UNIVERSITY OF CALIFORNIA, SAN DIEGO

METHODS AND DEVICES FOR FABRICATING AND ASSEMBLING DNA AND PROTEIN ARRAYS FOR HIGH-THROUGHPUT ANALYSES

A dissertation submitted in partial satisfaction of the requirements
for the degree Doctor of Philosophy

in

Bioengineering

by

Kristopher David Barbee

Committee in charge:

Professor Xiaohua Huang, Chair
Professor Sadik Esener
Professor Michael Heller
Professor Bing Ren
Professor Shankar Subramaniam

2010

The dissertation of Kristopher David Barbee is approved, and it is acceptable in quality and form for publication on microfilm and electronically:

_____

_____

_____

_____

_____

Chair

University of California, San Diego

2010

EPIGRAPH

The key is to get it to work.

Xiaohua Huang

Table of Contents

LIST OF FIGURES

ACKNOWLEDGEMENTS

First and foremost, I thank my advisor, Professor Xiaohua Huang, for his guidance, mentorship, advice, assistance, encouragement, and support. He has given me the flexibility and freedom to pursue many different projects and approaches to various problems. He has also given me the opportunity to conduct my research at other institutions so that I could have access to the best equipment available. His door has always been open and his technical expertise, which spans multiple disciplines, has always been extremely helpful and inspiring.

I thank the rest of my committee members, Professor Sadik Esener, Professor Michael Heller, Professor Bing Ren and Professor Shankar Subramaniam, for their time and advice.

I thank Alexander Hsiao for contributing significantly to several projects related to the fabrication and assembly of DNA and protein arrays using electric fields. Without his assistance, this work would not have been possible.

I thank Matt Chandrangsu for contributing significantly to several projects related to the fabrication and synthesis of linear DNA polymer arrays. Without his assistance, this work would not have been possible.

I thank Aric Joneja for his expert advice on numerous topics such as PCR primer design, DNA enzymology and general molecular biology techniques. His extensive knowledge and experience has also been extremely helpful in troubleshooting our experiments and interpreting our results.

I thank Eric Roller for his work involving the integration and automation of our imaging systems. His work has enabled us to perform sensitive and quantitative epifluorescence imaging for a variety of projects

I thank Nora Theilacker for her expert advice on antibodies and immunoassays. Her image analysis routines were also instrumental to several projects presented here.

I also thank Ying-Ja Chen for her advice and her help setting our imaging systems, Robert Mifflin for his expert advice on electrical circuits and devices, Erin McElfish for her assistance with RCA and Joyce Chuang for her help formatting and editing this dissertation.

A portion of this work was performed in the Nano3 facility at CalIT2 at UCSD. I would like to thank Ryan Anderson, Larry Grissom, Dr. Maribel Montero, Dr. Bernd Fruhberger and Sean Parks at the Nano3 Facility for providing advice, training and technical support. I would also like to thank Michael Clark for dicing some of our wafers.

A portion of this work was performed in the Nanotech Facility at the University of California, Santa Barbara, part of the NSF National Nanotechnology Infrastructure Network. I would like to thank Dr. Brian Thibeault, Bob Hill, Dr. Adam Abrahamsen, and Mike Silva at UCSB for their advice, training and technical support.

A portion of this work was performed at the Triangle National Lithography Center at North Carolina State University (NCSU). I would like to thank David Vellenga and Marcio Cerullo at NCSU for their training, technical support and services,

which included DUV photolithography and BARC etching. I would also like to thank Jonathan Pierce at the Analytical Instrumentation Facility at NCSU for his help with some of our SEM imaging.

I would like to acknowledge the NSF National Nanotechnology Infrastructure Network for enabling access to the Nanotech Facility at UCSB. I would also like to acknowledge the NIH/NHGRI, NSF and the Department of Bioengineering at UCSD for their financial support.

Chapter 2, in part, is a reproduction of the material as it appears in: Barbee, K.D.; Huang, X., *Analytical Chemistry* **2008** 80 (6); 2149 - 2154, 2008; copyright 2008 American Chemical Society. Used with permission. The dissertation author was the primary investigator and author of this paper.

Chapter 3, in part, is a reproduction of the material as it appears in: Barbee, K.D.; Hsiao, A.P.; Heller, M.J.; Huang, X., *Lab on a Chip* **2009** 9 (22); 3268 - 3274; copyright 2009 Royal Society of Chemistry. Used with permission. The dissertation author was the primary investigator and author of this paper.

Chapter 4, in part, has been submitted for publication. Barbee, K.D.; Hsiao, A.P.; Roller, E.E.; Huang, X. Used with permission. The dissertation author was the primary investigator and author of this paper.

Chapter 5, in part, has been submitted for publication. Barbee, K.D.; Chandrangsu, M.; Huang, X. Used with permission. The dissertation author was the primary investigator and author of this paper.

VITA

Education

- Ph.D., Bioengineering
  The University of California, San Diego - *La Jolla, CA (2010)*
- M.S., Bioengineering
  The University of California, San Diego - *La Jolla, CA (2005)*
- Graduate Studies, Biomedical Engineering
  The Ohio State University - *Columbus, OH (2001 - 2003)*
- B.S., Mechanical Engineering**,** *Summa Cum Laude*
  The Ohio State University - *Columbus, OH (2001)*

Research Experience

- **Research Associate, Department of Bioengineering** *(2004 - 2010)*
  The University of California, San Diego - La Jolla, CA. Developed new methods and technologies for (1) massively parallel solid-phase amplification of DNA on microfabricated substrates; (2) assembling high-density microbead-based DNA and antibody arrays via electric and magnetic fields; (3) multiplexed protein detection in microfluidic devices; (4) high-throughput, single molecule DNA sequencing by ligation
- **Research Associate, Department of Cell Biology** *(2004)*
  The Scripps Research Institute, La Jolla, CA. Advisor: Prof. John Yates III. Studied murine protein expression levels using multi-dimensional HPLC and mass spectrometry.
- **Research Associate, Department of Chemical Engineering** *(2002 - 2003)*
  The Ohio State University, Columbus, OH. Advisor: Prof. Shang-Tian Yang. Studied the effects of 2-D and 3-D micro-environments on the maintenance and neuronal differentiation of murine embryonic stem cells.

Publications

- Barbee, K. D.; Chandrangsu, M.; Huang, X. **Fabrication of DNA Polymer Brush Arrays Using Destructive Micropatterning and Rolling Circle Amplification.** Submitted.
- Barbee, K. D.; Hsiao, A. P.; Roller, E. E.; Huang, X. **Multiplexed Protein Detection on Antibody- Conjugated Microbead Arrays in a Microfabricated Electrophoretic Device.** Submitted.
- Theilacker, N.; Roller, E.E.; Barbee, K.D.; Franzreb, M.; Huang, X. **Encoded Antibody-conjugated Microbeads for Protein Analysis**. Submitted.
- Barbee, K. D.; Hsiao, A. P.; Heller, M. J.; Huang, X. **Electric Field Directed Assembly of High-Density Microbead Arrays.** Lab on a Chip 2009 9 (22); 3268 - 3274.

- Barbee, K. D.; Huang, X. **Magnetic Assembly of High-Density DNA Arrays for Genomic Analyses.** Analytical Chemistry 2008 80 (6); 2149 - 2154.

Technical Skills

- **Microfabrication and nanofabrication techniques:** Contact and projection photolithography, e-beam and nanoimprint lithography, soft lithography, thin film deposition and reactive ion etching.
- **Surface chemistry:** Glass and polymer surface chemistry, bioconjugation chemistry, self-assembly and thin film fabrication.
- **Molecular and cellular biology**: DNA enzymology, PCR, RCA, gel electrophoresis, immunoassays, cell culture and recombinant DNA technology.
- **DNA and protein chemistry:** Development of new methods, devices and technologies for high-throughput DNA sequencing, multiplexed protein detection and solid-phase DNA amplification.
- **Imaging and characterization techniques:** AFM, SEM, TIRF and epifluorescence microscopy, spectrometry, interferometry and profilometry.
- **Device prototyping and fabrication:** Glass and PDMS-based microfluidic devices, solid-state thermal cyclers, bioreactors and CNC milling/machining.
- **Computation and modeling:** Design, modeling, analysis, automation and control software including AutoCAD, COMSOL Multiphysics, MATLAB, Excel, ImageJ and LabVIEW.

Patents & Invention Disclosures

- Barbee, K.D.; Hsiao, A.P.; Huang, X. **Methods and Devices for Multiplexed Protein Detection on Antibody-Conjugated Microbead Arrays**. *UCSD Technology Transfer Disclosure (2010).*
- Barbee, K.D.; Hsiao, A.P.; Huang, X. **Microfabricated Devices for Electric Field Directed Assembly of DNA and Protein Arrays**. *UCSD Technology Transfer Disclosure (2010).*
- Barbee, K.D.; Huang, X. **Methods and Devices for Biomolecular Arrays**. *USPTO App. No. 60/887,244 (2007); WIPO App. No. PCT/US2008/052484 (2008).*

Teaching Experience

- **Senior Teaching Associate**
  Department of Bioengineering, UCSD, La Jolla, CA (2005 - 2007)
  Developed, organized and directed training sessions for all Bioengineering TAs.
- **Instructor**
  Academic Connections, UCSD, La Jolla, CA (2005 - 2006)
  Designed and taught two biotechnology courses with laboratory sections and supervised TAs

- **Teaching Associate**
  Department of Bioengineering, UCSD, La Jolla, CA (2004 -2006)
  Taught discussion sections in physical chemistry and biomolecular engineering.
- **Teaching Associate**
  Department of Chemistry UCSD, La Jolla, CA (2004)
  Instructed a laboratory section in general chemistry.
- **Teaching Associate**
  Department of Mathematics, OSU, Columbus, OH (1999 - 2003)
  Taught over twenty algebra, trig. and pre-calc. recitation sections and lectured a pre-calc. course.
- **Instructional Assistant**
  Student Athlete Support Services, OSU, Columbus, OH (1998 - 2003)
  Tutored hundreds of student-athletes in mathematics, chemistry and physics.
- **Teaching Associate**
  Department of Chemistry, OSU, Columbus, OH (1999 - 2002)
  Instructed six laboratory sections and two recitation sections in four different courses.
- **Instructional Assistant**
  Department of Mathematics, OSU, Columbus, OH (1997 - 1999)
  Tutored hundreds of students in calculus at the Mathematics and Statistics Learning Center.

Invited Talks

- Barbee, K.D. **Biosystems Research and Development Department at Sandia National Laboratories**, Livermore, CA (2010).
- Barbee, K.D. **Clemson University and Medical University of South Carolina Joint Bioengineering Program**, Charleston, SC (2010).
- Barbee, K.D. **Illumina, Inc**., San Diego, CA (2010).
- Barbee, K.D. **Institute of Nanobiotechnology at Johns Hopkins University**, Baltimore, MD (2010).
- Barbee, K.D. **Life Technologies,** Eugene, OR. (2010)

Conference Presentations

- Barbee, K.D.; Chandrangsu, M.; Joneja, A.; Huang, X. **Linear Strand Displacement Amplification and Linear Polymer Arrays for Genome Amplification**. *National Human Genome Research Institute* (*NHGRI) Sequencing Technology Meeting*. Chapel Hill, NC (2010).
- Barbee, K.D.; Hsiao, A.P.; Heller, M.J.; Huang, X. **Electric Field Directed Assembly of High-Density Microbead Arrays**. *Lab on a Chip World Congress.* San Francisco, CA (2009).

- Barbee, K.D.; Roller. E.E.; Hsiao, A.P.; Chaisson, M.; Heller, M.J.; Pevzner, P.; Huang, X. **Single Molecule DNA Sequencing by Ligation**. *NHGRI Sequencing Technology Meeting*. San Diego, CA (2009).
- Roller. E.E.; Barbee, K.D.; Heller, M.J.; Pevzner, P.; Huang, X. **Genome Sequencing by Ligation Using Nano-Arrays of Single DNA Molecules.** *NHGRI Sequencing Technology Meeting*. San Diego, CA (2008).
- Huang, X.; Barbee, K.D. **Microfabricated Arrays for High-Throughput DNA Sequencing**. *National Nanotechnology Infrastructure Network Annual Meeting*. Ann Arbor, MI (2007).
- Chen. Y.-J.; Barbee, K.D.; Roller, E.E.; Chen, R.; Wong, S.-Y.; Huang, X. **Massively Parallel Cloning and Sequencing of DNA.** *NHGRI Sequencing Technology Meeting*. Marco Island, FL (2007).
- Barbee, K.D.; Huang, X. **A Novel Technique for Fabricating Biomolecular Nano-Arrays**. *NSTI Nanotechnology Conference*. Boston, MA (2006).

Appointments

- Representative, **Bioengineering Graduate Student Task Force**
  UCSD, La Jolla, CA (2008 - 2009)
- Representative, **Affiliated Housing Advisory Committee**
  UCSD, La Jolla, CA (2006 - 2007)
- Recruitment Officer**, Bioengineering Graduate Student Group**
  UCSD, LA Jolla, CA (2004 - 2007)
- Representative, **Grad. & Pro. Student Satisfaction Committee**
  UCSD, La Jolla, CA (2005 - 2006)

Professional & Honorary Societies

- Member, **Tau Beta Pi National Engineering Honor Society**
- Member, **Pi Tau Sigma Honorary Mechanical Engineering Society**
- Member, **The Honor Society of Phi Kappa Phi**

ABSTRACT OF THE DISSERTATION

METHODS AND DEVICES FOR FABRICATING AND ASSEMBLING DNA AND PROTEIN ARRAYS FOR HIGH-THROUGHPUT ANALYSES

by

Kristopher David Barbee

Doctor of Philosophy in Bioengineering
University of California, San Diego, 2010

Professor Xiaohua Huang, Chair

Recent developments in DNA sequencing technologies have resulted in substantial reductions in time and cost for large scale sequencing efforts. However, the routine sequencing of individual human genomes for personalized medicine and point-of-care clinical applications will require future-generation DNA sequencing

technologies to achieve unprecedented multiplexing, sample throughput and cost reductions. There is also a need for tools and techniques for interrogating proteins in a sensitive, quantitative, multiplexed and high-throughput manner. To enable further miniaturization and parallelization for such analyses, I have developed new methods and technologies for fabricating and assembling high-density DNA and protein arrays. Microfabrication techniques were utilized to construct various platforms upon which DNA and protein conjugated microbeads can be assembled. Electric and magnetic fields are employed to accelerate the assembly process and achieve unprecedented filling efficiencies. I have also demonstrated the utility of such arrays as a platform for multiplexed protein detection. In addition, I have developed a method for fabricating DNA polymer brush arrays in microfluidic devices. These arrays may be useful for enhancing the sensitivity of microarrays and the yield, efficiency and order of solid-phase DNA amplification.

1 Introduction

1.1 High-throughput technologies

The advent of high-throughput technologies in biomedical research has enabled varying degrees of multiplexed sample or biomolecular analyses via a wide range of platforms and methodologies[1-6]. For instance, enzyme-linked immunosorbent assays[7] (ELISA) performed on multi-well plates have provided a means for the parallel screening of tens to a few hundred samples in a relatively efficient and economical manner. In addition, protein arrays fabricated via robotic spotting have provided a means for the simultaneous analysis of as many as several thousand proteins on a single microscope slide[8-15]. Even more impressive are DNA microarrays, which have enabled the parallel detection of hundreds of thousands of single nucleotide polymorphisms (SNPs) on relatively small solid supports such as glass slides and wells etched into the faces of fiber optic bundles[16-20]. Second-generation genome sequencing technologies

have also achieved massive parallelization with unprecedented multiplexing and throughput[21-23]. While these technologies have lead to some of the greatest breakthroughs in biomedical research, there is still plenty of room for improvements in terms of size, throughput and cost[24]. Further improvements in these areas should enable more complex proteomics studies and the routine sequencing of individual human genomes for personalized medicine, point-of-care clinical applications and advanced cancer research.

1.2 DNA arrays

DNA arrays fabricated by robotic printing and photolithographic methods have enabled numerous large-scale assays such as gene expression studies and genotyping[16-18]. Other platforms have utilized DNA-conjugated microbeads, which offer several advantages over the aforementioned methods[19, 20]. For instance, the microbeads provide more surface area than a planar surface within a given footprint, thereby enabling higher loading capacities for more sensitive assays. The microbeads also serve as carrier particles, which allow the DNA oligos to be synthesized directly on the microbeads in a more traditional and efficient, column-based approach. The different microbead populations can then be combined and deposited at once onto a solid substrate for later use. Another powerful advantage is the ability to clonally amplify genomic DNA templates on microbeads using microemulsions[25]. Once deposited onto an appropriate surface, these clones can be sequenced in a massively parallel manner using a variety of approaches.

Despite these advantages, there are several limitations involved with using microbeads to fabricate DNA arrays. For instance, assembling the microbeads in an efficient and timely manner can be very challenging. In fact, gravity and Brownian motion alone are not sufficient for microbead deposition or assembly, especially for the popular polystyrene microbeads that have a density near that of water. The sedimentation time can be approximated by assuming terminal velocities and summing the relevant forces:

$$\sum F = F_{gravity} - F_{buoyancy} - F_{drag} = m\frac{du}{dt} = 0$$

and thus

$$\rho_p V_p g - \rho_s V_p g - f u_T = 0 ,$$

where ρ_p and V_p are the density and volume of the particle, respectively, g is the gravitational acceleration, ρ_s is density of the solution and u_T is the terminal velocity of the particle f is the frictional factor of a sphere and is given by $f = 6\pi\eta r$, where η is the viscosity of the medium and r is the radius of the particle. Solving for u_T and simplifying, we get:

$$u_T = \frac{2r^2 g}{9n}\left(\rho_p - \rho_s\right)$$

For 1 μm beads with a density of about 1.5 times that of water, the terminal velocity is less than 0.3 μm/second. Microbeads of this density, which include the popular superparamagnetic beads from Dynal Corp., would have an average settling

time of approximately 7.5 minutes for a 250 μm chamber thickness. This may be an acceptable amount of time for some applications but these microbeads are much more dense than plain polystyrene microbeads. With a specific gravity of approximately 1.05, their settling time would be approximately ten times longer. This problem has made passive assembly methods undesirable if not impractical. Solvent evaporation and controlled dewetting methods have been used to overcome this issue but these approaches are often very slow, not easily scaled and not compatible with certain biomolecules and attachment chemistries[26,27]. Other groups have employed electric[28-30] and magnetic[31-33] assembly methods to overcome these issues, but these active approaches require multistep fabrication processes and complex field generation schemes. In addition, large, high-density arrays with high filling efficiencies and low defects rates have yet to be demonstrated using many of these approaches.

Another disadvantage associated with current microbead-based DNA arrays is related to the random, non-structured arrangements of the microbeads, which can result in reduced throughput and imaging efficiency, complicated image processing and high reagent costs[22]. To create structured microbead arrays, other groups have employed the use of microwell arrays, which guide the assembly of the microbeads into defined locations on the substrate[26, 34-36]. The wells are typically fabricated using photolithographic methods or by etching wells into fiber optic bundles. The microbeads are usually about the same size as the microwells such that each microwell can only accommodate one microbead. The major disadvantage with this basic strategy comes back to the speed and efficiency of the assembly process. Since the microbeads will not

passively assemble and remain fixed within these microwells, evaporation, dewetting or centrifugation-based methods[21] must be employed.

1.3 Protein arrays

Protein and antibody arrays fabricated via robotic spotting[8,9,11-13,37-40] enable greater multiplexing and significantly reduced sample volumes compared to analyses performed with western blots[41] or ELISA[7]. However, assays that employ protein- and antibody-conjugated microbeads allow for even greater multiplexing and scalability than those performed on spotted arrays[42-49]. Unfortunately, many microbead-based protein array platforms suffer from the same difficulties with assembly as their nucleic acid counterparts. Several methods for assembling or capturing antibody-conjugated microbeads on chip-based platforms have been demonstrated. These include micromanipulation[44], microfluidic trapping[45,46], evaporation of microbead suspensions on etched silicon[47] or fiber-optic bundles[48] and electrostatic self-assembly on chemically-modified substrates[49]. These approaches are limited in that they are either very slow, very complex or cannot be easily scaled. Other limitations may include flexibility, sensitivity and difficulty in automating the processes.

1.4 DNA amplification

The state of the art in genome-scale DNA amplification includes the emulsion polymerase chain reaction (emPCR) process[25] and bridge PCR[23,50,51]. The emPCR method uses water-in-oil micro-emulsions to isolate microbeads and fragmented genomic DNA templates so that monoclonal products can be produced on the beads. Micro-emulsions that contain both a bead and a single DNA template must occur at

very low frequencies to ensure clonal amplification, a requirement that leads to wasted reagents and added costs. In addition, the size of the micro-emulsions is difficult to control, resulting in large variations in the amount of amplified product as well as inefficient use of expensive reagents. Prior to depositing these microbeads on a surface for DNA sequencing, the population must be enriched to remove the large portion of microbeads that do not contain any PCR products.

In contrast, the bridge PCR method involves the amplification of genomic DNA templates directly on the surface of a glass substrate that contains both forward and reverse PCR primers[23]. The genomic DNA templates are first allowed to hybridize to the covalently bound primers. After synthesizing their compliments, the original templates are removed to prevent cross talk between the clonal clusters of DNA that will then be synthesized via ~40 cycles of PCR. Although this method may be better suited for automation, it suffers from low yields and very poor reaction kinetics. This poor yield limits the signal that can be obtained from each cluster during sequencing, which makes imaging very difficult and limits the read length. These platforms use confluent lawns of DNA primers, which result in random arrangements of the DNA clusters. If the original template density is too low, the cluster density will be also be very low and sequencing throughput will suffer. On the other hand, if the original template density is too high, the clusters will be too dense, rendering many of them indistinguishable from one another[52].

1.5 Scope of the dissertation

The objective of this dissertation work was to develop new technologies for fabricating and assembling high-density DNA and protein arrays for genomic and proteomic analyses. New methods and devices were developed to overcome the limitations of current microbead-based DNA and protein fabrication and assembly methods. New methods and devices were also developed to generate polymer brush arrays that may overcome the limitations currently associated with solid-phase DNA amplification.

In part of this work, we utilized microfabrication techniques to create various microwell arrays upon which DNA and protein conjugated microbeads could be assembled. Electric and magnetic fields were employed to accelerate the assembly process and achieve unprecedented filling efficiencies on these arrays. We have demonstrated the utility of such arrays as platforms for multiplexed protein detection. The electrophoretic microdevices may also be useful for actively accelerating diffusion-limited biomolecular interactions and reactions.

In another part of this work, we utilize microfabrication techniques to generate arrays of DNA polymer brushes for genome-scale single molecule amplification. Oligonucleotide arrays are first fabricated using photolithography and plasma etching. The linear DNA polymers are then synthesized via rolling circle amplification (RCA). These polymer brush arrays may be useful for enhancing the sensitivity of microarrays and the efficiency and yield of bridge PCR.

1.6 References

1. Brenner, S., Johnson, M., Bridgham, J., Golda, G., Lloyd, D.H., Johnson, D., Luo, S., McCurdy, S., Foy, M., Ewan, M. *et al.* Gene expression analysis by massively parallel signature sequencing (MPSS) on microbead arrays. *Nat. Biotechnol.* **18**, 630-634 (2000).

2. Lander, E.S., Linton, L.M., Birren, B., Nusbaum, C., Zody, M.C., Baldwin, J., Devon, K., Dewar, K., Doyle, M., FitzHugh, W. *et al.* Initial sequencing and analysis of the human genome. *Nature* **409**, 860-921 (2001).

3. Venter, J.C., Adams, M.D., Myers, E.W., Li, P.W., Mural, R.J., Sutton, G.G., Smith, H.O., Yandell, M., Evans, C.A., Holt, R.A. *et al.* The sequence of the human genome. *Science* **291**, 1304-1351 (2001).

4. Burbaum, J. & Tobal, G.M. Proteomics in drug discovery. *Curr. Opin. Chem. Biol.* **6**, 427-433 (2002).

5. Shendure, J., Mitra, R.D., Varma, C. & Church, G.M. Advanced sequencing technologies: Methods and goals. *Nat. Rev. Genet.* **5**, 335-344 (2004).

6. Bentley, D.R. Whole-genome re-sequencing. *Curr. Opin. Genet. Dev.* **16**, 545-552 (2006).

7. Engvall, E. & Perlmann, P. Enzyme-linked immunosorbent assay (ELISA) quantitative assay of immunoglobulin g. *Immunochemistry* **8**, 871-874 (1971).

8. Holt, L.J., Bussow, K., Walter, G. & Tomlinson, I.M. By-passing selection: Direct screening for antibody-antigen interactions using protein arrays. *Nucleic Acids Res.* **28**, e72- (2000).

9. MacBeath, G. & Schreiber, S.L. Printing proteins as microarrays for high-throughput function determination. *Science* **289**, 1760 - 1763 (2000).

10. Pandey, A. & Mann, M. Proteomics to study genes and genomes. *Nature* **405**, 837-846 (2000).

11. de Wildt, R.M.T., Mundy, C.R., Gorick, B.D. & Tomlinson, I.M. Antibody arrays for high-throughput screening of antibody-antigen interactions. *Nat. Biotechnol.* **18**, 989 - 994 (2000).

12. Haab, B.B., Dunham, M.J. & Brown, P.O. Protein microarrays for highly parallel detection and quantitation of specific proteins and antibodies in complex solutions. *Genome Biology* **2**, 0004.0001-0004.0013 (2001).

13. Zhu, H., Bilgin, M., Bangham, R., Hall, D., Casamayor, A., Bertone, P., Lan, N., Jansen, R., Bidlingmaier, S., Houfek, T. *et al.* Global analysis of protein activities using proteome chips. *Science* **293**, 2101-2105 (2001).

14. MacBeath, G. Protein microarrays and proteomics. *Nat. Genet.* **32**, 526-532 Suppl (2002).

15. Phizicky, E., Bastiaens, P.I.H., Zhu, H., Snyder, M. & Fields, S. Protein analysis on a proteomic scale. *Nature* **422**, 208-215 (2003).

16. Fodor, S.P.A., Read, J.L., Pirrung, M.C., Stryer, L., Lu, A.T. & Solas, D. Light-directed, spatially addressable parallel chemical synthesis. *Science* **251**, 767-773 (1991).

17. Chee, M., Yang, R., Hubbell, E., Berno, A., Huang, X.C., Stern, D., Winkler, J., Lockhart, D.J., Morris, M.S. & Fodor, S.P. Accessing genetic information with high-density DNA arrays. *Science* **274**, 610-614 (1996).

18. Schena, M., Shalon, D., Heller, R., Chai, A., Brown, P.O. & Davis, R.W. Parallel human genome analysis: Microarray-based expression monitoring of 1000 genes. *Proc. Natl. Acad. Sci. U. S. A.* **93**, 10614-10619 (1996).

19. Ferguson, J.A., Steemers, F.J. & Walt, D.R. High-density fiber-optic DNA random microsphere array. *Anal. Chem.* **72**, 5618-5624 (2000).

20. Gunderson, K.L. Whole-genome genotyping on bead arrays. *Methods Mol. Biol.* **529**, 197-213 (2009).

21. Margulies, M., Egholm, M., Altman, W.E., Attiya, S., Bader, J.S., Bemben, L.A., Berka, J., Braverman, M.S., Chen, Y.J., Chen, Z. *et al.* Genome sequencing in microfabricated high-density picolitre reactors. *Nature* **437**, 376-380 (2005).

22. Shendure, J., Porreca, G.J., Reppas, N.B., Lin, X., McCutcheon, J.P., Rosenbaum, A.M., Wang, M.D., Zhang, K., Mitra, R.D. & Church, G.M. Accurate multiplex polony sequencing of an evolved bacterial genome. *Science* **309**, 1728-1732 (2005).

23. Bentley, D.R., Balasubramanian, S., Swerdlow, H.P., Smith, G.P., Milton, J., Brown, C.G., Hall, K.P., Evers, D.J., Barnes, C.L., Bignell, H.R. *et al.* Accurate whole human genome sequencing using reversible terminator chemistry. *Nature* **456**, 53-59 (2008).

24. Shendure, J. & Ji, H. Next-generation DNA sequencing. *Nat. Biotechnol.* **26**, 1135-1145 (2008).

25. Dressman, D., Yan, H., Traverso, G., Kinzler, K.W. & Vogelstein, B. Transforming single DNA molecules into fluorescent magnetic particles for detection and enumeration of genetic variations. *Proc. Natl. Acad. Sci. U. S. A.* **100**, 8817-8822 (2003).

26. Michael, K.L., Taylor, L.C., Schultz, S.L. & Walt, D.R. Randomly ordered addressable high-density optical sensor arrays. *Anal. Chem.* **70**, 1242-1248 (1998).

27. Cui, Y., Bjork, M.T., Liddle, J.A., Sonnichsen, C., Boussert, B. & Alivisatos, A.P. Integration of colloidal nanocrystals into lithographically patterned devices. *Nano Lett.* **4**, 1093-1098 (2004).

28. Yeh, S.-R., Seul, M. & Shraiman, B.I. Assembly of ordered colloidal aggregrates by electric-field-induced fluid flow. *Nature* **386**, 57-59 (1997).

29. Li, A.X., Seul, M., Cicciarelli, J., Yang, J.C. & Iwaki, Y. Multiplexed analysis of polymorphisms in the hla gene complex using bead array chips. *Tissue Antigens* **63**, 518-528 (2004).

30. Winkleman, A., Gates, B.D., McCarty, L.S. & Whitesides, G.M. Directed self-assembly of spherical particles on patterned electrodes by an applied electric field. *Adv. Mater.* **17**, 1507-1511 (2005).

31. Wen, W., Wang, N., Zheng, D.W., Chen, C. & Tu, K.N. Two- and three-dimensional arrays of magnetic microspheres. *J. Mater. Res.* **14** (1999).

32. Roberts, L.A., Crawford, A.M., Zappe, S., Jain, M. & White, R.L. Patterned magnetic bar array for high-throughput DNA detection. *IEEE Trans. Magnet.* **40**, 3006-3008 (2004).

33. Yellen, B.B. & Friedman, G. Programmable assembly of colloidal particles using magnetic microwell templates. *Langmuir* **20**, 2553-2559 (2004).

34. Yin, Y., Lu, Y., Gates, B. & Xia, Y. Template-assisted self-assembly: A practical route to complex aggregates of monodispersed colloids with well-defined sizes, shapes, and structures. *J. Am. Chem. Soc.* **123**, 8718-8729 (2001).

35. Xia, Y., Yin, Y., Lu, Y. & McLellan, J. Template-assisted self-assembly of spherical colloids into complex and controllable structures. *Adv. Funct. Mater.* **13**, 907-918 (2003).

36. Steemers, F.J. & Gunderson, K.L. Whole genome genotyping technologies on the beadarray platform. *Biotechnol. J.* **2**, 41-49 (2007).

37. Silzel, J.W., Cercek, B., Dodson, C., Tsay, T. & Obremski, R.J. Mass-sensing, multianalyte microarray immunoassay with imaging detection. *Clin. Chem.* **44**, 2036-2043 (1998).

38. Arenkov, P., Kukhtin, A., Gemmell, A., Voloshchuk, S., Chupeeva, V. & Mirzabekov, A. Protein microchips: Use for immunoassay and enzymatic reactions. *Anal. Biochem.* **278**, 123 - 131 (2000).

39. Moody, M.D., Van Arsdell, S.W., Murphy, K.P., Orencole, S.F. & Burns, C. Array-based ELISAs for high-throughput analysis of human cytokines. *Biotechniques*, 186-194 (2001).

40. Huang, R.-P., Huang, R., Fan, Y. & Lin, Y. Simultaneous detection of multiple cytokines from conditioned media and patient's sera by an antibody-based protein array system. *Anal. Biochem.* **294**, 55-62 (2001).

41. Renart, J., Reiser, J. & Stark, G.R. Transfer of proteins from gels to diazobenzyloxymethyl-paper and detection with antisera: A method for studying antibody specificity and antigen structure. *Proc. Natl. Acad. Sci. U. S. A.* **76**, 3116-3120 (1979).

42. Dasso, J., Lee, J., Bach, H. & Mage, R.G. A comparison of ELISA and flow microsphere-based assays for quantification of immunoglobulins. *J. Immunol. Methods* **263**, 23-33 (2002).

43. Kellar, K.L. & Iannone, M.A. Multiplexed microsphere-based flow cytometric assays. *Exp. Hematol.* **30**, 1227-1237 (2002).

44. Goodey, A., Lavigne, J.J., Savoy, S.M., Rodriguez, M.D., Curey, T., Tsao, A., Simmons, G., Wright, J., Yoo, S.-J., Sohn, Y. *et al.* Development of multianalyte sensor arrays composed of chemically derivatized polymeric microspheres localized in micromachined cavities. *J. Am. Chem. Soc.* **123**, 2559-2570 (2001).

45. Herrmann, M., Roy, E., Veres, T. & Tabrizian, M. Microfluidic ELISA on non-passivated pdms chip using magnetic bead transfer inside dual networks of channels. *Lab Chip* **7**, 1546-1552 (2007).

46. Diercks, A.H., Ozinsky, A., Hansen, C.L., Spotts, J.M., Rodriguez, D.J. & Aderem, A. A microfluidic device for multiplexed protein detection in nano-liter volumes. *Anal. Biochem.* **386**, 30-35 (2009).

47. Qiu, X., Thompson, J.A., Chen, Z., Liu, C., Chen, D., Ramprasad, S., Mauk, M., Ongagna, S., Barber, C., Abrams, W.R. *et al.* Finger-actuated, self-contained immunoassay cassettes. *Biomed. Microdev.* **11**, 1175-1186 (2009).

48. Blicharz, T.M., Siqueira, W.L., Helmerhorst, E.J., Oppenheim, F.G., Wexler, P.J., Little, F.F. & Walt, D.R. Fiber-optic microsphere-based antibody array for the analysis of inflammatory cytokines in saliva. *Anal. Chem.* **81**, 2106-2114 (2009).

49. Sivagnanam, V., Song, B., Vandevyver, C. & Gijs, M.A.M. On-chip immunoassay using electrostatic assembly of streptavidin-coated bead micropatterns. *Anal. Chem.* **81**, 6509-6515 (2009).

50. Adessi, C., Matton, G., Ayala, G., Turcatti, G., Mermod, J.-J., Mayer, P. & Kawashima, E. Solid phase DNA amplification: Characterisation of primer attachment and amplification mechanisms. *Nucleic Acids Res.* **28**, e87- (2000).

51. Fedurco, M., Anthony Romieu, Scott Williams, Isabelle Lawrence and & Turcatti, G. BTA, a novel reagent for DNA attachment on glass and efficient generation of solid-phase amplified DNA colonies. *Nucleic Acids Res.* **34**, e22 (2006).

52. Quail, M.A., Kozarewa, I., Smith, F., Scally, A., Stephens, P.J., Durbin, R., Swerdlow, H. & Turner, D.J. A large genome center's improvements to the Illumina sequencing system. *Nat. Meth.* **5**, 1005-1010 (2008).

2 Rapid magnetic assembly of high-density DNA arrays for genomic analyses

2.1 Abstract

A method for rapidly assembling high-density DNA arrays with near perfect order is described. Photolithography is used to generate a wafer-scale array of microwells in a layer of photoresist on a chemically functionalized glass cover slip. The array is enclosed within a microfluidic device and a suspension of superparamagnetic microbeads conjugated to DNA molecules is introduced into the chamber. A permanent magnet is used to direct the rapid assembly of the beads into the wells, with each well containing a single bead. These beads are immobilized on the glass surface via affinity binding and excess beads can be recycled or washed away. Non-specifically bound beads are removed by dissolving the photoresist. The result is a high-density array of

beads with virtually no background. This method can be used to produce protein arrays for chip-based assays and DNA arrays for genotyping or genome sequencing.

2.2 Introduction

Some of the greatest breakthroughs in biomedical research can be attributed to the development of the numerous high throughput technologies for quantitative measurements of biomolecules. Many of these technologies are made possible by microfabrication techniques commonly used in the semiconductor industry. For example, DNA and protein arrays fabricated by robotic printing and photolithographic methods have enabled extremely large-scale surveys of biomolecules[1-4]. The emerging "next generation" genome sequencing technologies, many of which utilize massive parallelization and miniaturization to achieve unprecedented multiplexing, throughput and cost reductions[5-10], promise to revolutionize biomedical research and enable personalized healthcare. However, some of these technology platforms utilize randomly distributed DNA-conjugated microbeads or clones on a glass slide within a reaction chamber. The random arrangements of the beads or clones result in low throughput and imaging efficiency, complicated image processing and high reagent costs[6-10]. One approach to improving these devices involves the use of microfabricated arrays to eliminate overlap and to minimize the area between the beads or clones.

Such arrays can be generated by depositing samples onto glass slides using robotic contact printing[2], microcontact printing[11-13] or dip pen lithography.[14] These arrays can also be generated by assembling beads onto microfabricated arrays of wells on glass or silicon substrates[15-18], or in etched wells on the face of a fiber-optic bundle[18-

[20]. Since bead assembly will not occur in an efficient and reliable manner if the process depends solely upon gravitational forces and Brownian motion, this process is typically achieved via solvent evaporation or dewetting[17-21]. However, these approaches are not suitable when rapid assembly is required or sample drying is undesirable. Other groups have employed electric[22] and magnetic[23-25] assembly methods to overcome these issues, but these active approaches require multistep fabrication processes and complex field generation schemes. For many genomic and proteomic applications, the array fabrication and assembly processes need to be scalable and inexpensive. The format of the arrays must also be compatible with high-throughput imaging and microfluidic devices. Our approach satisfies these criteria by combining a single photolithographic step with the facilitated self-assembly of magnetic microbeads to create large, high-density DNA arrays on cover glass.

Our method for fabricating high-density biomolecular arrays is illustrated in Figure 2.1. The process begins with the silanization and biotinylation of the surface of a glass cover slip. Photolithography is then used to generate high-density arrays of micrometer to sub-micrometer-scale wells in a thin layer of photoresist that has been spin coated on the glass surface. The patterned glass cover slip is enclosed within a flow cell and a suspension of streptavidin-coated superparamagnetic microbeads conjugated to DNA molecules is introduced into the device. A permanent magnet is briefly dragged along the backside of the cover glass to direct the rapid assembly of the microbeads into the wells. The beads are immobilized in the wells via biotin-streptavidin affinity binding with only one bead fixed within each well due to physical constraints. Excess

beads are washed away and non-specifically bound beads are removed by dissolving the photoresist with ethanol. The result is a high-density array of single beads with virtually no background.

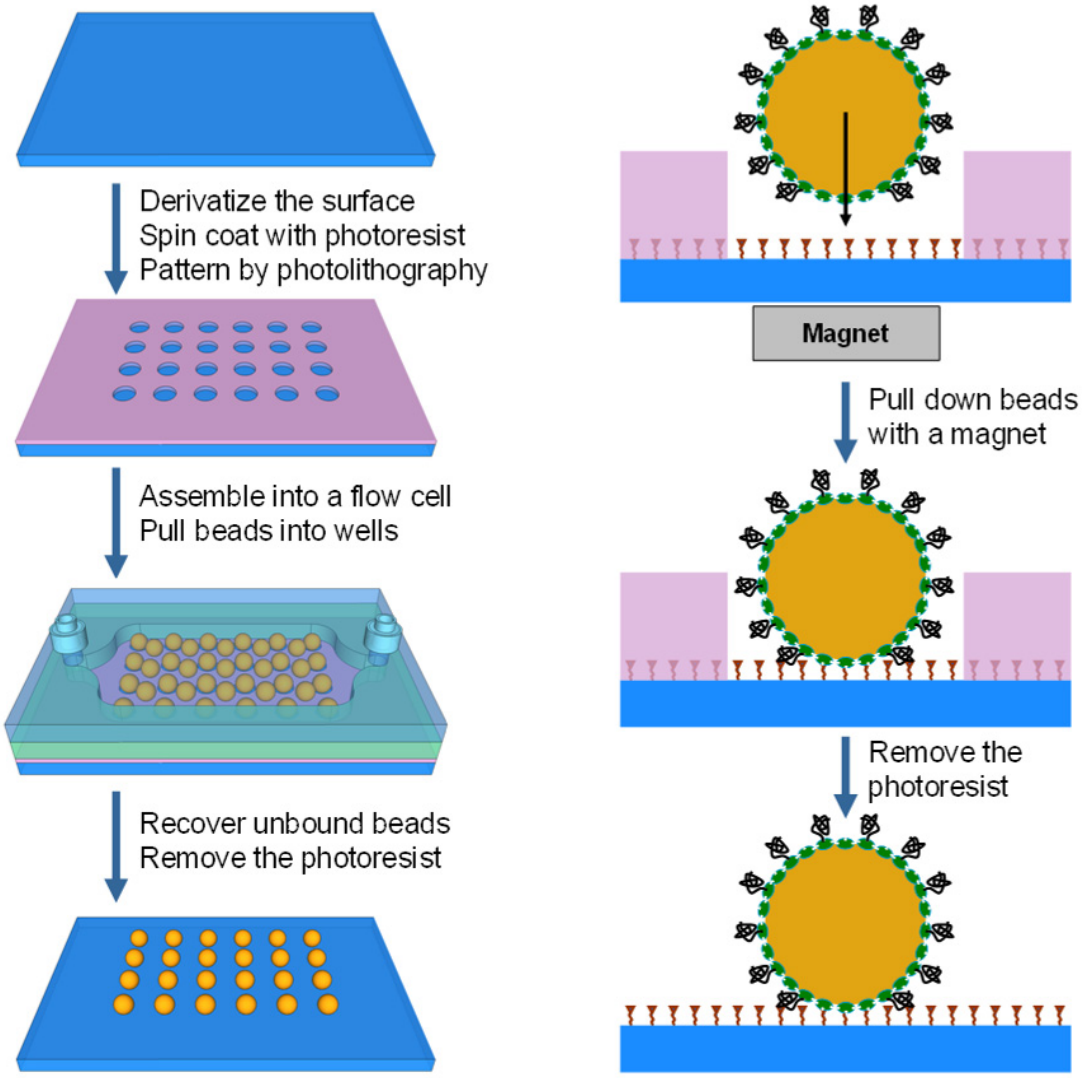

Figure 2.1: Rapid magnetic assembly of high-density DNA arrays.
The schematic illustrates the steps involved in the fabrication and assembly process. The left panel shows the basic procedure whereas the right panel illustrates the surface chemistry used to attach the beads to the array and the DNA to the beads. See text for a detailed description. The final microbead array is shown without the flow cell for illustrative purposes only. The drawing is not to scale.

2.3 Materials and methods

2.3.1 Chemical derivatization of glass surfaces

50 x 75 x 0.170 mm^3 borosilicate glass cover slips (Erie Scientific) were washed with a detergent solution and rinsed with 18 MΩ-cm de-ionized water. They were further cleaned by soaking in methanol and then acetone for 5 minutes each in an ultrasonic bath and dried in a convection oven at 110 ºC for 10 minutes. The cover slips were then soaked in a 2 M nitric acid solution for 30 minutes at room temperature and rinsed with de-ionized water. Silanization was performed using a 2% solution of 3-aminopropyltriethoxysilane (Gelest) in 95:5 acetone: water for 15 minutes at room temperature. The cover slips were then rinsed 3 times with acetone and cured at 110 ºC for 15 minutes in a convection oven. A 1 mM solution of N-hydroxylsuccinimidyl-PEG-biotin, MW 5000 (Nektar Therapeutics) in dry N, N-dimethylformamide with 1 mM triethylamine was prepared and 300 uL was spotted onto each cover slip and then covered with another cover slip using a #1 cover slip as a spacer. After one hour of incubation at room temperature, the cover slips were rinsed with acetone and treated with a 1% ammonium hydroxide + 0.1 % sodium dodecyl sulfate solution for 15 minutes. The cover slips were rinsed with de-ionized water followed by acetone and dried at 65 ºC for 10 minutes. The derivatized cover slips were stored in a vacuum desiccator.

2.3.2 Microfabrication

A layer of Microposit S1805 photoresist (Rohm & Haas) about 500 nm thick was applied to the surface of the glass by spinning at 3500 rpm for 30 seconds with a

spin coater. The glass was then heated on a hotplate at 110 ºC for 60 seconds. The array of wells were patterned by a 0.2 second exposure to 365 nm light (~475 mW/cm^2) through a chrome-on-quartz photomask using a wafer stepper system (GCA Autostep 200) equipped with an Olympus 2145 lens (5x reduction/0.45 NA). The resist was developed in MIF 701 (Rohm & Haas) for 60 seconds at room temperature then rinsed with water and dried with nitrogen gas.

2.3.3 Conjugation of DNA to microbeads

Three oligonucleotides with both biotin and fluorescence dye labels are: 5'-Fluorescein-TCC AGT TGA CCT GAG AGT C-TEG-biotin-3', 5'-Cy3-TCC TGA CTG AGT AGC ATC G-TEG-biotin-3' and 5'-Cy5-TCA CGT ACT GAG GTC GTC A-TEG-biotin-3'. The microbeads were prepared by adding drop wise a 10 μM solution of a labeled oligonucleotide to 0.1% (w/v) suspension of 1-μm streptavidin-coated superparamagnetic beads (Dynal MyOne, Invitrogen) in a DNA binding buffer (10 mM Tris-HCl, pH 7.5, 2.0 M NaCl, 1 mM EDTA). The amount of the biotinylated oligonucleotides is sufficient to bind approximately one third of the biotin binding sites on the beads (~150,000 oligonucleotides per bead). The mixture was shaken for 2 hours at room temperature and washed 3 times with a wash buffer (WB: 50 mM sodium phosphate, pH 7.05, 150 mM NaCl, 1 mM EDTA, 0.02% Tween-20). The beads were re-suspended in the wash buffer to give a final concentration of 0.25% (w/v). For the color image shown in Figure 2.3, the mixture contained the 3 bead populations in roughly equal molar ratio. For the gray-scale image shown in Figure 2.4, the beads contained only the Cy5-labeled oligonucleotides.

2.3.4 Rapid magnetic assembly of microbead arrays

The microbead assembly was performed within a flow cell, which consists of a 1 mm thick glass slide, a 250 μm-thick silicone rubber gasket and the cover glass with the array (Figure 2.1). Prior to the assembly of the flow cell, small holes were drilled through the slide and tubing connectors were fixed to the slide with epoxy. The gasket was laid onto the slide and the middle portion was cut out to form the flow chamber. The cover glass was aligned and pressed to the gasket to form a liquid-tight seal between the slide and the cover glass.

The chamber was first rinsed with a wash buffer (WB) and then the suspension containing the DNA-conjugated microbeads was introduced into the chamber via a syringe pump. A small neodymium iron boron magnet (Cat. # 5848K21, McMaster-Carr Co.) was quickly dragged along the backside of the array to pull the beads into the wells. The suspension was slightly agitated using the syringe pump and then the beads were drawn back towards the surface of the array using the magnet. This process was repeated 3-5 times. The suspension containing any excess beads was then reclaimed and the chamber was washed extensively with the wash buffer. The resist was dissolved by briefly exposing it to a 95% ethanol solution. The ethanol was then removed by rinsing with the wash buffer. For more sensitive biomolecules, the resist can also be removed under milder conditions using a flood exposure followed by a brief wash with a basic buffer solution.

2.3.5 Bright field and fluorescence microscopy

Bright field images were acquired with a 63x/0.7 NA objective on a DM LFSA microscope (Leica Microsystems) equipped with an ORCA-ER CCD camera (Hamamatsu Photonics). Fluorescent images were acquired with an Axiovert 200M epifluorescence microscope (Carl Zeiss). The chamber containing the bead array was placed on a BioPrecision XY microscope stage (Ludl Electronic Products) and illuminated with a Lambda DG-5 light source (Sutter Instrument Co.) using FITC, Cy3, and Cy5 excitation filters and a Pinkel set filter cube (Semrock). The images were acquired with either a 10x/0.45 NA or a 20x/0.80 NA objective (Carl Zeiss) and an iXon Plus 1-megapixel EMCCD camera with 8 x 8 μm^2 pixels (Andor Technology). Background subtraction and image processing was performed with ImageJ.[26]

2.3.6 AFM imaging

The atomic force micrograph was acquired with a Multimode Scanning Probe Microscope and NanoScope IV controller (Digital Instruments, Veeco Metrology Group). The instrument was operated in tapping mode using an AS-12NM scanner and a RTESP probe (Veeco Probes). Height and phase information was recorded using the NanoScope software and image processing and rendering was performed using WSxM.[27]

2.3.7 SEM imaging

Scanning electron micrographs were acquired with a Phillips XL30 Environmental SEM in high vacuum mode at 10 kV. All samples were washed with deionized water, air dried, and then sputter coated with a thin layer of gold or chromium

using a Denton Discovery 18 sputter system or EMITECH K575X sputter tool prior to SEM imaging.

2.4 Results and discussion

Using this procedure, we are able to fabricate wafer-scale high-density arrays of microbeads on glass cover slips. Specifically, we have demonstrated that large arrays of wells with micrometer to sub-micrometer dimensions can be fabricated on derivatized cover glass and that millions of DNA-conjugated superparamagnetic beads can be assembled within these wells in seconds by active manipulation with a magnetic field gradient. Example light micrographs, AFM and SEM images of these arrays are shown in Figure 2.2. A false-colored fluorescence micrograph of a DNA-conjugated microbead array is shown in Figure 2.3.

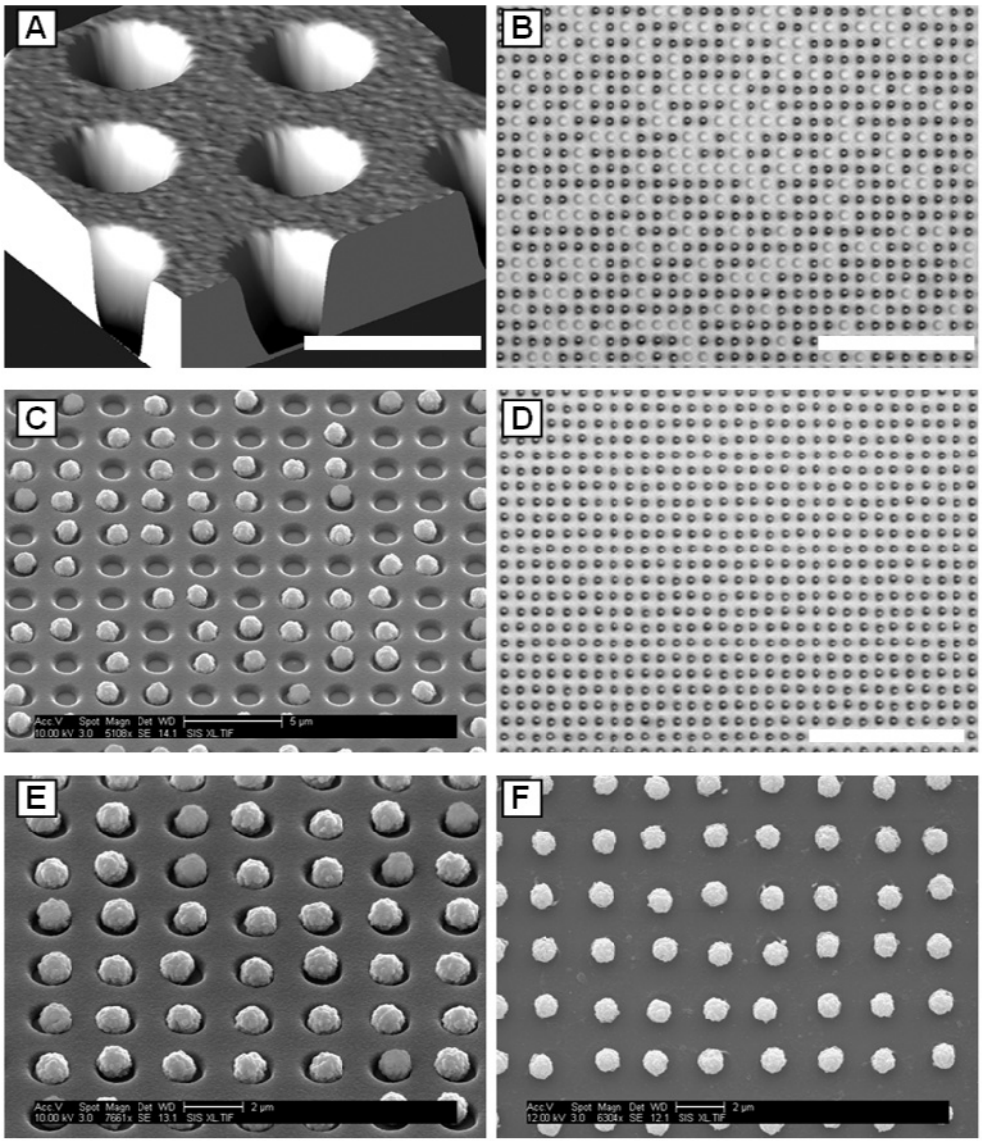

Figure 2.2: High-density array of wells and microbeads.
(A) AFM image of a small section of an array of wells in photoresist on a glass cover slip. (B) Light micrograph and (C) SEM image of a small section of an array of wells partially filled with streptavidin-conjugated superparamagnetic microbeads. We left about half of the wells unfilled for illustrative purposes. (D) Light micrograph and (E) SEM image of a highly ordered array of microbeads in wells in the photoresist. (F) SEM image of an array of microbeads after removal of the photoresist. This array was fabricated on a 50 x 75 x 0.170 mm^3 glass cover slip and contained over 300 million wells. The wells are approximately 500 nm deep, 1.2 μm in diameter and have a center-to-center spacing of 2.4 μm. The beads have an average diameter of 1.05 μm with a maximum coefficient of variation of 3% according to the manufacturer's specifications. The scale bar in the xy-plane in (A) is 2 μm. The vertical dimension in this AFM image is not to scale. The scale bars in (B) and (D) are 24 μm.

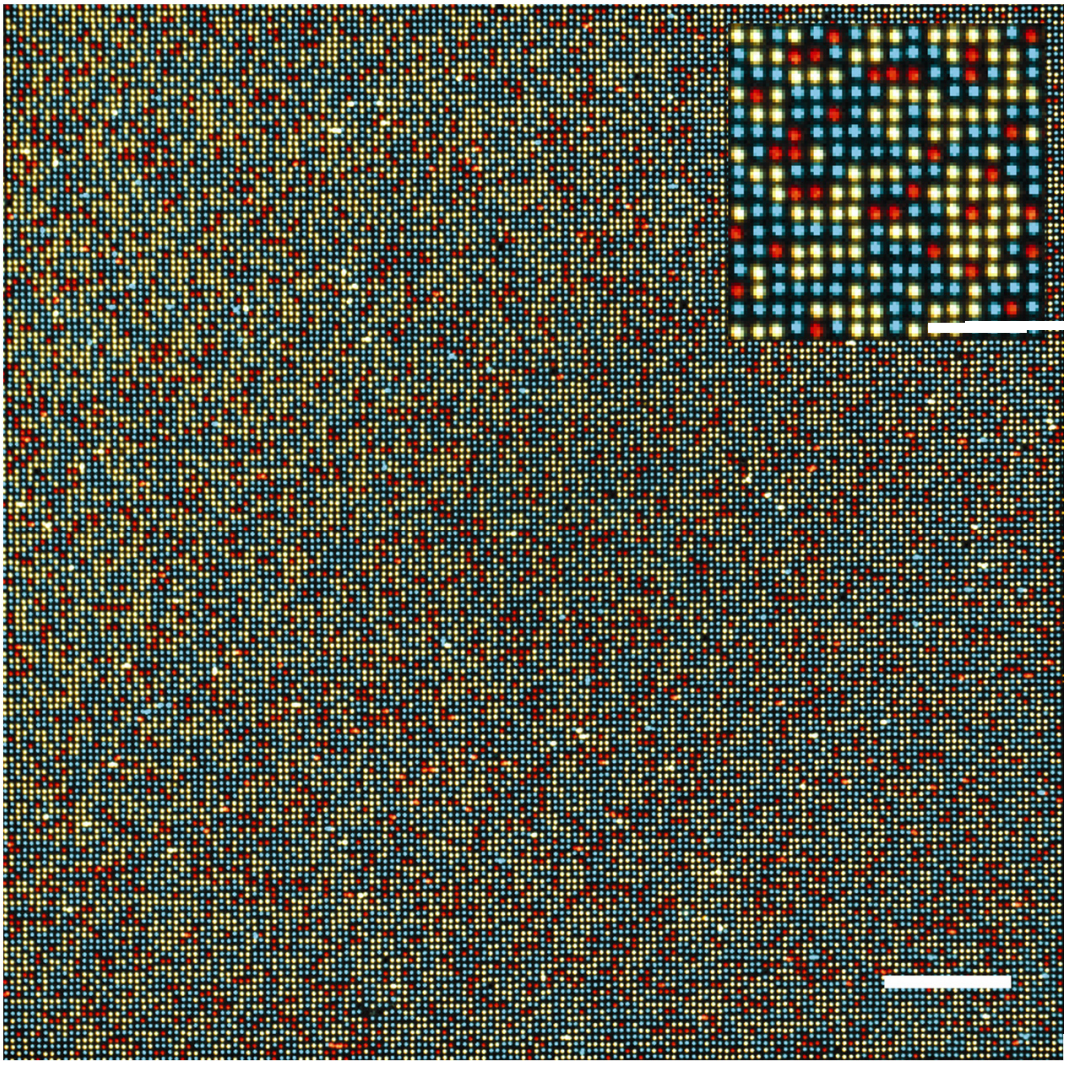

Figure 2.3: Assembly of a highly ordered DNA array.
A false-color composite fluorescence image of a small portion of a microbead array acquired with a 1-megapixel EMCCD camera with 8 x 8 μm^2 pixels through a 20x objective. A magnetic field gradient is applied to facilitate the rapid assembly of a mixture of three populations of 1 μm- superparamagnetic beads conjugated to fluorescent dye-labeled (Fluorescein-Cyan, Cy3-Yellow, and Cy5-Red) DNA molecules. The full image from the camera is shown. The inset is an enlarged image of a region of the array. It is pixelated because only 6 x 6 pixels are used for each feature. The assembly process is conducted within a fluidic chamber and results in greater than 99.9% filling, with only one bead in each well, in seconds. The rare occurrence of misplaced beads (< 0.5%) is very likely due to the presence of aggregates in the stock bead suspension. The center-to-center spacing of these beads is 2.4 μm. The scale bar in the main image is 48 μm. The scale bar in the inset is 12 μm.

Without the use of a magnetic field gradient, we found that the wells were filled very slowly and many of them remain empty despite prolonged incubation periods. This process is even more problematic when using beads with densities near that of water. Dewetting could be used to ensure a higher filling efficiency but it could take hours to days to fill the wells on a large array using this approach because of the slow rate at which the liquid front must move (~1 mm/h to ~1 μm/s)[17, 23]. The application of a magnetic field gradient overcomes this limitation by rapidly concentrating the superparamagnetic beads near the surface of the array and pulling them into the wells. Since the exposure to the magnetic field gradient is very brief and does not require micromagnets or solenoids, the formation of bead aggregates is transient and does not lead to any defects on the array[25]. Real time monitoring of the filling process can be used to determine when the assembly process is complete. Unbound beads can be drawn away from the surface using the magnet, which allows us to observe the surface of the array without having to remove the excess beads from the chamber.

The majority of the wells on a large array can be filled within seconds by quickly dragging an edge of a strong permanent magnet across the bottom of the glass substrate. By repeatedly agitating the suspension and concentrating the beads at the surface using the magnet, greater than 99.9% of the wells can be filled in less than one minute. Achieving this level of filling in such a short period of time requires a suspension containing at least 1.5 x 10^6 beads/μL for an array of wells with a pitch of 2.4 μm in a chamber with a height of 250 μm. This concentration corresponds to approximately twice as many beads as there are wells on this array. The use of lower

concentrations will generally result in an increase in the number of empty wells and the amount of time required to fill the wells. However, even if the bead to well ratio is reduced to one, we have shown that over 95% of the wells can be filled in less than 5 minutes.

Our method also provides an easy way to recycle excess beads and the process can be fully automated. These features may be much more difficult to implement when employing a dewetting[28] or solvent evaporation[20] approach. In addition, the immobilization of the beads onto the surface via biotin-streptavidin binding allows us to conduct various reactions and assays within the flow cell and perform rigorous washing steps without worrying about beads falling out of their wells[29]. Another advantage of using a capture mechanism rather than relying only on van der Waals interactions[18-21] to hold the beads in place is that it permits the removal of the resist after the assembly process is complete. This helps to remove any remaining unbound beads from the surface, reduces background fluorescent generated by the resist and prevents the non-specific binding of other molecules that will eventually be introduced into the flow cell as part of an assay or reaction. These important benefits can still be realized even if biotin-streptavidin chemistry is not suitable for a particular application. In such cases our process could be modified to incorporate other affinity binding modalities or covalent bonds if the surfaces of the beads and the glass substrate are appropriately functionalized, e.g. with alkyne groups on the beads and azide groups on the glass surface using the “click chemistry” strategy[30, 31].

Compared to fiber-optic bead arrays[19, 20], our approach offers more flexibility in terms of the substrates that can be used and the format and size of the arrays that can be produced. For instance, silicon wafers or various plastics could be used instead of glass. In addition, the photolithographic process allows us to modify the geometric parameters relevant to our arrays and gives us the ability to align the beads to virtually any CCD sensor using a standard microscope rather than a fiber optic couple. Many of the beads in our figures are not perfectly aligned with one another because the wells are slightly larger than the beads. The use of oversized wells results in shorter bead assembly times and ensures that beads with larger than average diameters can still be captured. However, the well size can be reduced to match the bead size if an array with more precise alignment is required. We have demonstrated that well diameters can be adjusted to some degree by varying the exposure time, which gives this process greater flexibility in terms of the size of beads than can be used with a given photomask. This benefit is illustrated in Figure 2.4.

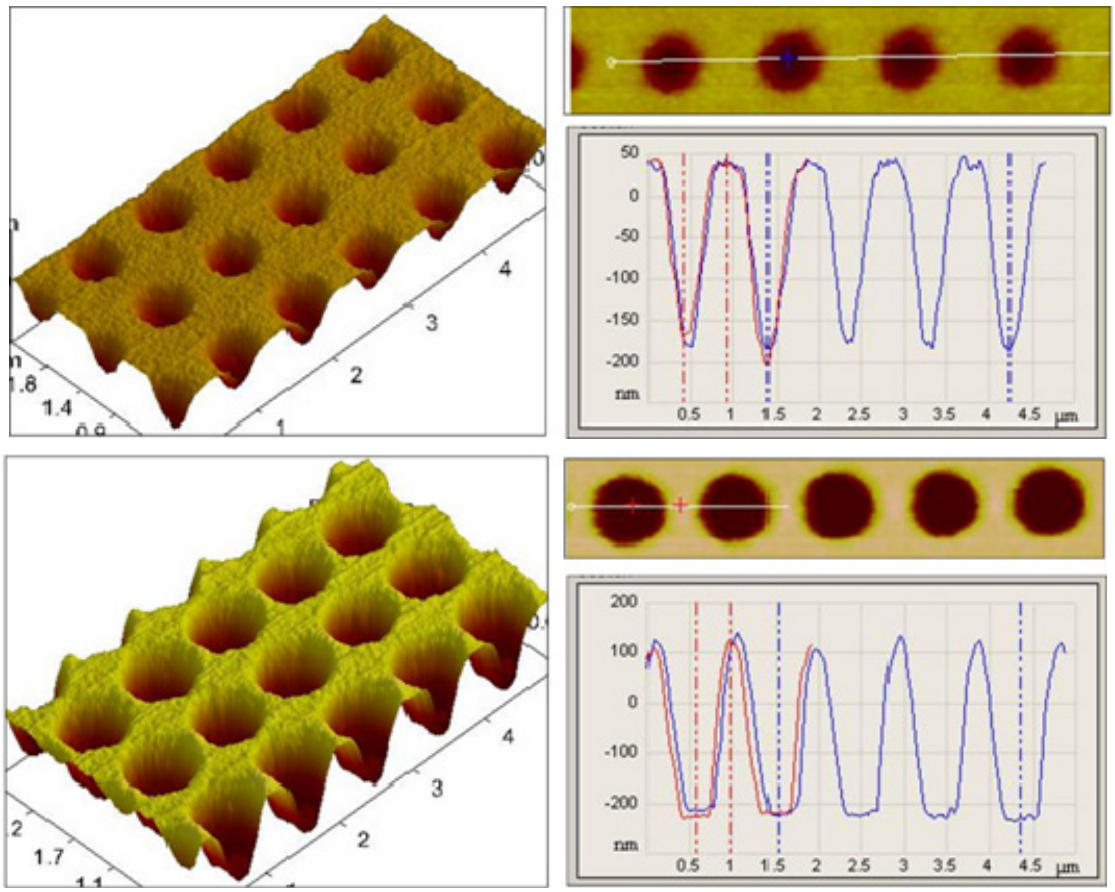

Figure 2.4: Fine dimensional control of the microwell diameter.
AFM images of arrays of wells produced using different exposure dosages but with the same photomask. The center-to-center spacing of the wells remains the same but the dimensions of the wells can be controlled by varying the exposure dosages during photolithographic processing. Shown here are isometric and top views of two arrays of wells generated with two different exposure times. The array on the top was produced using a shorter exposure time.

Not only does our fabrication process result in enhanced packing efficiency, but the usage of these ordered arrays can also improve imaging efficiency and dramatically simplify image processing. The imaging efficiency, in terms of the number of pixels needed to image each feature, is given by $(M*d/p)^2$, where M is the magnification, d is the periodic distance between two adjacent features and p is the pixel size. A feature

refers to a bead and its surrounding space and the equation assumes that the array is properly aligned to the CCD sensor. To achieve optimal alignment, precise adjustments to both the array and CCD are usually required. Translational positioning of the array can be performed using a motorized stage while angle adjustments can be made by rotating the camera. As shown in Figure 2.5, we have demonstrated that it is feasible to use only 3 x 3 pixels on the CCD sensor to image each feature with our current bead arrays and microscope configuration. In this image, the fluorescence from each bead is projected onto a maximum of 2 x 2 pixels and each signal cluster is separated from one another by a single row and column of pixels. At this level of efficiency, more than 10^5 beads can be imaged in a single field of view with our 1-megapixel camera. Profile plots across any 3 rows or columns in this figure reveal a clear distinction between the beads despite single pixel separation between adjacent beads.

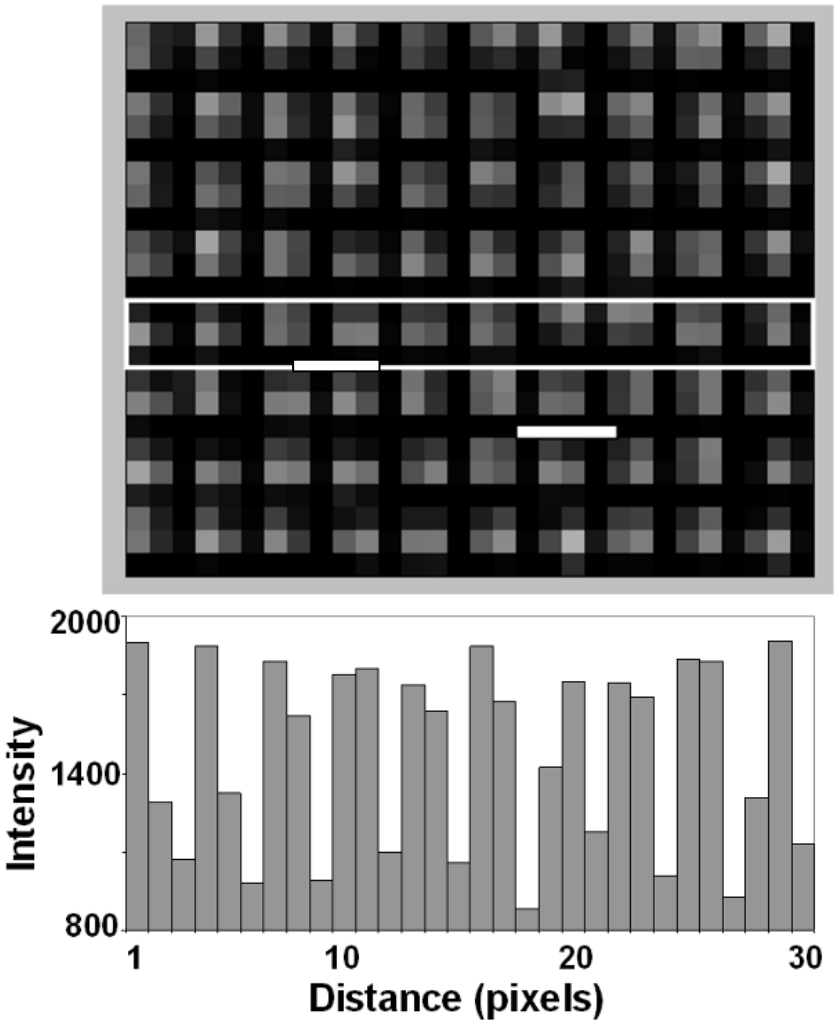

Figure 2.5: Improvement of imaging efficiency and processing.
The upper panel shows a small region of a fluorescent image of an array of 1-μm superparamagnetic beads conjugated to Cy5-labeled DNA probes. A 10x objective was used and an EMCCD with 8 x 8 μm^2 pixels was properly aligned to the array so that each feature can be imaged with 3 x 3 pixels. The lower panel shows the intensity profile of the pixels in the region highlighted by the rectangle. The periodicity of the signal clearly illustrates the separation between neighboring features. The different pixel intensities reflect the slight variation in the projection of the beads relative to the pixels on the CCD sensor. The scale bar is 4.8 μm.

Further improvements to both the imaging and packing efficiencies can be achieved by using smaller beads on an array with a reduced pitch as long as the format of the array matches that of the CCD sensor. For example, 4 pixels per feature could be

achieved if a 10x objective and a CCD camera with 8 x 8 μm^2 pixels are used to image 0.8 μm or smaller beads assembled into 0.8 μm wells that have a center-to-center spacing of 1.6 μm. In this case each bead would fill only one pixel and be separated from each neighboring bead by a single pixel. If we use a CCD camera with a larger pixel size, e.g. 16 x 16 μm^2, the maximum imaging efficiency of 1 pixel per feature could be feasible. However, special features may need to be built into the array to serve as markers for precise alignment of the array to the pixels of the CCD sensor. The maximum packing efficiency that can be achieved depends upon the optics and the wavelength of light being used for imaging. For instance, when using a diffraction-limited objective with a high numerical aperture, e.g. a 40x oil lens with 1.3 NA, and visible light with a wavelength of 500 nm, the theoretical minimum spacing of the features is approximately 230 nm. The efficient production of wafer-scale arrays with features on this scale will require deep UV photolithography or nanoimprint lithography. Our method can be modified slightly to accommodate these fabrication methods by derivatizing the glass surface after the fabrication of the wells to prevent the destruction of the biotin moieties during the imprinting or etching steps[32-34].

With the densities we have shown here, more than 20 million beads can be arrayed in 1 cm^2. We have also demonstrated the ability to fabricate arrays of wells with dimensions as small as 0.8 μm and densities approaching 40 million wells per cm^2 over a large area on a cover glass with the stepper system we used. With the appropriate beads and arrays of wells, many copies of a human genome can be fragmented (e.g. 100-1000 bp), cloned and assembled onto a single glass cover slip. The genomic DNA

clones can be generated by amplification of single DNA molecule on beads by PCR in microemulsions[35]. The usage of these high-density arrays of DNA-conjugated microbeads can significantly increase the throughput and capacity of the emerging genome sequencing technologies[7-9] and other array-based genomic and proteomic assays. In our arrays, there is a minimal amount of space between each bead and overlap is virtually eliminated. These characteristics will also help reduce reagent waste and the need for expensive computer clusters to perform the image analysis and base calling algorithms.

2.5 Conclusions

We have developed a scalable method for fabricating large-scale, high-density arrays of DNA-conjugated superparamagnetic microbeads on glass cover slips. The single-step photolithographic process along with the speed and simplicity of the bead assembly step gives our approach many advantages over existing bead array technologies[15-25]. We have shown that arrays with densities approaching 20 million beads per cm^2 can be produced over an area as large as 12 cm^2 using well established, production-scale manufacturing processes. Our low-defect arrays are free of background caused by non-specifically bound beads and are compatible with automated processes, microfluidics devices and conventional microscopy. The highly ordered arrays, when properly sized and aligned to a given CCD sensor, can also greatly improve imaging efficiency and reduce the complexities of image processing. We have shown that as few as 3 x 3 pixels are required to image each feature. By combining these arrays with the emerging sequencing technologies, the time and cost required to

sequence a human genome could be reduced by at least one order of magnitude. The described method can also be used for fabricating and assembling arrays of other molecules such as antigens, lipids and proteins.

2.6 Acknowledgements

We thank Dr. Brian Thibeault and Bob Hill at the Nanotech Facility at the University of California, Santa Barbara, and Ryan Anderson, Larry Grissom, and Dr. Maribel Montero at the Calit2 Nano3 Facility at the University of California, San Diego for providing advice, training and technical support to K.B. Access to the UCSB Nanotech facility was made possible by the NSF National Nanotechnology Infrastructure Network. This work was supported in part by the NIH/NHGRI (HG003587 and HG004130), and by NSF under a CAREER award to X.H (BES-0547193).

2.7 References

1. Fodor, S.P.A., Read, J.L., Pirrung, M.C., Stryer, L., Lu, A.T. & Solas, D. Light-directed, spatially addressable parallel chemical synthesis. *Science* **251**, 767-773 (1991).

2. Schena, M., Shalon, D., Davis, R.W. & Brown, P.O. Quantitative monitoring of gene expression patterns with a complementary DNA microarray. *Science* **270**, 467-470 (1995).

3. Lockhart, D.J., Dong, H., Byrne, M.C., Follettie, M.T., Gallo, M.V., Chee, M.S., Mittmann, M., Wang, C., Kobayashi, M., Horton, H. *et al.* Expression monitoring by hybridization to high-density oligonucleotide arrays. *Nat. Biotechnol.* **14**, 1675-1680 (1996).

4. Zhu, H., Bilgin, M., Bangham, R., Hall, D., Casamayor, A., Bertone, P., Lan, N., Jansen, R., Bidlingmaier, S., Houfek, T. *et al.* Global analysis of protein activities using proteome chips. *Science* **293**, 2101-2105 (2001).

5. Emrich, C.A., Tian, H., Medintz, I.L. & Mathies, R.A. Microfabricated 384-lane capillary array electrophoresis bioanalyzer for ultrahigh-throughput genetic analysis. *Anal. Chem.* **74**, 5076-5083 (2002).

6. Margulies, M., Egholm, M., Altman, W.E., Attiya, S., Bader, J.S., Bemben, L.A., Berka, J., Braverman, M.S., Chen, Y.J., Chen, Z. *et al.* Genome sequencing in microfabricated high-density picolitre reactors. *Nature* **437**, 376-380 (2005).

7. Shendure, J., Porreca, G.J., Reppas, N.B., Lin, X., McCutcheon, J.P., Rosenbaum, A.M., Wang, M.D., Zhang, K., Mitra, R.D. & Church, G.M. Accurate multiplex polony sequencing of an evolved bacterial genome. *Science* **309**, 1728-1732 (2005).

8. Bentley, D.R. Whole-genome re-sequencing. *Curr. Opin. Genet. Dev.* **16**, 545-552 (2006).

9. Church, G.M. Genomes for all. *Sci. Am.* **294**, 46-54 (2006).

10. Johnson, D.S., Mortazavi, A., Myers, R.M. & Wold, B. Genome-wide mapping of in vivo protein-DNA interactions. *Science* **316**, 1497-1502 (2007).

11. Thibault, C., Berre, V.L., Casimirius, S., Trévisiol, E., François, J. & Vieu, C. Direct microcontact printing of oligonucleotides for biochip applications. *J. Nanobiotech.* **3**, 1-12 (2005).

12. Pla-Roca, M., Fernandez, J.G., Mills, C.A., Martinez, E. & Samitier, J. Micro/nanopatterning of proteins via contact printing using high aspect ratio pmma stamps and nanoimprint apparatus. *Langmuir* **23**, 8614-8618 (2007).

13. Tan, H., Huang, S. & Yang, K.L. Transferring complementary target DNA from aqueous solutions onto solid surfaces by using affinity microcontact printing. *Langmuir* **23**, 8607-8613 (2007).

14. Nam, J.-M., Han, S.W., Lee, K.-B., Liu, X., Rathner, M.A. & Mirkin, C.A. Bioactive protein nanoarrays on nickel oxide surfaces formed by dip-pen nanolithography. *Angew. Chem. Int. Ed.* **43**, 1246-1249 (2004).

15. Xia, Y., Yin, Y., Lu, Y. & McLellan, J. Template-assisted self-assembly of spherical colloids into complex and controllable structures. *Adv. Funct. Mater.* **13**, 907-918 (2003).

16. Michel, R., Reviakine, I., Sutherland, D., Fokas, C., Csucs, G., Danuser, G., Spencer, N.D. & Textor, M. A novel approach to produce biologically relevant chemical patterns at the nanometer scale: Selective molecular assembly

patterning combined with colloidal lithography. *Langmuir* **18**, 8580-8586 (2002).

17. Cui, Y., Bjork, M.T., Liddle, J.A., Sonnichsen, C., Boussert, B. & Alivisatos, A.P. Integration of colloidal nanocrystals into lithographically patterned devices. *Nano Lett.* **4**, 1093-1098 (2004).

18. Steemers, F.J. & Gunderson, K.L. Whole genome genotyping technologies on the beadarray platform. *Biotechnol. J.* **2**, 41-49 (2007).

19. Michael, K.L., Taylor, L.C., Schultz, S.L. & Walt, D.R. Randomly ordered addressable high-density optical sensor arrays. *Anal. Chem.* **70**, 1242-1248 (1998).

20. Ferguson, J.A., Steemers, F.J. & Walt, D.R. High-density fiber-optic DNA random microsphere array. *Anal. Chem.* **72**, 5618-5624 (2000).

21. Yin, Y., Lu, Y., Gates, B. & Xia, Y. Template-assisted self-assembly: A practical route to complex aggregates of monodispersed colloids with well-defined sizes, shapes, and structures. *J. Am. Chem. Soc.* **123**, 8718-8729 (2001).

22. Li, A.X., Seul, M., Cicciarelli, J., Yang, J.C. & Iwaki, Y. Multiplexed analysis of polymorphisms in the hla gene complex using bead array chips. *Tissue Antigens* **63**, 518-528 (2004).

23. Wen, W., Wang, N., Zheng, D.W., Chen, C. & Tu, K.N. Two- and three-dimensional arrays of magnetic microspheres. *J. Mater. Res.* **14** (1999).

24. Roberts, L.A., Crawford, A.M., Zappe, S., Jain, M. & White, R.L. Patterned magnetic bar array for high-throughput DNA detection. *IEEE Trans. Magnet.* **40**, 3006-3008 (2004).

25. Yellen, B.B. & Friedman, G. Programmable assembly of colloidal particles using magnetic microwell templates. *Langmuir* **20**, 2553-2559 (2004).

26. Abramoff, M.D., Magelhaes, P.J., Ram, S.J. Image processing with imagej. *Biophotonics Intl.* **11**, 36-42 (2004).

27. Horcas, I., Fernandez, R., Gomez-Rodriguez, J.M., Colchero, J., Gomez-Herrero, J. & Baro, A.M. Wsxm: A software for scanning probe microscopy and a tool for nanotechnology. *Rev. Sci. Instrum.* **78**, 013705 (2007).

28. Yin, Y., Lu, Y. & Xia, Y. A self-assembly approach to the formation of asymmetric dimers from monodispersed spherical colloids. *J. Am. Chem. Soc.* **123**, 771-772 (2001).

29. Gunderson, K.L., Kruglyak, S., Graige, M.S., Garcia, F., Kermani, B.G., Zhao, C., Che, D., Dickinson, T., Wickham, E., Bierle, J. *et al.* Decoding randomly ordered DNA arrays. *Genome Res.* **14**, 870-877 (2004).

30. Wu, P., Feldman, A.K., Nugent, A.K., Hawker, C.J., Scheel, A., Voit, B., Pyun, J., Frechet, J.M., Sharpless, K.B. & Fokin, V.V. Efficiency and fidelity in a click-chemistry route to triazole dendrimers by the copper(i)-catalyzed ligation of azides and alkynes. *Angew. Chem. Int. Ed. Engl.* **43**, 3928-3932 (2004).

31. Rozkiewicz, D.I., Gierlich, J., Burley, G.A., Gutsmiedl, K., Carell, T., Ravoo, B.J. & Reinhoudt, D.N. Transfer printing of DNA by "Click" Chemistry. *Chembiochem.*, DOI: 10.1002/cbic.200700402 (2007).

32. Hoff, J.D., Cheng, L.J., Meyhofer, E., Guo, L.J. & Hunt, A.J. Nanoscale protein patterning by imprint lithography. *Nano Lett.* **4**, 853-857 (2004).

33. Gao, H., Tan, H., Zhang, W., Morton, K. & Chou, S.Y. Air cushion press for excellent uniformity, high yield, and fast nanoimprint across a 100 mm field. *Nano Lett.* **6**, 2438-2441 (2006).

34. Truskett, V.N. & Watts, M.P. Trends in imprint lithography for biological applications. *Trends Biotechnol.* **24**, 312-317 (2006).

35. Dressman, D., Yan, H., Traverso, G., Kinzler, K.W. & Vogelstein, B. Transforming single DNA molecules into fluorescent magnetic particles for detection and enumeration of genetic variations. *Proc. Natl. Acad. Sci. U. S. A.* **100**, 8817-8822 (2003).

This chapter, in part, is a reproduction of the material as it appears in: Barbee, K.D.; Huang, X., *Analytical Chemistry* **2008** 80 (6);: 2149 - 2154, 2008; copyright 2008 American Chemical Society. Used with permission. The dissertation author was the primary investigator and author of this paper.

3 Electric field directed assembly of high-density microbead arrays

3.1 Abstract

We report a method for rapid, electric field directed assembly of high-density protein-conjugated microbead arrays. Photolithography is used to fabricate an array of micron to sub-micron-scale wells in an epoxy-based photoresist on a silicon wafer coated with a thin gold film, which serves as the primary electrode. A thin gasket is used to form a microfluidic chamber between the wafer and a glass coverslip coated with indium-tin oxide, which serves as the counter electrode. Streptavidin-conjugated microbeads suspended in a low conductance buffer are introduced into the chamber and directed into the wells via electrophoresis by applying a series of low voltage electrical pulses across the electrodes. Hundreds of millions of microbeads can be permanently

assembled on these arrays in as little as 30 seconds and the process can be monitored in real time using epifluorescence microscopy. The binding of the microbeads to the gold film is robust and occurs through electrochemically induced gold-protein interactions, which allows excess beads to be washed away or recycled. The well and bead sizes are chosen such that only one bead can be captured in each well. Filling efficiencies greater than 99.9% have been demonstrated across wafer-scale arrays with densities as high as 69 million beads per cm^2. Potential applications for this technology include the assembly of DNA arrays for high-throughput genome sequencing and antibody arrays for proteomic studies. Following array assembly, this device may also be used to enhance the concentration-dependent processes of various assays through the accelerated transport of molecules using electric fields.

3.2 Introduction

Microbead-based platforms have become a popular technology for many high-throughput biological assays such as genotyping[1], DNA sequencing[2], and protein detection[3] due to the ease in which they enable multiplexing and miniaturization. Microbeads have been captured or assembled onto various surfaces via evaporation[4-6], gravity[7], centrifugation[8], and magnetic[9, 10] and electric fields[11-18]. While all these methods have been successfully utilized, each has some limitations. For instance, controlled evaporation, or dewetting, can take hours to assemble large arrays on microfabricated templates[5]. In addition, achieving sufficient filling efficiencies with sub-micron particles may require multiple aliquots and highly concentrated microbead suspensions[19]. Gravity-dependent assembly methods can also be relatively slow and

often result in lower packing efficiencies[7]. Centrifugation-based approaches face similar issues and cannot be easily automated[8]. We recently reported a method for the rapid assembly of superparamagnetic microbeads into arrays with near perfect order using a magnetic field[10]. However, it may be difficult to scale due to the limited availability of uniform and monodisperse sub-micron magnetic beads as shown in Figure 3.1.

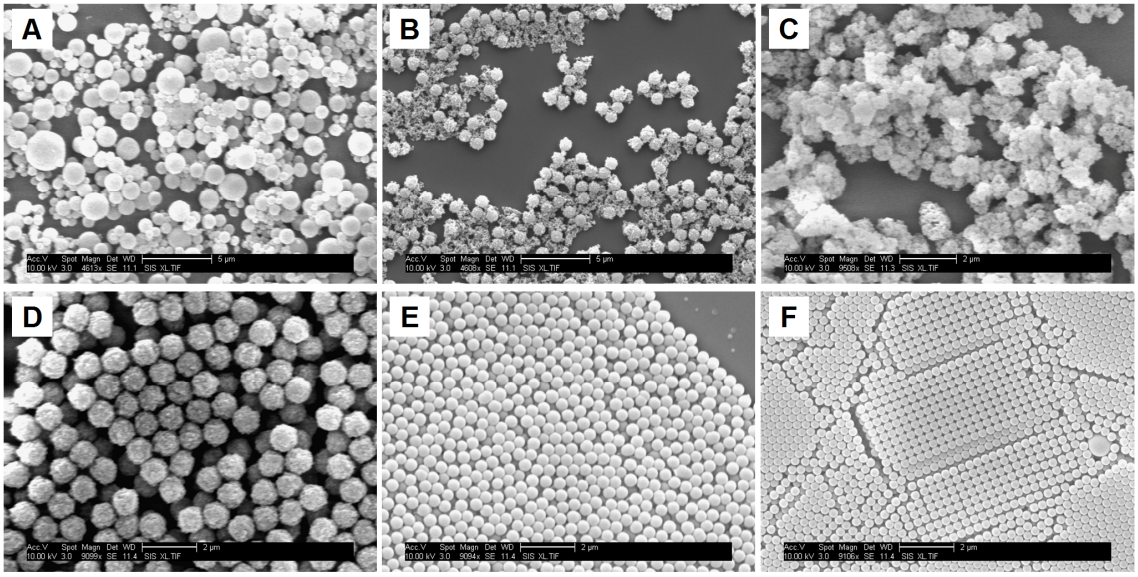

Figure 3.1: Uniformity and monodispersity of sub-micron beads.
Many commercially available magnetic microbeads suffer from a high degree of polydispersity (A), nanoparticle contamination (B) or irregular and non-uniform shapes (C). The magnetic microbeads in (D) are of much higher quality in terms of uniformity and monodispersity but they are not available with sub-micron diameters. Polystyrene (E) and silica (F) microbeads have excellent uniformity and monodispersity. They are also commercially available in many sizes well below 1 μm.

Methods employing electric field directed assembly on microfabricated templates offer certain advantages in that they can be fast, automatable, scalable, and used to assemble non-magnetic particles. These types of platforms also have the potential to accelerate via an electric field various diffusion-limited processes such as DNA hybridization[20] and antibody-antigen binding[21]. Many of the reported electric-

field-based methods are often used to direct the assembly of microbeads or nanoparticles into colloidal crystals or clusters with little control over their number, order or position. A few others have demonstrated more control over microbead position and order[14-16]. However, their methods might be difficult to scale or they may not be compatible with microfluidics, biological assays and real-time bright-field and epifluorescence microscopy.

We have developed a device and process that utilizes an electric field to direct the assembly of high-density arrays of protein-conjugated microbeads in a rapid, automatable and scalable fashion. Our method, unlike those previously reported, can be used to assemble wafer-scale arrays of individual microbeads with near perfect order. The microfabrication process and the fluidic device are illustrated in Figure 3.2. A high-density array of wells in an epoxy-based photoresist is fabricated on a silicon wafer coated with a gold film that serves as the primary electrode (Figure 3.2A). The counter electrode consists of a glass coverslip coated with indium-tin oxide (ITO), which serves as the counter electrode. A flow cell is formed by sandwiching a thin adhesive silicone gasket that contains a cut-out of a flow channel between the wafer and the coverslip (Figure 3.2B).

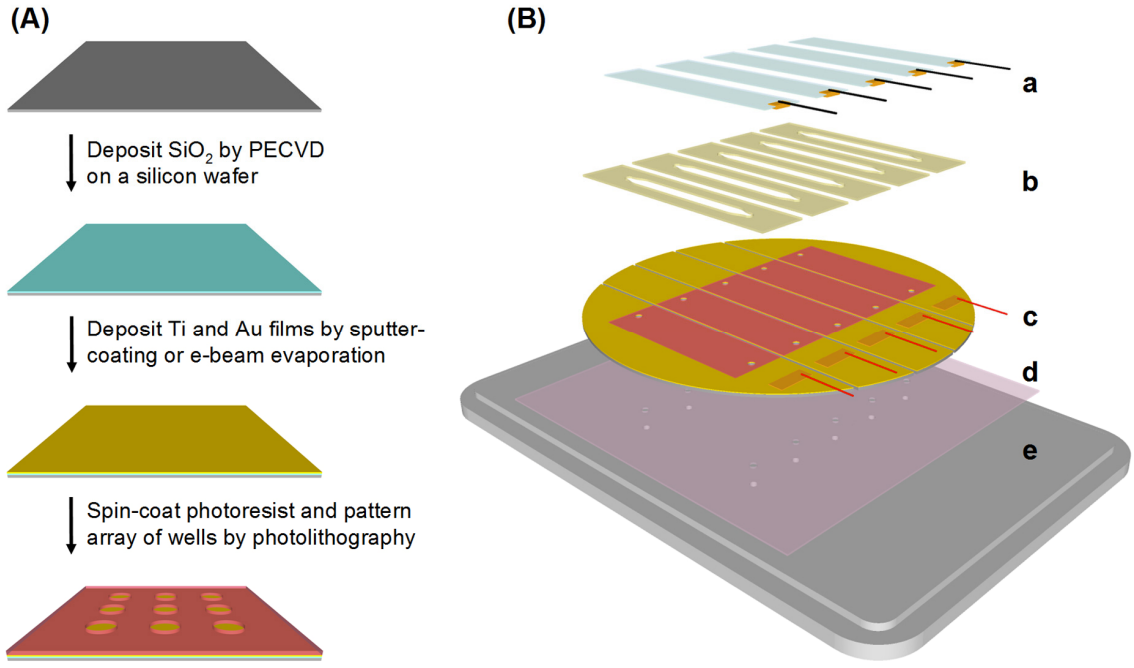

Figure 3.2: Device fabrication and assembly.
(A) Fabrication of an array of microwells on a silicon wafer. (B) Exploded view of the device. a: ITO-coated glass coverslip; b: silicone gaskets with flow channels; c: silicon wafer with a high-density array of wells in photoresist on a thin layer of gold; d: double-coated adhesive gasket to couple the wafer to the stage insert; and e: microscope stage insert with fluidic ports.

As illustrated in Figure 3.3, a series of low voltage electrical pulses is applied to the electrodes. The negatively charged, streptavidin-coated microbeads are directed into the wells by electrophoresis. The microbeads are permanently captured within the wells through electrochemically-induced binding between the gold and streptavidin. Using this approach, we have demonstrated that hundreds of millions of 0.5 μm and 1 μm microbeads can be captured in a rapid, efficient and ordered manner. The diameter of the wells in the photolithographically-defined templates can be easily adjusted to the desired bead size, ensuring that each well can accommodate only one microbead. This spatial control supports higher imaging efficiencies for demanding applications such as

genome sequencing by reducing the total number of pixels required to image each microbead[10, 22]. Our assembly method is also simple and practical in that it utilizes low frequency, direct current (DC) pulses applied across a flow cell that is suitable for biological assays using epifluorescence microscopy.

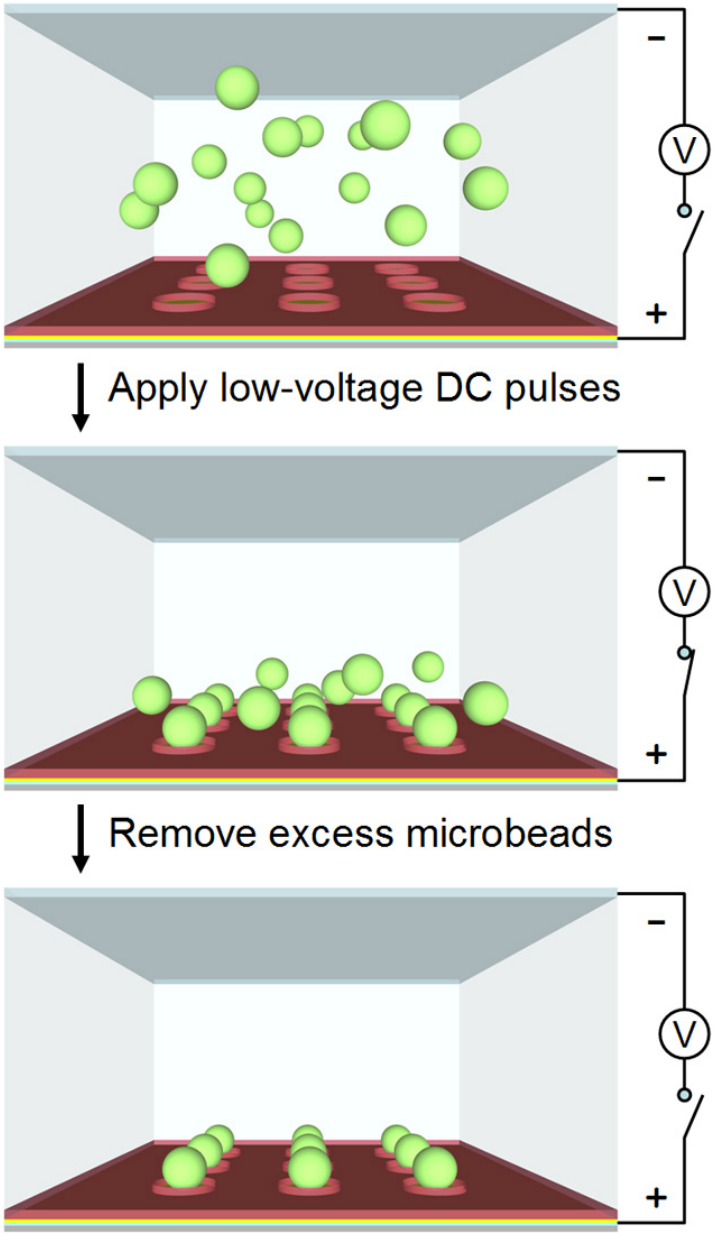

Figure 3.3: Electric field directed assembly of microbead arrays.
A cross-sectional view of a small portion of the flow cell is illustrated. By applying a series of low-voltage electrical pulses, the protein-conjugated microbeads are directed into the wells via electrophoresis and captured onto the gold surface through electrochemically-induced interactions between the gold and proteins. The counter electrode consists of an ITO-coated glass coverslip. The flow cell is formed between the glass coverslip and the patterned wafer using a thin, double-coated silicone tape. Drawings are not to scale.

3.3 Materials and methods

3.3.1 Device fabrication

The general procedure for fabricating an array of wells on a silicon wafer coated with a thin oxide layer and metal films is illustrated in Figure 3.2A. The silicon wafers (100 mm) were cleaned in a 3:1 mixture of 98% H_2SO_4: 30% H_2O_2 at 85 °C for 15 min and then rinsed extensively with deionized water (dH_2O). (CAUTION: H_2SO_4-H_2O_2 mixtures are extremely dangerous and should be handled with care.) The wafers were then dipped in a buffered oxide etch (6:1 of 40% NH_4F: 49% HF) for 30 s and rinsed with dH_2O. (CAUTION: HF is extremely dangerous and should be handled with care). The wafers were blown dry with nitrogen and coated with a 200-300 nm layer of silicon dioxide using a plasma-enhanced chemical vapor deposition (PECVD) system (Plasmalab, Oxford Instruments). Oxide deposition was conducted at 350 °C and 20 W RF using 710 sccm N_2O and 170 sccm SiH_4 at 1 Torr.

Titanium and gold films were deposited on the oxide-coated wafers using a Discovery 18 sputter system (Denton Vacuum) or VES2550 electron-beam evaporation system (Temescal). The deposition chambers were typically evacuated to a base pressure of 9×10^{-7} Torr or less. Sputtered-coated titanium and gold films were deposited at 200 W DC in Ar at 3.0×10^{-3} Torr and 36 sccm. Evaporated Ti and Au films were deposited at 0.1-0.2 nm s^{-1}. The titanium layer, which serves as an adhesion layer between the oxide and the gold films, was approximately 30 nm thick. Gold film thicknesses ranged from 300-400 nm.

Following metallization, SU-8 2000.5, an epoxy-based, negative-tone photoresist (Microchem), was applied directly to the gold film by spin-coating at 2000 rpm for 30 s. After baking on a hotplate at 95 °C for 1 min, the wafer was patterned via i-line photolithography using a chrome on quartz photomask on a GCA Autostep 200 stepper system equipped with an Olympus 2145/0.45 NA reduction lens. With an intensity of ~475 mW cm^{-2}, typical exposure times ranged from 0.29 s for ~0.6 μm features up to 0.415 s for ~1.2 μm features. The exposed wafers were baked at 95 °C for 1 min, developed for 2 min in SU-8 developer (Microchem Corp.), then rinsed with isopropyl alcohol and dried with nitrogen. The thickness of the SU-8 layer is estimated to be about 200 nm.

3.3.2 ITO deposition on glass coverslips

Using a custom-built PTFE rack, 50 × 75 × 0.170 mm^3 glass coverslips (Erie Scientific) were washed in batch mode in a 2% solution of Micro-90 detergent (Cole-Parmer) and rinsed extensively with dH_2O. The coverslips were soaked in acetone and then methanol with sonication for at least 30 min each. The coverslips were further cleaned in a 1:1:5 mixture of 30% H_2O_2:30% NH_4OH:H_2O at 85 °C for 1 hour and then in a 3:1 mixture of 98% H_2SO_4: 30% H_2O_2 at 85 °C for 1 hour. The coverslips were rinsed extensively in dH_2O and dried in an oven at 110 °C for 30 min.

The ITO films were deposited on the coverslips using an ATC Orion 8 Sputter System (AJA International). The deposition chamber was evacuated to a base pressure of 5×10^{-7} Torr or less and the substrates were heated to 325 °C.

Sputtering was performed at 325 W RF and 2×10^{-3} Torr for 10 min with argon and oxygen flow rates of 20 and 0.1 sccm, respectively. The ITO films were characterized using a FPP-100 four-point probe system (Veeco) and a Lambda 20 UV-Vis spectrometer (Perkin Elmer). Typical values for the sheet resistance were 12-15 Ω. Typical values for the optical transmittance were 90-95% over a range of 450-800 nm as shown in Figure 3.4. Prior to device assembly, the coverslips were diced into 8-10 mm x 50 mm strips using a diamond scribing tool.

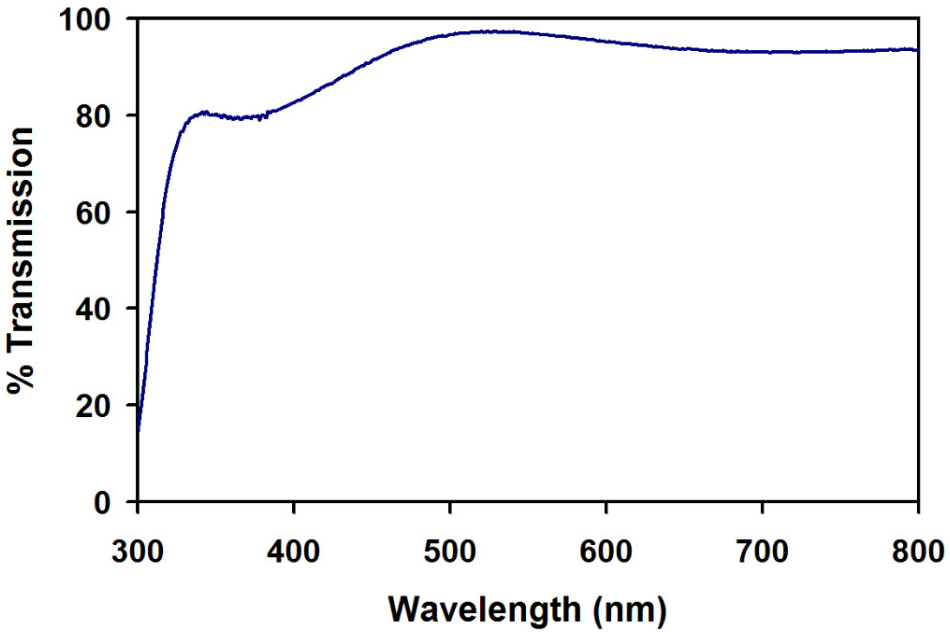

Figure 3.4: ITO transmission curve.
Light transmission through an ITO-coated glass coverslip as measured by a UV-Vis spectrometer.

3.3.3 Device assembly

After completion of the fabrication process, the wafers were covered with a protective layer of Shipley Megaposit SPR220-7.0 photoresist (Rohm and Haas) by spin-coating at 2000 rpm for 30 s and then baked on a hotplate at 115 °C for 5 min.

Holes were drilled through the wafer in an automated fashion using a 1.0 mm diamond-coated drill bit (C. R. Laurence Co.) and a high-speed rotary tool mounted to a computer numerical control milling machine (PCNC 1100, Tormach). The wafers were then diced by hand into 12 mm-wide pieces using a scribing tool and the resist was stripped by soaking in acetone for 2 min. Each die was then rinsed with isopropyl alcohol and dried with nitrogen. Prior to use, the dice were further cleaned in a Technics PEII-B plasma system at 100W and 3.00×10^{-1} Torr O_2 for 3 min and then rinsed with dH_2O. After drying with nitrogen, the dice were fixed via double-coated acrylic tape (DC-UHB10FA-C, J. V. Converting Co.) to a custom-built aluminum plate, which contains ports for fluidic connections and fits securely within the aperture of our microscope stage (Figure 3.2B).

The channels that form the flow cells within the device were designed in a computer-aided design program and cut out of a ~110 μm-thick, double-coated silicone tape (No. 702, Scapa Group) using a cutting plotter (CC200-20, Graphtec Corp.). Typical channel dimensions ranged from 2-6 mm in width by 26-32 mm in length. The tape containing the channel cut-out was then aligned and fixed to the wafer. Narrow strips of copper tape ~30 μm thick (Cat. No. 77802, Electron Microscopy Sciences) were attached to both ends of the counter electrode and then wrapped around the ends and onto the backside of the coverslip. The coverslip was then attached to the wafer with the silicone tape to create the fluidic chamber. Electrical connections to both the gold film and the copper tape on the coverslip were made by additional pieces of copper tape, each soldered to an insulated copper

wire. An exploded view of the complete device is shown in Figure 3.2B.

3.3.4 Electric field directed assembly of microbead arrays

Streptavidin-coated, fluorescent polystyrene microbeads with diameters of 0.5 μm and 1 μm (CPO1F/7066 and CP01F/7677, Bangs Laboratories) were diluted to 0.1%-0.2% solids in a low conductance buffer (4.5 mM tris(hydroxymethyl) aminomethane, 4.5 mM boric acid, and 0.02% Triton X-100, pH 8.6, with a conductance of 61 μS cm^{-1}) (LCB). The microbead suspensions were washed 3 times with LCB. Prior to each buffer exchange, the suspensions were centrifuged for 6 min at 3000 g and then resuspended by vortexing for ~30 sec. Suspensions were sonicated by placing them in an ultrasonic water bath for 5-10 min immediately prior to use.

The chambers were connected to a syringe pump (Cavro XR Rocket, Tecan Group) using 1/16″ OD × 0.03″ ID Teflon tubing, ¼-28 Upchurch (Idex Corp.) and 062 MINSTAC fittings (The Lee Co.) and washed with LCB. The microbead suspensions were introduced and the total circuit resistance was measured with a digital multimeter (2010, Keithley Instruments). Typical values ranged from ~100-200 kΩ. A function generator (33220A, Agilent Technologies) was used to apply a series of 1 Hz, 3.0 V DC pulses with a 10% duty cycle for 30-60 s either continuously or in 10-15 s intervals with 2 min periods between each interval. The electrical waveforms were monitored using an oscilloscope (TDS 224B, Tektronix). Following the assembly process, excess microbeads were washed away with LCB at a flow rate of 16-40 μL s^{-1} . An illustration of the assembly process is shown in

Figure 3.3.

3.3.5 Fluorescence imaging

Real-time imaging of the assembly process was performed on an epifluorescence microscope (DM LFSA, Leica Microsystems) with a 40x/0.55 NA objective, and a CCD camera (ORCA-ER, 1024 × 1344, 6.45 x 6.45 μm^2 pixels, Hamamatsu Photonics). Excitation light was from an Osram 100W HBO mercury arc lamp. The images and movies were recorded with SimplePCI software (Hamamatsu Photonics). Image analysis and background subtraction was performed with Image J[23].

3.3.6 SEM imaging

To disassemble the chamber and release the substrate for SEM imaging, the entire device was submersed in liquid nitrogen. The low temperature simplified the release of the wafer from the aluminum plate and the coverslip from the wafer. The diced samples were then coated for 30 s with chromium or iridium at 130 mA in Ar using a K575X sputter tool (Emitech). The images were obtained with a Phillips XL30 environmental SEM operating at 10 kV in high-vacuum mode. The aluminum plate is prepared for further use by soaking it in acetone, which aids in the removal of the acrylic tape.

3.4 Results and discussion

3.4.1 Rapid assembly of microbead arrays

We have demonstrated the ability to rapidly assemble high-density arrays of protein-conjugated microbeads on photolithographically-defined templates using an

electric field. Standard thin film deposition and photolithography techniques are used in the fabrication process. The microbead assembly process utilizes a function generator to deliver 3.0 V DC pulses at a frequency of 1 Hz and a duty cycle of 10%. Figures 3.5A and 3.5B shows the fluorescence and SEM images of a typical array of 1 μm beads assembled into ~1 μm wells at a pitch of 2.4 μm. As can be seen, arrays with near perfect order can be assembled with filling efficiencies as high as 99.9%. Using this approach, we have also demonstrated the ability to assemble 1 μm (Figure 3.5C) and 0.5 μm beads (Figure 3.5D) on arrays with densities approaching 69 million microbeads per cm^2.

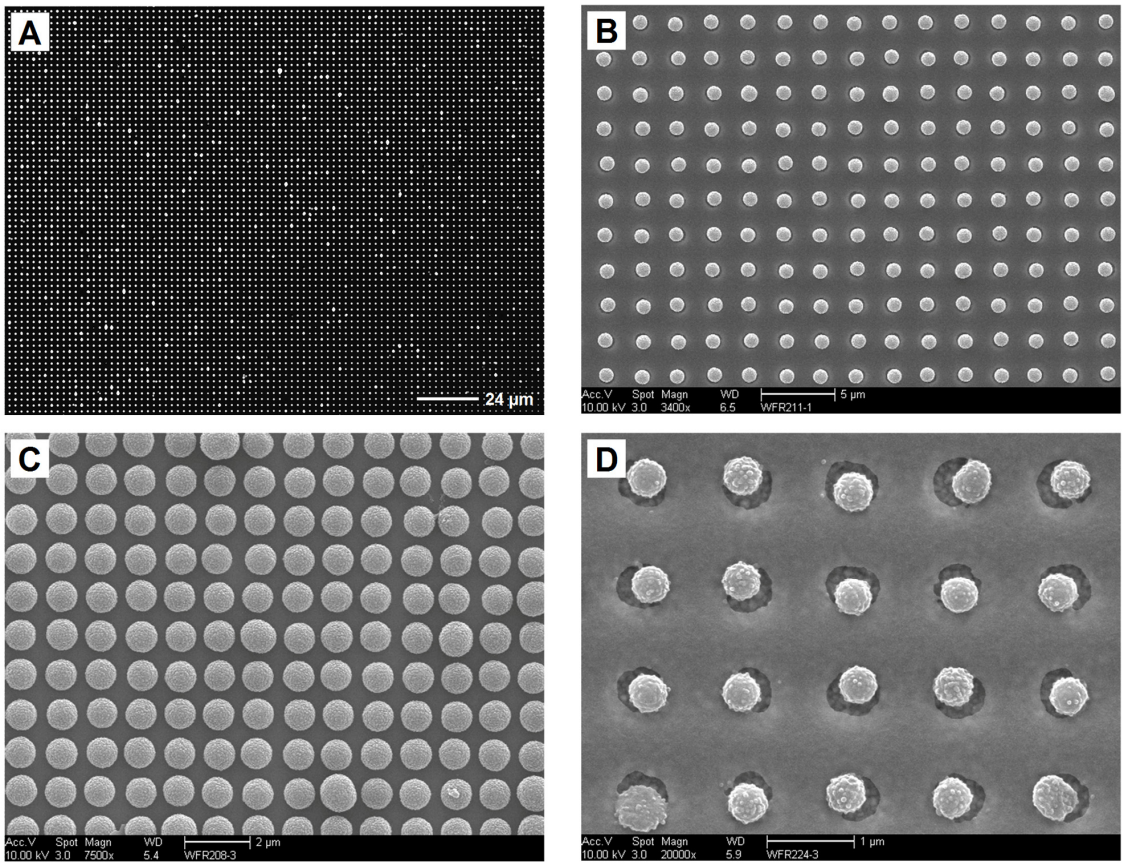

Figure 3.5: High-density microbead arrays assembled using an electric field. (A) Fluorescence micrograph and (B) SEM image of small portions from the same assembled array of 1 µm streptavidin-conjugated polystyrene microbeads at a 2.4 µm pitch. This full-frame fluorescence micrograph was acquired with a 40x/0.55 NA objective and a Hamamatsu ORCA-ER CCD camera. (C). SEM image of a small portion of an array of 1 µm beads assembled into ~0.8 µm wells at a pitch of 1.2 µm. (D). SEM image of a small portion of an array of ~0.5 µm beads assembled into ~0.6 µm wells at a pitch of 1.2 µm.

Defect rates in the assembled arrays are typically less than a few percent. Common defects include unfilled wells and microbead doublets (Figure 3.5A). For example, in Figure 3.5A only 5 wells remain unfilled, which corresponds to a filling efficiency of 99.9%. The variation in fluorescence intensity observed in Figure 3.5A is due to the presence of doublets as well as considerable differences in microbead

size as seen in Figure 3.6B. There are approximately 0.2% wells containing smaller, less visible microbeads and 1.5% wells containing brighter doublets or abnormally large microbeads. We found that some doublets and larger aggregates were often present in the stock and LCB microbead suspensions. Therefore, the doublets observed in the arrays may not be caused by the assembly process.

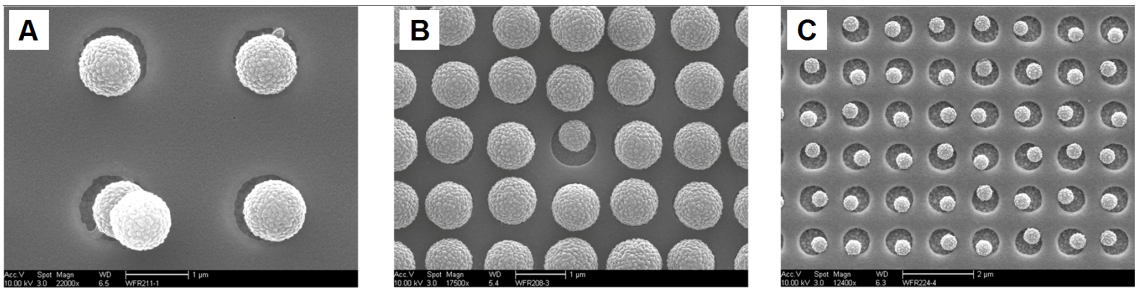

Figure 3.6: Microbead doublets, size variation and alignment.
(A) An SEM image with a microbead doublet in one well. (B) An SEM image showing the size variation among the 1 µm beads. (C) An SEM image of 0.5 µm beads assembled into over-sized wells. The microbead positioning and well occupancy rates may be compromised if the wells are significantly larger than the microbeads.

3.4.2 Materials considerations

Gold was chosen for the electrode upon which the microbeads were assembled primarily due to its affinity towards proteins. As described elsewhere, proteins can be adsorbed directly onto gold surfaces, with[24] or without[25] the use of an electric field. By exploiting this phenomenon, we are able to capture permanently streptavidin-coated microbeads onto the gold electrodes without any surface modifications. The binding of the microbeads is sufficient to withstand both stringent washes and the application of a reverse bias of 1.5 V DC. It is even more astounding that the assembled arrays are able to survive the liquid nitrogen treatment and the SEM imaging process. The use of

platinum and ITO for the primary electrode was also investigated. However, we found that the microbeads were less likely to bind to these materials under our assembly conditions.

The choice of materials used for the counter electrodes is subject to other design constraints, with an emphasis on imaging. ITO-coated coverslips were used as counter electrodes to provide a suitable window through which optical imaging of the arrays can be performed. However, ITO films are not very robust and can be damaged easily. Therefore, it is imperative that the assembly conditions are compatible with this material. By using a low conductance buffer and minimizing the strength and duration of the electrical pulses, no obvious damage was found to occur to the ITO films.

The material used to fabricate the arrays of wells needs to meet several criteria. It must be a robust dielectric with good adhesion to gold, compatible with sub-micron photolithography and able to withstand the potentially damaging by-products of electrolysis. Positive resists such as Shipley S1805 were initially used to simplify the fabrication process. Although suitable as dielectrics, these materials were prone to delamination after prolonged exposure to the assembly conditions. In contrast, the epoxy-based negative photoresist, SU-8 2000.5, was able to withstand electrophoretic conditions well beyond those required for assembly. SU-8 2000.5 is also suitable for sub-micron photolithography, albeit with some minor defects that can be attributed to the resolution limit of the stepper system. Despite the apparent advantages of SU-8, compatibility issues may arise if this device is to be used as a

platform for biological assays. In such cases, silicon dioxide or silicon nitride films may be employed. However, the use of such materials will require a more involved fabrication process.

Flow cells were created using a thin, double-coated silicone tape. Using a cutting plotter, this material can be quickly cut into various shapes and sizes. This allows channels to be created much more easily than through conventional microfabrication processes. The tape backing is made of polyester and the adhesive is silicone-based. This makes it suitable as an electrical insulator and stable in aqueous environments. Since the tape is only 110 μm thick, high field strengths can be achieved within the device at relatively low voltages. The shallow chamber height also enables the use of microscope objectives with high numerical apertures, which tend to have relatively short working distances.

The buffer system, tris(hydroxymethyl) aminomethane and boric acid (Tris-borate), was chosen for its low conductivity and its pH value. At a concentration of 4.5 mM, this solution has a conductivity of only 61 μS cm^{-1} and a pH value of 8.6, yet still provides adequate buffering capacity under the electrophoretic assembly conditions. With an isoelectric point of ~5, streptavidin is negatively charged and thus the streptavidin-conjugated microbeads are also negatively charged in this buffer[26]. In contrast, phosphate and bicarbonate buffering systems with similar concentrations and pH values have much higher conductivity values. With the low conductivity of the Tris-borate buffer, the microbeads can be pulled rapidly toward the electrode while the current is kept at a minimum. However, we found that the

binding of the microbeads was less efficient after they were stored in such a buffer for more than one week.

The types of the microbeads that can be assembled and captured onto the gold surface depend on their surface properties, especially the charges and the nature of the chemical functionality. The streptavidin-coated microbeads were used for two reasons. First, the streptavidin molecules can serve as the functional groups for further attachment of biotinylated molecules or other moieties through the strong biotin-streptavidin affinity binding. Second, we found that under the conditions used, streptavidin-coated microbeads can be assembled and captured with ease. The electrochemically-induced binding of microbeads to the gold surface is probably due to the dative bonding between the chemical groups on the protein and gold, and other interactions such as electrostatic and van der Waals interactions[24, 25, 27]. The binding of the microbeads to the gold surface is robust in that the assembled arrays can withstand the prolonged application of a bias of -1.5 V DC and harsh conditions such as exposure to liquid nitrogen, sputter coating and SEM imaging. We have also experimented with 0.5 μm and 1 μm carboxylate-modified polystyrene microbeads. Even though these microbeads could be pulled into the wells using an electric field, permanent binding was rarely observed. This suggests that electrochemically induced binding of the carboxylate groups on the microbeads to the gold surface is less efficient under our conditions.

3.4.3 Assembly conditions

Various electric field conditions were examined to optimize the microbead

transport and assembly process. With our electrode configuration, AC dielectrophoresis was found to be an inadequate means for assembly, even at 20 Vpp over a wide range of frequencies. However, a DC potential difference of only ~2.0 V was required to observe appreciable electrophoretic migration of the negatively charged, streptavidin-coated microbeads towards the positive electrode. Potentials up to ~2.9 V DC, even when applied for extended periods of time (>30 s), did not result in a significant degree of microbead binding. However, potentials at or above ~3.0 V DC with durations as short as 50 ms enabled rapid and permanent microbead binding. In our device, a 3.0 V potential corresponds to an electric field strength of ~270 V cm^{-1}, although stronger fields are likely to exist around the edges of the wells[28]. Potential differences greater than ~3.5 V DC, when applied continuously for more than 30 seconds, resulted in damage to the ITO and substantial gas evolution due to the electrolysis of water.

To minimize the possibility of bubble formation and damage to the electrodes, photoresist or microbeads, we used low frequency (1 Hz), 3.0 V DC pulses with a short, 10% duty cycle. These conditions were sufficient for rapid, directed assembly with a minimal amount of time in which the substrate and microbeads were subjected to the field. The low-frequency pulsing of the field also helped reduce the lateral microbead aggregation seen at higher frequencies or with continuously applied potentials. Frequencies lower than 1 Hz resulted in less efficient assembly as the microbeads have more time to diffuse away from the surface between pulses. Aggregation of the microbeads, which appeared to hinder

their ability to be captured efficiently, was further reduced by applying the electric field in two to three 15-second intervals with a two-minute recess in between each interval. Although the electric field is generally applied for a total of 30-45 pulses, the majority of the wells will have captured a microbead within the first 20-30 pulses. The additional time is usually spent filling the remaining 10-15% of the wells. The drop in the assembly rate can be attributed to both the depletion of microbeads from the suspension and the formation of aggregates near the surface of the array[12, 13, 29, 30]. Some microbeads are dislodged during the washing step. This is likely due to irregularities in the microbead population or inadequate contact and binding with the gold surface.

The microbead concentration is chosen such that the suspension contains approximately 2-4 times as many microbeads as the number of wells in the chamber. Higher concentrations tend to lead to field-induced aggregation. For the smaller 0.5 μm beads, we could not achieve 100% filling with a single batch of the microbead suspension. Even though there were plenty of microbeads left in the suspension, the assembly process did not proceed any further after about 15 pulses. This was probably due to buffer depletion because the assembly process could be resumed to complete the filling of the wells by using an additonal batch of microbeads.

Following the assembly process, the integrity of the streptavidin on the microbeads was verified by introducing into the chamber a solution containing biotinylated, fluorophore-labeled oligonucleotides. After a 60 min incubation, the chamber was washed and the microbeads were imaged. A comparison of the images

before and after the incubation period revealed a substantial gain in the fluorescence signal on the microbeads, indicating that an ample amount of streptavidin was still intact and functional. We also tested the ability to accelerate the capture of these biotinylated, fluorophore-labeled oligonucleotides.using an electric field. For this demonstration, an array of microbeads was assembled and then the oligos were introduced into the chamber at a concentration of 100 nM. A series of electrical pulses (1.0 V DC pulse at 1 Hz and 10% duty cycle) was then applied to the chip for 5 minutes. The resulting fluorescence signal, as shown in Figure 3.7, was significantly greater than the passive control. The signal is concentrated around the perimeter of the microbeads as a result of field concentrating effects brought about by the microbeads.

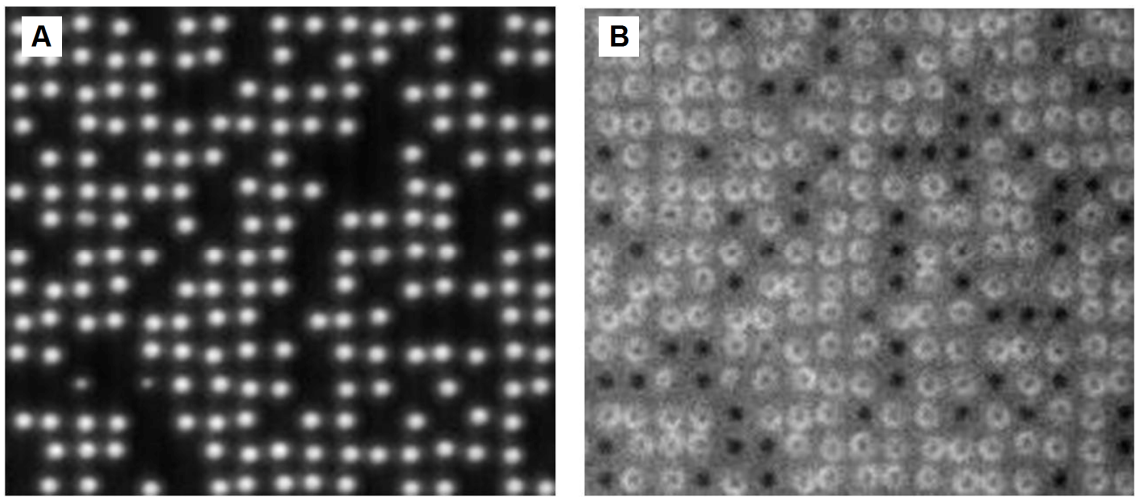

Figure 3.7: Accelerated capture of DNA oligonucleotides using an electric field. (A) Fluorescence image of a partially assembled array of FITC labeled, streptavidin-coated microbeads. (B) Fluorescence image of the microbead array shown in (A) after the electrophoretic capture of biotinylated, Cy5-labeled oligonucleotides.

Assembly can still be performed using wells that are smaller than the microbeads as long as the wells are not too deep and the pitch is large enough to

prevent contact between the microbeads. As is observed in Figure 3.5C, the microbeads are better aligned under such a condition. If the wells are hexagonally packed and the microbeads are appropriately sized, it is very likely that the microbeads can be assembled into an array with the highest achievable packing density. However, if the microbeads are much smaller than the wells, the microbead alignment may be compromised to some degree (Figure 3.6C).

As compared to magnetic assembly methods[9, 10], the choices of the microbeads or particles available for electric field directed assembly are much greater since microbeads with magnetic properties are not required. In principle, any protein-conjugated microbeads can be used. The size of the wells that can be fabricated is only limited by the resolution of the photolithography system and perhaps by the types of photoresist used. Therefore, our method offers great flexibility and scalability for the rapid assembly of microbead arrays with various patterns, densities and pitches.

3.5 Conclusions

In summary, we have demonstrated the ability to use electric fields to direct the rapid assembly of arrays of 0.5 and 1 μm protein-conjugated microbeads on photolithographically defined templates. Standard microfabrication procedures are used to generate wafer-scale arrays of wells on gold in a robust, epoxy-based photoresist. Hundreds of millions of microbeads can be assembled within these wells in 30-45 seconds by applying low-voltage, low-frequency DC electrical pulses. Each well contains only one microbead and filling rates as high as 99.9% are

easily achieved with minimal defects. Array assembly takes place within a microfluidic device that is compatible with real-time bright-field and epifluorescence imaging. The methods presented here may be applied to colloidal lithography[31, 32], micro- and nano-fabrication, and the assembly of arrays of microbeads conjugated to biomolecules such as antibodies and DNA for use in high-throughput assays. In addition, the use of such a platform may provide a means of accelerating diffusion-limited assays by actively concentrating molecules of interest via an electric field[20, 21].

3.6 Acknowledgements

This work was supported in part by grants from the NIH/NHGRI (R21HG003587, R21HG004130 and 1R01HG005096) and the NSF under a CAREER award to X. H. (BES-0547193). A portion of this work was done in the UCSB nanofabrication facility, part of the NSF funded NNIN network. We thank Dr. Brian Thibeault, Dr. Adam Abrahamsen, and Mike Silva for training and technical support at UCSB. Part of this work was also performed in the Nano3 facility at CalIT^2 at UCSD. We thank Larry Grissom, Dr. Bernd Fruhberger, Ryan Anderson and Dr. Maribel Montero for training and technical support at Nano3.

3.7 References

1. Gunderson, K.L. Whole-genome genotyping on bead arrays. *Methods Mol. Biol.* **529**, 197-213 (2009).

2. Cloonan, N., Forrest, A.R.R., Kolle, G., Gardiner, B.B.A., Faulkner, G.J., Brown, M.K., Taylor, D.F., Steptoe, A.L., Wani, S., Bethel, G. *et al.* Stem cell transcriptome profiling via massive-scale mrna sequencing. *Nat. Meth.* **5**, 613-619 (2008).

3. Blicharz, T.M., Siqueira, W.L., Helmerhorst, E.J., Oppenheim, F.G., Wexler, P.J., Little, F.F. & Walt, D.R. Fiber-optic microsphere-based antibody array for the analysis of inflammatory cytokines in saliva. *Anal. Chem.* **81**, 2106-2114 (2009).

4. Ferguson, J.A., Steemers, F.J. & Walt, D.R. High-density fiber-optic DNA random microsphere array. *Anal. Chem.* **72**, 5618-5624 (2000).

5. Yin, Y., Lu, Y., Gates, B. & Xia, Y. Template-assisted self-assembly: A practical route to complex aggregates of monodispersed colloids with well-defined sizes, shapes, and structures. *J. Am. Chem. Soc.* **123**, 8718-8729 (2001).

6. Cui, Y., Bjork, M.T., Liddle, J.A., Sonnichsen, C., Boussert, B. & Alivisatos, A.P. Integration of colloidal nanocrystals into lithographically patterned devices. *Nano Lett.* **4**, 1093-1098 (2004).

7. Shendure, J., Porreca, G.J., Reppas, N.B., Lin, X., McCutcheon, J.P., Rosenbaum, A.M., Wang, M.D., Zhang, K., Mitra, R.D. & Church, G.M. Accurate multiplex polony sequencing of an evolved bacterial genome. *Science* **309**, 1728-1732 (2005).

8. Margulies, M., Egholm, M., Altman, W.E., Attiya, S., Bader, J.S., Bemben, L.A., Berka, J., Braverman, M.S., Chen, Y.J., Chen, Z. *et al.* Genome sequencing in microfabricated high-density picolitre reactors. *Nature* **437**, 376-380 (2005).

9. Wen, W., Wang, N., Zheng, D.W., Chen, C., Tu, K.N. Two- and three-dimensional arrays of magnetic microspheres. *J. Mater. Res.* **14**, 1186-1189 (1999).

10. Barbee, K.D. & Huang, X. Magnetic assembly of high-density DNA arrays for genomic analyses. *Anal. Chem.* **80**, 2149-2154 (2008).

11. Richetti, P., Prost, J. & Barois, P. Two-dimensional aggregation and crystallization of a colloidal suspension of latex spheres. *J. Physique Lett.* **45**, 1137-1143 (1984).

12. Trau, M., Saville, D.A. & Aksay, I.A. Field-induced layering of colloidal crystals. *Science* **272**, 706-709 (1996).

13. Yeh, S.-R., Seul, M. & Shraiman, B.I. Assembly of ordered colloidal aggregrates by electric-field-induced fluid flow. *Nature* **386**, 57-59 (1997).

14. Chiou, P.Y., Ohta, A.T. & Wu, M.C. Massively parallel manipulation of single cells and microparticles using optical images. *Nature* **436**, 370-372 (2005).

15. Winkleman, A., Gates, B.D., McCarty, L.S. & Whitesides, G.M. Directed self-assembly of spherical particles on patterned electrodes by an applied electric field. *Adv. Mater.* **17**, 1507-1511 (2005).

16. Dziomkina, N.V., Hempenius, M.A. & Vancso, G.J. Symmetry control of polymer colloidal monolayers and crystals by electrophoretic deposition on patterned surfaces. *Adv. Mater.* **17**, 237-240 (2005).

17. Dehlinger, D.A., Sullivan, B.D., Esener, S. & Heller, M.J. Directed hybridization of DNA derivatized nanoparticles into higher order structures. *Nano Lett.* **8**, 4053-4060 (2008).

18. Hwang, H. & Park, J.K. Rapid and selective concentration of microparticles in an optoelectrofluidic platform. *Lab Chip* **9**, 199-206 (2009).

19. Tam, J.M., Song, L. & Walt, D.R. DNA detection on ultrahigh-density optical fiber-based nanoarrays. *Biosens. Bioelectron.* **24**, 2488-2493 (2009).

20. Sosnowski, R.G., Tu, E., Butler, W.F., O'Connell, J.P. & Heller, M.J. Rapid determination of single base mismatch mutations in DNA hybrids by direct electric field control. *Proc. Natl. Acad. Sci. U. S. A.* **94**, 1119-1123 (1997).

21. Harper, J.C., Polsky, R., Wheeler, D.R., Dirk, S.M. & Brozik, S.M. Selective immobilization of DNA and antibody probes on electrode arrays: Simultaneous electrochemical detection of DNA and protein on a single platform. *Langmuir* **23**, 8285-8287 (2007).

22. Shendure, J. & Ji, H. Next-generation DNA sequencing. *Nat. Biotechnol.* **26**, 1135-1145 (2008).

23. Abramoff, M.D., Magelhaes, P.J. & Ram, S.J. Image processing with imagej. *Biophotonics Intl.* **11**, 36-42 (2004).

24. Moulton, S.E., Barisci, J.N., Bath, A., Stella, R. & Wallace, G.G. Investigation of protein adsorption and electrochemical behavior at a gold electrode. *J. Colloid Interface Sci.* **261**, 312-319 (2003).

25. De Roe, C., Courtoy, P.J. & Baudhuin, P. A model of protein-colloidal gold interactions. *J. Histochem. Cytochem.* **35**, 1191-1198 (1987).

26. Sivagnanam, V., Sayah, A., Vandevyver, C. & Gijs, M.A.M. Micropatterning of protein-functionalized magnetic beads on glass using electrostatic self-assembly. *Sensors and Actuators B: Chemical* **132**, 361-367 (2008).

27. Gu, Z., Huang, S. & Chen, Y. Biomolecular nanopatterning by magnetic electric lithography. *Angew. Chem. Intl. Ed. Engl.* **48**, 952-955 (2009).

28. Cordovez, B., Psaltis, D. & Erickson, D. Trapping and storage of particles in electroactive microwells. *Appl. Phys. Lett.* **90**, 024102 (2007).

29. Giersig, M. & Mulvaney, P. Preparation of ordered colloid monolayers by electrophoretic deposition. *Langmuir* **9**, 3408-3413 (1993).

30. Bohmer, M. In situ observation of 2-dimensional clustering during electrophoretic deposition. *Langmuir* **12**, 5747-5750 (1996).

31. Fischer, U.C. & Zingsheim, H.P. Submicroscopic pattern replication with visible light. *J. Vac. Sci. Technol.* **9**, 881-885 (1981).

32. Haginoya, C., Ishibashi, M. & Koike, K. Nanostructure array fabrication with a size-controllable natural lithography. *Appl. Phys. Lett.* **71**, 2934-2936 (1997).

This chapter, in part, is a reproduction of the material as it appears in: Barbee, K.D.; Hsiao, A.P.; Heller, M.J.; Huang, X., *Lab on a Chip* **2009** 9 (22); 3268 - 3274; The dissertation author was the primary investigator and author of this paper.

4 Multiplexed protein detection on antibody-conjugated microbead arrays in a microfabricated electrophoretic device

4.1 Abstract

We report the development of a microfabricated electrophoretic device for assembling high-density arrays of antibody-conjugated microbeads for chip-based protein detection. The device consists of a flow cell formed between a gold-coated silicon chip with an array of microwells etched in a silicon dioxide film and a glass coverslip with a series of thin gold counter electrode lines. We have demonstrated that 0.4 and 1 μm beads conjugated with antibodies can be rapidly assembled into the microwells by applying a pulsed electric field across the chamber. We have shown that

these antibody-conjugated microbead arrays can be used to perform on-chip sandwich immunoassays to detect test antigens at concentrations as low as 40 pM (6.4 ng/mL). We also demonstrate the ability to identify each microbead type on the array using a combination of fluorescence and spatial encoding strategies. A finite element model was also developed to examine the electric field distribution within the device for different counter electrode configurations over a range of line pitches and chamber heights. This device will be useful for assembling high-density, encoded antibody arrays for multiplexed detection of proteins and other types of protein-conjugated microbeads for applications such as the analysis of protein-protein interactions.

4.2 Introduction

The ability to interrogate proteins in a sensitive, quantitative, multiplexed and high-throughput manner has many applications in proteomic analysis[1-3], cancer research[4, 5], diagnostics[6] and drug discovery[7]. Although established methods such as western blots[8] and enzyme-linked immunosorbent assays[9] (ELISA) can be used for sensitive and reliable protein detection and quantification, they are labor-intensive and require large sample volumes. Furthermore, they allow for the analysis of only a small number of samples and proteins at a time. Alternatively, the use of spotted protein and antibody microarrays enable greater multiplexing and significantly reduced sample volumes[10-18]. Other groups have demonstrated the potential advantages of assays that employ protein- and antibody-conjugated microbeads, which allow for even greater multiplexing and scalability than those performed in microtiter plates or on spotted arrays[19-26]. The majority of these microbead-based immunoassays are typically

performed in solution[19, 20] or on-chip[21-26]. The solution-based formats are fast and sensitive but they require specialized flow cytometry equipment for sample analysis. In contrast, chip-based formats are well suited for analysis via epifluorescence microscopy and allow for the integration of additional lab-on-a-chip processes such as nucleic acid extraction and genetic profiling from single cells or whole blood[27, 28].

Methods for assembling or capturing antibody-conjugated microbeads on chip-based platforms include micromanipulation[21], microfluidic trapping[22, 23], evaporation of microbead suspensions on etched silicon[24] or fiber-optic bundles[25], and electrostatic self-assembly on chemically-modified substrates[26]. Many of these platforms enable multiplexed analysis by using a mixed population of encoded microbeads or by physically isolating each population in separate microfluidic channels. In this work, we report the development of a new approach for fabricating and assembling microbead arrays. We utilize an electric field to direct the assembly of antibody-conjugated microbeads onto a microfabricated array of wells. The process takes place within a microfluidic device and arrays of micron to sub-micron beads can be assembled in 15-45 seconds. Moreover, we have demonstrated that these arrays of antibody-conjugated microbeads can be assembled and used for sensitive, multiplexed protein detection in many samples in parallel. In contrast to previously reported methods, our approach enables much faster and more scalable array assembly. The array format provides the order and spatial separation necessary for packing a large number of microbeads into an extremely small footprint. For instance, nearly 7000 sub-micron beads can be rapidly assembled on an array just 100 μm x 100 μm in size. This small footprint may enable

the analysis of entire proteomes at the single cell level[29, 30]. In addition, our device may provide a means for electrophoretically accelerating the transport of antigens to decrease assay times and to enhance sensitivity[31-33].

Another key advantage of our approach is the ability to assemble our arrays in a controlled, stepwise fashion, thus providing a means in which we can spatially encode and decode the identity of each microbead on the array[34]. By introducing and assembling a small number of microbeads from a single population at a time, we can record the location of these microbeads as they are assembled. This encoding method produces a spatial map of every microbead on the array, thus enabling a large range of multiplexing capabilities without the need for fluorescence encoding[35, 36] or other more complex strategies[37, 38]. In this study, we demonstrate the feasibility of a combined encoding approach by assembling two different fluorescence microbead populations per round. This combination of both fluorescence and spatial encoding schemes gives us even greater multiplexing potential.

The method and device described here also encompass significant improvements over those previously reported for rapid electric-field directed assembly of streptavidin-conjugated microbead arrays[39]. In our previous work, the high-density array of wells was patterned in an epoxy-based photoresist on a gold-coated silicon wafer. The gold served as the working electrode, whereas the counter electrode consisted of an indium-tin oxide (ITO) film on a glass coverslip. In this study, the array of microwells is fabricated in a silicon dioxide film and the counter electrode consists of a series of thin gold lines on a glass coverslip. The silicon dioxide helps create a more robust platform

than those fabricated with an epoxy-based photoresist. For instance, the silicon dioxide film can withstand harsher cleaning processes and electrophoretic conditions. The use of an oxide layer also allows for more precise geometric control of the microwells by chemical vapor deposition, high-resolution photolithography and reactive ion etching. Furthermore, the oxide may be chemically modified prior to use to prevent non-specific adsorption of biomolecules. The use of a glass coverslip with a series of thin, microfabricated gold lines as counter electrodes offers certain advantages over an ITO-coated glass coverslip. For instance, ITO films are not fully transparent in the visible spectrum, which can reduce the sensitivity of assays that require fluorescence imaging for detection. Furthermore, ITO films are easily degraded by high electrical currents, presumably due to the by-products of electrolysis[40]. As the ITO film is degraded, its transparency is reduced and its resistivity tends to increase. In contrast, our use of properly spaced counter electrode lines on the coverslip allows for completely unobstructed fields of view without the loss of transparency or electrical conductivity.

4.3 Materials and methods

4.3.1 Fabrication of arrays of microwells in an oxide on gold

Figure 4.1 illustrates the general procedure for the fabrication and assembly of the electrophoretic device. Silicon wafers (100-150 mm) were cleaned in a 3:1 mixture of 98% H_2SO_4: 30% H_2O_2 at 85 °C for 15 min and then rinsed extensively with 18 MΩ-cm deionized water (dH_2O). (CAUTION: This mixture is extremely dangerous). The wafers were then dipped in a buffered oxide etch (6:1 of 40% NH_4F: 49% HF) for 30 s and then rinsed with dH_2O. (CAUTION: HF is extremely dangerous). The wafers were

blown dry with nitrogen and then baked at 200 °C on a hotplate for 5 min to remove any remaining water. A 200-500 nm layer of silicon dioxide was then deposited on each wafer using an Oxford Plasmalab plasma-enhanced chemical vapor deposition (PECVD) system. Oxide deposition was conducted at 350 °C and 20 W RF using 710 sccm N_2O and 170 sccm SiH_4 at 1 Torr.

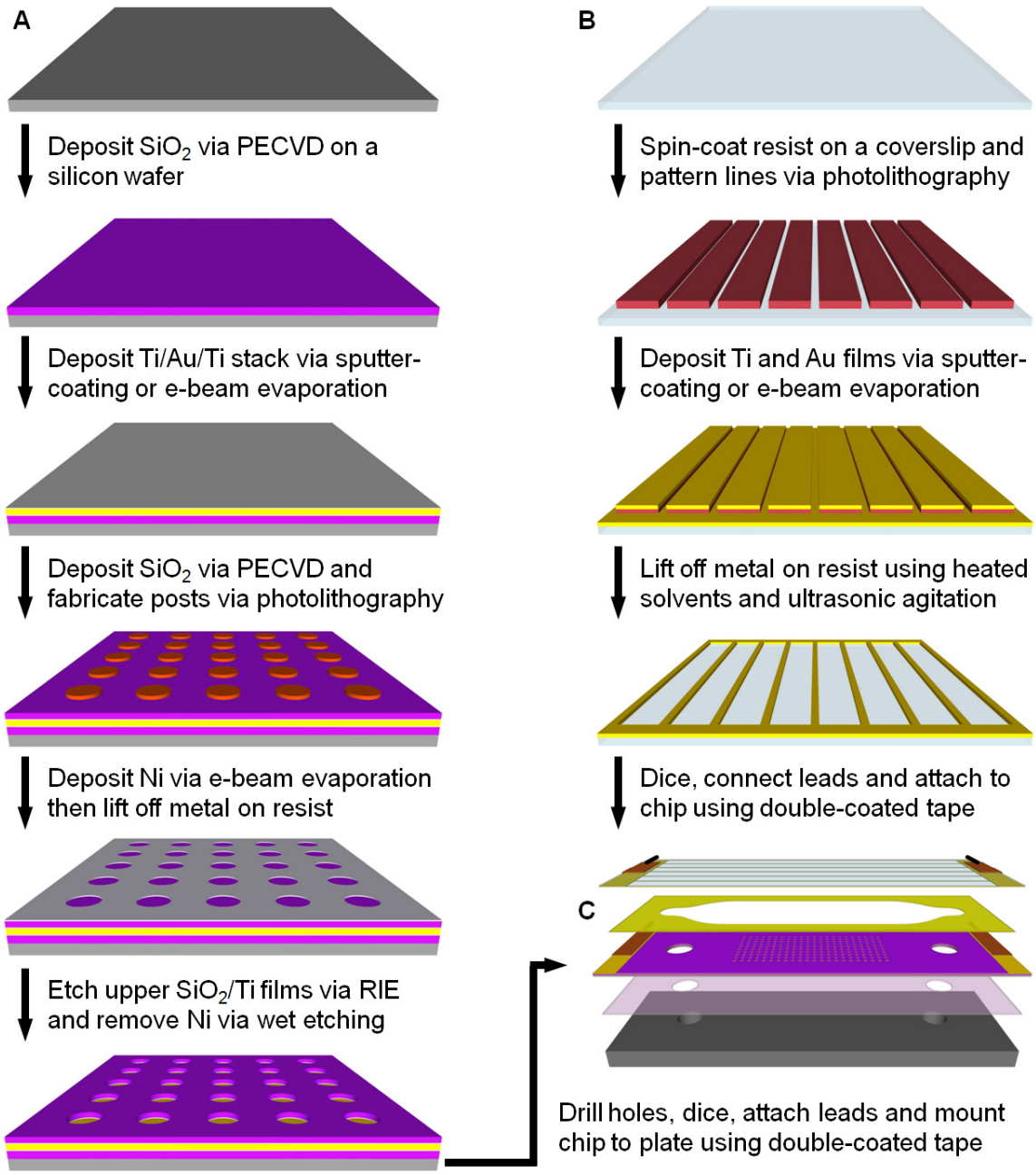

Figure 4.1: Fabrication and assembly of the electrophoretic device.
(A) Fabrication of an array of microwells in silicon dioxide on a titanium-gold-titanium stack on a silicon wafer. (B) Fabrication of gold counter electrode lines on a glass coverslip via a lift-off process. The gold lines serve as counter electrodes in the assembled chamber and are only 25 µm wide with a pitch of 320 µm to allow for imaging of the microbead arrays. (C) Assembly of the device and mounting to a custom-built aluminum plate with tapped ports for fluidic connections. Drawings are not to scale.

Films of titanium, gold and titanium were sequentially deposited on the oxide-coated wafer using a Denton Discovery 18 sputter system. The deposition chamber was typically evacuated to a base pressure of 9 $\times 10^{-7}$ Torr or less and the films were deposited at 150-200 W DC in 3.0 $\times$ 10^{-3} Torr Ar flowing at a rate of ~36 sccm. The two titanium layers, which serve as adhesion layers between the oxide and gold films, were approximately 10 nm thick. The thickness of the gold film was ~300 nm. Following metallization, another 100-300 nm of silicon dioxide was deposited via PECVD using the same tool and conditions described above. A Filmetrics F20 measurement system was used to determine the oxide film thickness.

For arrays fabricated using an i-line stepper system, hexamethyl disilazane (HMDS) (Shin-Etsu MicroSi) was applied to the wafers and allowed to sit for 30 s before spin-drying at 4000 rpm for 30 s. Shipley Microposit S1805 photoresist (Rohm & Haas Electronic Materials) was then applied via spin-coating at 3500 rpm for 30 s. After baking on a hotplate at 110 °C for 60 s, the wafers were patterned via i-line photolithography on a GCA Autostep 200 stepper system using a quartz reticle containing an array of chrome contacts on a clear background. With an intensity of ~475 mW/cm^2, an exposure time of 0.15 s was used to generate posts with a diameter of ~1 μm. The exposed wafers were developed for 60 s in MF-701 or MF-24A (Rohm & Haas Electronic Materials), then rinsed with dH_2O and dried with nitrogen. Residual resist was removed by exposing the wafers for 30 s to an oxygen-based plasma at 100 W RF and 3.0 $\times$ 10^{-1} Torr O_2 in a Technics PEII-A plasma system

For arrays fabricated using a deep UV (DUV) scanner system, the wafers were first coated with a bottom anti-reflective coating (BARC) (ARC 29A-8, Brewer Science) by spin-coating at 2250 rpm for 30 s. After baking the BARC at 220 °C for 60 s, a 250 nm-thick film of DUV resist (ARF AR1682J-15, JSR Micro) was applied via spin-coating at 1000 rpm for 40 s. Edge bead was removed from the front and back sides of the wafers with propylene glycol monomethyl ether acetate (Baker BTS-220, J. T. Baker). All coating, baking and edge bead removal steps were performed on a SVG 90-SE coat track. The resist was baked at 110 °C for 90 s and then exposed on a PAS 5500/950B Step and Scan System (ASML) equipped with a 10 W, 193 nm ArF excimer laser (ELS-6610A, Cymer.). Arrays of posts were patterned on the substrates using a quartz reticle containing chrome contacts on a clear background. Typical doses ranged from 12-24 mJ/cm^2. The exposed wafers were baked at 110 °C for 60 s, developed in MF-319 (Rohm & Haas Electronic Materials) for 60 s and rinsed with dH_2O in a quick dump rinser. The wafers were then rinsed and dried in a spin-rinse-dry tool (PSC-101, Semitool). To remove the BARC, the wafers were exposed to an oxygen-based plasma for 75 s at 50 W RF at 8 sccm and 4.0×10^{-2} Torr in a RIE system (System VII, Plasma-Therm).

Next, the patterned wafers were coated with 30-50 nm of nickel via a Temescal BJD 1800 or VES 2550 electron-beam evaporation system. The chambers were typically evacuated to base pressures of 7×10^{-7} Torr or less and nickel films were deposited at 1.0-2.0 Å/s. The resist and unwanted metal was removed using Shipley Microposit Remover 1165 (Rohm & Haas Electronic Materials) at 70 °C with ultrasonic

agitation for ~1 hr. After rinsing in dH_2O and drying with nitrogen, the exposed oxide was etched in a Panasonic FP-EA01A ICP etcher using 40 sccm CHF_3 at 0.5 Pa with 900 W forward RF power and 200 W reverse RF power. The substrates were cooled via backside helium flow at 15 sccm and 700 mTorr. Under these conditions, the average etch rate for PECVD-grown silicon dioxide was ~0.20 μm/min. However, etch times were extended by as much as 50% to ensure that the upper layer of titanium was also completely removed to fully expose the underlying gold film.

Following the etching process, the wafers were coated with a thick layer of Shipley Megaposit SPR220-7.0 (Rohm & Haas Electronic Materials) photoresist by spin-coating at 2000 rpm for 30 s and then baking at ~100 °C for 5 min. Holes for fluidic connections were then drilled in the wafers using a 1.0 mm diamond-coated drill bit (Cat. # MD16, C. R. Laurence Co.) and a high speed rotary tool (38481 IB/E, Proxxon) mounted to a CNC milling machine (PCNC-1100, Tormach). The wafers were secured in a custom-built jig and submersed under dH_2O or flooded with a dilute coolant solution (Formula #77, Kool Mist) while drilling. The wafers were then diced manually with a carbide scribing tool or automatically with a dicing saw (DAD3220, Disco). The resist was stripped by soaking in acetone for 3 min and then in isopropanol for 1 min. After drying with compressed air, the nickel layer was stripped for 10 min at room temperature in a nickel etchant (Type TFB, Transene Co.). The wafers were then rinsed with dH_2O and dried with nitrogen.

4.3.2 Fabrication of counter electrode lines on glass coverslips

Using custom-built PTFE racks, 45 mm × 50 mm × 0.170 mm (Propper Manufacturing Co.) or 50 mm × 75 mm × 0.170 mm (Erie Scientific Co., Inc.) glass coverslips were washed with sonication in batch mode using a solution of 2% Micro-90 detergent and rinsed extensively with dH_2O. The coverslips were further cleaned in a 1:1:5 mixture of 30% H_2O_2:30% NH_4OH:H_2O at 85 °C for 2 hr and then in a 3:1 mixture of 98% H_2SO_4: 30% H_2O_2 at 85 °C for 2 hr. (CAUTION: These mixtures are extremely dangerous). The coverslips were rinsed extensively in dH_2O and stored under dH_2O until use.

Prior to fabrication, the coverslips were blown dry with nitrogen and then baked on a hotplate at ~200 °C for 5 min to remove any remaining moisture. After cooling, HMDS was applied and allowed to sit for 30 s before spin-drying at 4000 rpm for 30 s. A layer of Shipley Megaposit SPR220-3.0 or SPR518-A photoresist (Rohm & Haas Electronic Materials) was then applied by spin-coating at 3500 rpm for 30 s or at 2000 rpm for 40 s, respectively. The resist was baked at 115 °C (SPR220-3.0) or 90 °C (SPR518-A) for 90 s and then exposed to 365-405 nm light on a Quintel contact aligner using a photomask printed on a transparency film. An exposure time of 16-21 s at ~10 mW/cm^2 was typically used to print 25 μm wide lines at a pitch of 320 μm. After baking the exposed coverslip at 115 °C for 90 s (SPR220-3.0) or 110 °C for 60 s (SPR518-A), the resist was developed for 90 s in MF-24A or MF-321 developer (Rohm & Haas Electronic Materials), rinsed with dH_2O, and dried with nitrogen.

After a 3 min oxygen plasma treatment in a Technics PEII-B plasma system at 100 W RF and 3.0×10^{-1} Torr O_2, a Denton Discovery 18 sputter system was used to deposit a 10 nm-thick titanium film followed by a 300 nm-thick Au film. Sputtering was performed at 150 W with 3.0×10^{-3} Torr Ar at 36-38 sccm. The resist and unwanted metal was then removed by soaking the substrate in Shipley Microposit Remover 1165 at 70 °C in an ultrasonic bath for up to 1 hr. The coverslip was then washed with acetone, rinsed with dH_2O and dried with nitrogen. Line height measurements were obtained with a Dektak 150 surface profiler (Veeco Instruments).

4.3.3 Device assembly

An exploded view of the fluidic device is shown in Figure 4.1C. The general method for assembly of this device has been described elsewhere[32]. Briefly, each chip was cleaned just prior to use by exposing it to oxygen-based plasma at 100 W RF and 3×10^{-1} Torr O_2 for 3 min in a Technics PEII-B plasma system. After rinsing with dH_2O and drying with compressed air, the chip was mounted to a custom-built aluminum plate (Figure 4.2) using a double-coated adhesive tape. The flow cell was then formed by attaching the coverslip with the counter electrodes to the chip via a second double-coated adhesive tape containing a cutout of the fluidic channel. Channel dimensions were typically 2 mm wide by 10 mm long with a height of ~110 μm. Electrical connections were made to the gold film on the chip and the counter electrode lines using copper tape. Fluidic connections were made via ports in the aluminum plate.

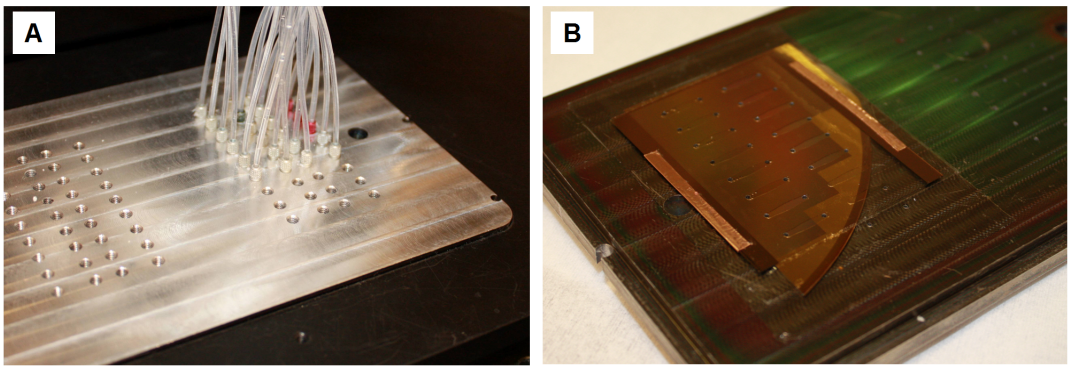

Figure 4.2: Photographs of the aluminum plate and an assembled electrophoretic device.
(A) Top view of the custom-built aluminum plate through which the fluidic connections are made to each channel in the device. (B) Bottom view of the plate and an assembled device containing 14 separate channels. The bottom side of the aluminum plate has been coated with titanium and silicon dioxide films to aid in the adhesion of the double-coated tape.

4.3.4 Antibody conjugation to microbeads

Biotinylated antibodies (biotin-XX goat anti-mouse IgG (H+L), Cat. # B2763 and biotin-XX F(ab')$_2$ fragment of goat anti-rabbit IgG (H+L), Cat. # B21078, Invitrogen) were conjugated to 0.4 or 1 μm streptavidin-coated green (ex. 480/em. 520) and red (ex. 660/em. 690) fluorescent polystyrene beads (Cat. # CP01F/8682, CP01F/7678 and CP01F/8963, Bangs Laboratories) by adding drop-wise a 0.2% microbead suspension to a solution containing one of the biotinylated antibody species. Each conjugation was performed in phosphate buffered saline (PBS, 137 mM sodium chloride, 2.7 mM potassium chloride, 10 mM sodium phosphate dibasic and 2 mM potassium phosphate monobasic, pH 7.4) at an antibody concentration corresponding to five to ten times the amount required to cover the surface of all microbeads in the suspension. A 4 μL drop of the microbead suspension was delivered to the antibody

solution every 5 s using a syringe pump (Cavro XR Rocket Pump, Tecan Group) and the mixture was vortexed throughout the mixing process. After the addition of the entire microbead suspension, the mixture was shaken at room temperature for 1 hr. The microbeads were then washed four times with PBS and stored at 4 °C until use.

4.3.5 Microbead array assembly

NeutrAvidin- (Cat. # F8776, Invitrogen), streptavidin-, and antibody-conjugated microbeads were assembled as described elsewhere[32]. Briefly, the microbeads were exchanged into a low conductance buffer (LCB, 4.5 mM tris(hydroxymethyl) aminomethane, 4.5 mM boric acid and 0.02% Triton X-100, pH 8.6) and introduced into the flow cell at a concentration of 0.02 or 0.2% solids. The microbeads were assembled by applying 3.0 V DC pulses at 1 Hz and a 10% duty cycle for 15-45 s in 15 s intervals with a 1-2 min pause between each interval. The microbeads were pulled into the wells via electrophoresis where they bind permanently to the gold surface through electrochemically-induced interactions. Excess microbeads were then washed away using a syringe pump.

4.3.6 Spatial and fluorescence encoding of microbeads

A mixture of two populations of antibody-conjugated microbeads, one with green fluorescence and one with red fluorescence, were introduced into the flow cell and then subjected to exactly four electrical pulses. Microbeads that were not captured were washed away and then the array was imaged using a DM LFSA epifluorescence microscope (Leica Microsystems) equipped with a 40x/0.55 NA objective, a Cascade 650 CCD camera (Photometrics) and a fast wavelength-switching light source with a

300 W xenon arc lamp (Lambda DG-5, Sutter Instrument Co.). Array scanning was achieved via a BioPrecision 2 XY microscope stage and a MAC 5000 controller system (Ludl Electronic Products). This process was repeated a total of ten times to demonstrate the principle of combining both fluorescence and spatial encoding schemes to record and map 20 different microbead populations. The images were aligned and combined using custom macros in ImageJ[41].

4.3.7 Sandwich immunoassays

In the sandwich immunoassays, two antibody-conjugated microbead populations (goat anti-mouse IgG microbeads and goat anti-rabbit IgG microbeads) were combined at a 1:1 ratio and diluted to ~0.02% for each species. The microbeads were assembled into an array using 5-15 pulses then washed with PBS with 0.05% Tween-20 (PBS-5T). A blocking solution (SuperBlock blocking buffer in Tris-buffered saline, pH 7.4, Cat. # 37545, Pierce Biotechnology) with 0.05% Tween-20 (SB-5T) was then introduced into the chamber. After a 30 min incubation, the chamber was washed with PBS-5T. A solution containing the antigens diluted to specified concentrations using PBS-5T with 10% SB-5T was then loaded. After a 90 min incubation, the chamber was washed with PBS-5T and a solution containing both detection antibodies was introduced into the chamber. After a 30 min incubation, the chamber was washed with PBS-5T and the array was imaged on a fluorescence microscope. The test antigens were mouse and rabbit immunoglobulin proteins (Mouse IgG, Cat. # 2-6502; Rabbit IgG, Cat. # 2-6102, Invitrogen) and the detection antibodies were fluorescently labeled antibodies (Alexa Fluor 568 goat anti-rabbit IgG (H+L), Cat. # A11036; Alexa Fluor 568 goat anti-mouse

IgG (H+L), Cat. # A11031, Invitrogen). To generate standard curves, 10 μL of the antigen solutions were introduced at concentrations ranging from 40 pM (6.4 ng/mL) to 625 pM (100 ng/mL). Experiments were repeated 3-4 times at each antigen concentration. Negative controls were also conducted using an identical procedure but without antigen in the solution. After a 90 min incubation, the chamber was washed with PBS-5T. A solution containing a mixture of the detection antibodies diluted with PBS-5T to a concentration of 2 μg/mL each was then introduced into the chamber. After a 30 min incubation, the chamber was washed with PBS-5T and then imaged with an automated epifluorescence microscopy system. The microbead assembly and sandwich immunoassay process is illustrated in Figure 4.3.

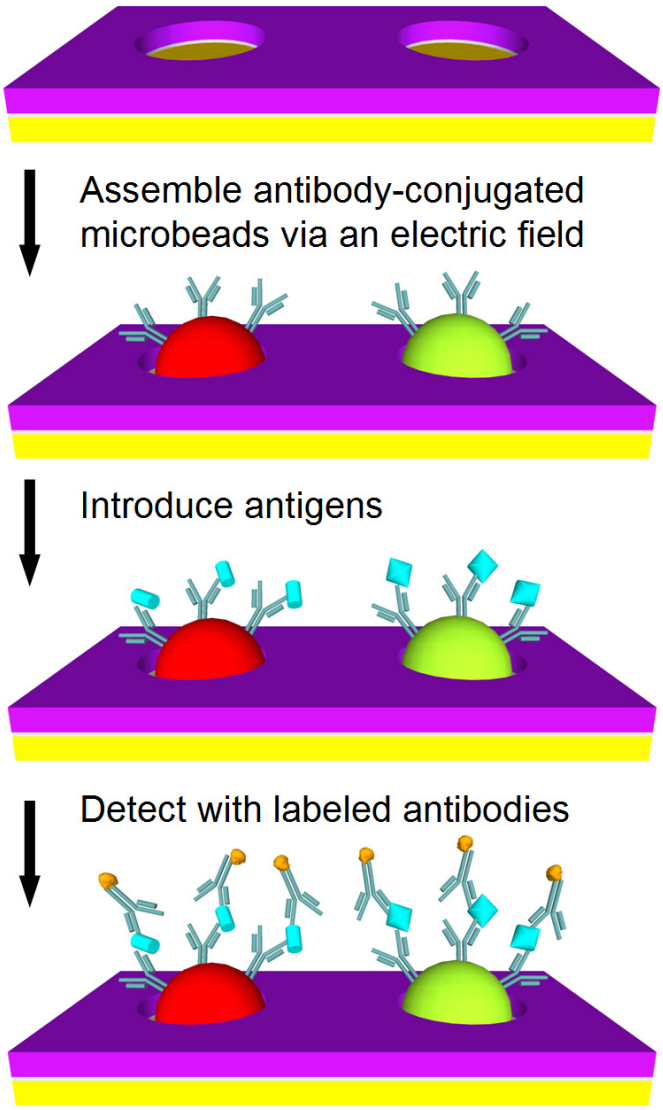

Figure 4.3: Sandwich immunoassay on antibody-conjugated microbeads assembled via electrophoretic deposition.
Antibody-conjugated microbeads are assembled on the microfabricated arrays via the application of a pulsed electric field. Multiplexed protein detection is then performed within the same microfluidic channel using a sandwich immunoassay. Drawings are not to scale.

4.3.8 Fluorescence imaging

Real-time fluorescence imaging was performed on a DM LFSA epifluorescence microscope (Leica Microsystems) equipped with a 40x/0.55 NA objective, a Cascade

650 CCD camera (Photometrics) and an X-Cite 120 illumination system (EXFO Photonics Solutions). Following the incubation with the detection antibodies, fluorescence imaging of the antibody arrays was performed on an Axio Observer.Z1 epifluorescence microscope (Carl Zeiss) equipped with a 40x/1.3 NA oil objective, a 1-megapixel EMCCD camera (iXon+ 885, Andor Technology) and a fast wavelength-switching light source with a 300 W xenon arc lamp (Lambda DG-5, Sutter Instrument Co.). Imaging on the Axio Observer.Z1 was fully automated using custom software. Auto focusing was performed with a Definite Focus System (Carl Zeiss) and array scanning was controlled via a BioPrecision 2 XY microscope stage and a MAC 5000 controller system (LUDL Electronic Products). For each antibody array, multiple fields of view were acquired along the length of the channel. For each field of view, images were taken in three fluorescence channels using the appropriate filter cubes (FITC-3540B, TXRED-4040B, and Cy5.5-A, Semrock). To image the microbeads in the FITC channel, a neutral density filter (ND 2.0 A, Chroma Technology) was used to reduce the output from the light source.

4.3.9 Image analysis

The data from the sandwich immunoassays was analyzed in ImageJ[41] using a custom macro. Briefly, the program generated a mask of the anti-rabbit and anti-mouse microbeads for each field of view using the images taken in the FITC and Cy5.5 channels, respectively. After locating the center of each microbead, the program identified the pixels associated with the microbead and calculated the mean pixel intensities in the corresponding Alexa 568 detection channel. Mean background pixel

intensities for each microbead type were obtained from negative control experiments in which no antigen was added. A microbead was considered to have detected a given antigen if its mean fluorescence intensity in the corresponding channel was greater than three times the standard deviation of the mean background intensity of the microbeads in the same channel[42]. A standard curve was then generated for each microbead type by plotting their mean, background subtracted intensities as a function of antigen concentration. Results were gathered from the analysis of multiple images and each image contained ~150 microbeads.

4.3.10 ITO transmission and resistivity measurements

The effects of electrophoretic assembly conditions on the optical transparency and resistivity of ITO films were studied using a modified chamber design. To enable easy disassembly, each ITO-coated glass slide (Cat. # CG-511N-S115, Delta Technologies) was positioned over a gold-coated slide outfitted with a PEEK gasket (Cat. # 5804K42, McMaster-Carr Co.) and held in place with binder clips. The gap between the two substrates was filled with LCB and then subjected to a 3 V DC potential in 1 min intervals. The device was disassembled after each interval and the optical transmittance of the ITO film was recorded with a Lambda 20 UV-Vis spectrometer (Perkin Elmer). The resistance across the ITO film was also measured after each interval using a digital multimeter (Model # 2010, Keithley Instruments).

4.3.11 SEM imaging

Scanning electron microscopy (SEM) was performed on a Phillips XL30 ESEM or FEI Sirion operating in high-vacuum mode. Prior to imaging with the XL30, the

samples were coated with either chromium or iridium using an Emitech K575X desktop sputtering system.

4.3.12 Finite element analysis

The variation in the electric field strength within the device was modeled using COMSOL Multiphysics v3.4 (COMSOL AB) and MATLAB 7.7.0 (The Mathworks). A cross-section of the chamber, which included ~830 microwells across a span of 2 mm, was drawn to scale and the conductive media DC application was used to plot the electric field strength in the media using different counter electrode configurations. In the first study, the chamber height was fixed at 110 μm and the pitch between the counter electrode lines was varied from 160 μm to 640 μm. In the second study, the counter electrode line pitch was fixed at 320 μm and the chamber height was varied from 55 μm to 220 μm. In both studies, the height of the counter electrode lines was 0.3 μm and the wells were 0.25 μm deep by 1.2 μm wide at a 2.4 μm pitch. The media was assigned a conductivity of 60 μS/cm and the bottom of each well was set to 3.0 V DC while the counter electrode lines were set to ground. All other entities were electrically insulating. Horizontal line plots were generated for each counter electrode line configuration at a height of 5 μm above the surface of the array and spanned between the centers of two adjacent counter electrode lines.

4.4 Results and discussion

We have developed a microfabricated electrophoretic device comprised of a high-density array of wells in silicon dioxide on a gold-coated silicon chip and a glass coverslip containing a series of thin gold lines. A typical SEM image of an array of

microwells fabricated in silicon dioxide on a gold film is shown in Figure 4.4A. By applying a pulsed electric field across the device, we have demonstrated that 0.4 and 1 μm antibody-conjugated microbeads can be rapidly assembled into high-density arrays with excellent filling efficiencies and near perfect order. A sample SEM image of a small portion of an array of antibody-conjugated microbeads assembled within the oxide wells is shown in Figure 4.4B. Sample fluorescence images of the antibody-conjugated microbead arrays are shown in Figure 4.5.

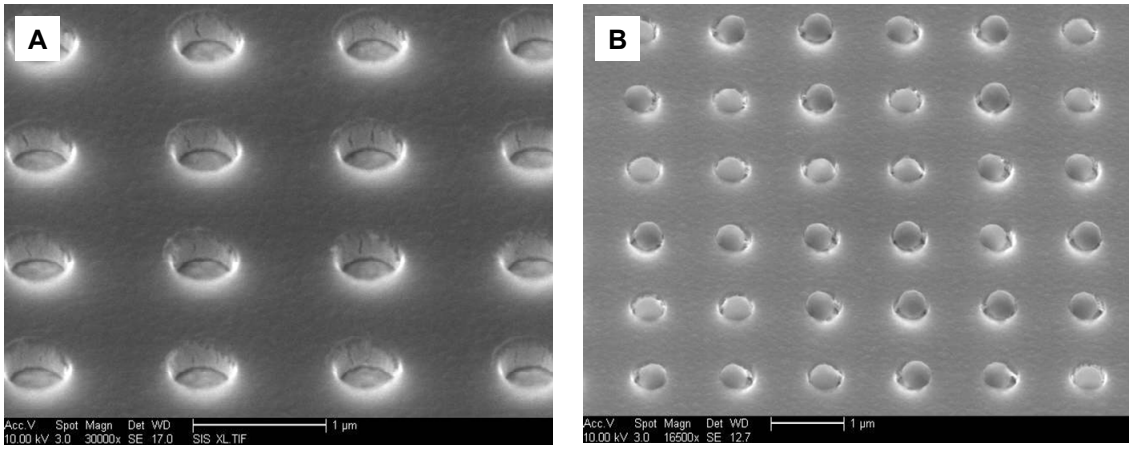

Figure 4.4: Microwell and antibody-conjugated microbead arrays.
(A) SEM image of a small portion of an array of ~0.5 μm wells at a 1.2 μm pitch etched in a silicon dioxide film that was deposited on a gold-coated wafer. (B) SEM image of a small portion of an assembled array of 0.4 μm antibody-conjugated beads at a 1.2 μm pitch.

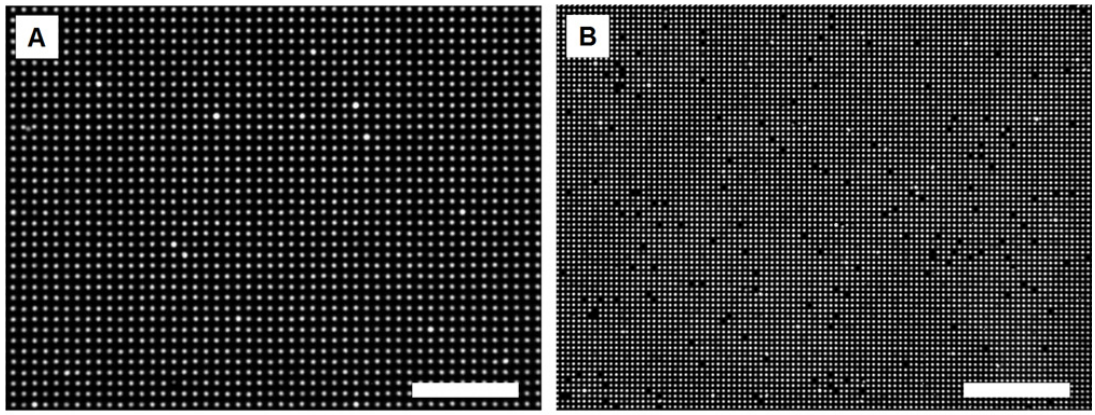

Figure 4.5: Fluorescence micrographs of high-density arrays of antibody-conjugated microbeads assembled via electrophoretic deposition.
(A) Raw fluorescence image of a small portion of an assembled array of a mixture of streptavidin- and antibody-conjugated 1 μm beads. (B) Raw fluorescence image of a small portion of an assembled array of a mixture of two types of antibody-conjugated, 0.4 μm beads at a 1.2 μm pitch. The scale bar in both images is 24 μm.

4.4.1 Spatial and fluorescence microbead encoding

To perform multiplexed immunoassays, we utilize both fluorescence and spatial encoding schemes to enable the identification of each microbead after it has been assembled on the array. An example of a combined encoding scheme is shown in Figure 4.6. In this instance, a mixture of two populations of microbeads with either red or green fluorescence were introduced into the flow cell and then subjected to exactly four electrical pulses. Microbeads that were not captured were then washed away and the array was imaged via epifluorescence microscopy, thus recording the exact locations of each microbead. This process, which only takes seconds per round, was repeated multiple times to demonstrate the gradual filling of the array and our ability to map each microbead type following each assembly round. The number of microbeads assembled in each round can be controlled by varying the microbead concentrations as well as the number of pulses applied during each round. Additionally, if more fluorescent barcodes

are used, many more populations of antibody-conjugated microbeads can be assembled simultaneously during each round, resulting in a much higher cumulative multiplexing ability.

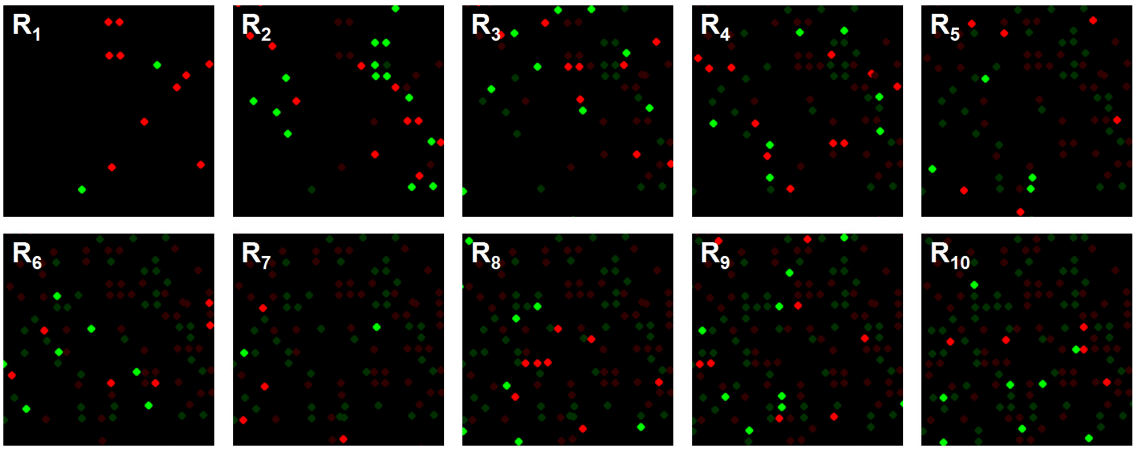

Figure 4.6: Spatial and fluorescence encoding of antibody-conjugated microbead arrays.
Fluorescent micrographs of a small portion of an antibody-conjugated microbead array assembled in a stepwise fashion. Two different fluorescent microbeads are assembled in each of ten rounds (R_1-R_{10}) to enable greater multiplexing capabilities. In each image, the newly assembled microbeads have been highlighted for emphasis.

4.4.2 Immunoassays

Sandwich immunoassays were conducted to demonstrate that our platform could support sensitive, quantitative and multiplexed protein detection. For each sandwich immunoassay, a mixture of two populations of antibody-conjugated microbeads were assembled onto an array via an electric field and then treated with a blocking solution prior to being exposed to a solution containing the antigens. The microbeads were then probed with fluorescently labeled detection antibodies and subsequently imaged via automated epifluorescence microscopy. With each type of detection antibody conjugated to a different fluorescently labeled microbead, we were able to detect

simultaneously two different antigens. The fluorescent signal from each microbead was measured in the detection channel (Alexa 568) and an antigen was considered present if the mean intensity in its corresponding channel was at least three times the standard deviation of the mean microbead background intensity in the same channel[42]. Standard curves were generated using antigen concentrations ranging from 0 to 625 pM and our detection limit was determined to be ~40 pM (6.4 ng/mL) (Figure 4.7), which is similar to the sensitivities of other microbead-based immunoassays[25, 26].

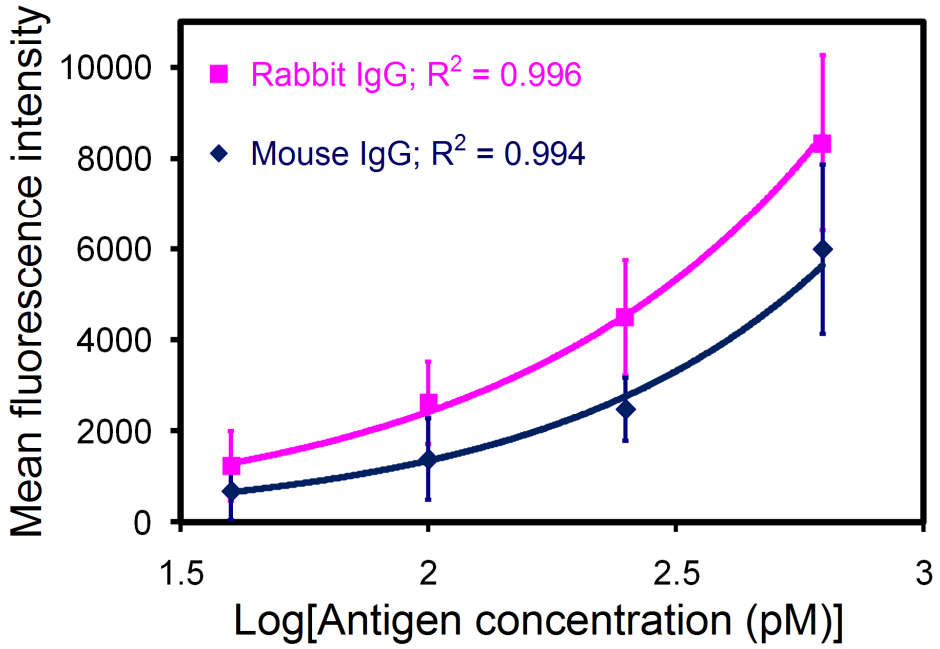

Figure 4.7: Standard curves for the sandwich immunoassays performed on antibody-conjugated microbead arrays.
Graph of the mean fluorescence intensity from 1 µm antibody-conjugated microbeads as a function of antigen concentration. Our detection limit was determined to be ~40 pM (6.4 ng/mL) for both antigens.

Optimization of parameters such as incubation times and the number of a given type of antibody-conjugated microbead assembled on the array may help bring the sensitivity of this approach closer to that of ELISA but without enzymatic signal

amplification. Of these factors, the latter may be of paramount importance, especially at very low antigen concentrations due to the small number of antigens available per microbead. Therefore, it may be beneficial to limit the number of microbeads of a given type to the minimum necessary to give statistically significant data. Other potential improvements include fluid oscillation, optimization of the incubation temperature and the application of an electric-field[31-33] to direct the antigens toward the electrode-bound microbeads. These approaches may enhance the diffusion-limited process of capturing antigens, thereby increasing the sensitivity of the assay and reducing the total assay time. Furthermore, the sensitivity of our immunoassays may also be improved through the use of an immunoRCA strategy[43].

4.4.3 Silicon dioxide wells

The use of silicon dioxide as a dielectric for the electrophoretic assembly of colloidal crystals has been demonstrated elsewhere[44]. We have utilized this material in our device because it offers numerous advantages over the epoxy-based photoresist used in previous work[39]. Although the fabrication process is simpler when using epoxy-based photoresist, the wells are partially destroyed during the plasma cleaning of the gold electrodes. In addition, the photoresist is more susceptible to chemical damage from the by-products of electrolysis during the microbead assembly process. On the other hand, silicon dioxide can withstand harsh environments and processes and may enable the use of various chip bonding techniques such as anodic and thermal bonding. It is also well-suited for direct bonding to PDMS. The use of silicon dioxide also enables more control over the geometric properties of the wells. For instance, oxide

films with precise thicknesses are easily produced. In addition, the use of a silicon dioxide layer facilitates the use of higher resolution microfabrication processes such as DUV lithography and RIE/ICP. Once the array of microwells have been fabricated, the surface properties of the oxide can be modified using silane-based chemistry, which would allow, for example, the passivation of the oxide with polyethylene glycol (PEG) to prevent non-specific binding of microbeads and biomolecules.

4.4.4 Counter electrode lines

The use of a counter electrode that consists of a series of gold lines fabricated on a glass coverslip offers several advantages over the use of an ITO-coated coverslip. One such advantage is that there is no loss of light when imaging between the gold lines. In contrast, ITO films are typically only 80-90% transparent to light in the visible spectrum, which could effectively reduce the sensitivity of epifluorescence-based assays. The use of gold lines is also favored because they can be fabricated using a relatively simple lift-off process whereas the deposition of high-quality ITO films typically requires the optimization of multiple parameters. Another key benefit of the gold lines is their durability. ITO films tend to degrade when subjected to high electrical currents or the by-products of electrolysis that are produced under electrophoretic conditions. While a small number of 3.0 V DC electrical pulses may not have a significant effect, continuous exposure to these electrophoretic conditions for just one minute can result in an major reduction in the transmission of visible light through the film. To demonstrate this phenomenon, we measured this transmittance of an ITO film after subjecting it to a continuous 3.0 V DC potential (Figure 4.8). The experimental

results indicate that the drop in transmittance is wavelength dependent, but is greater than 90% in the lower end of the visible spectrum after just three minutes. This decay would significantly affect the imaging sensitivity of a system using ITO as a counter electrode. The electrical properties of the ITO film were also affected to some degree as determined by a doubling of the sheet resistance after three minutes.

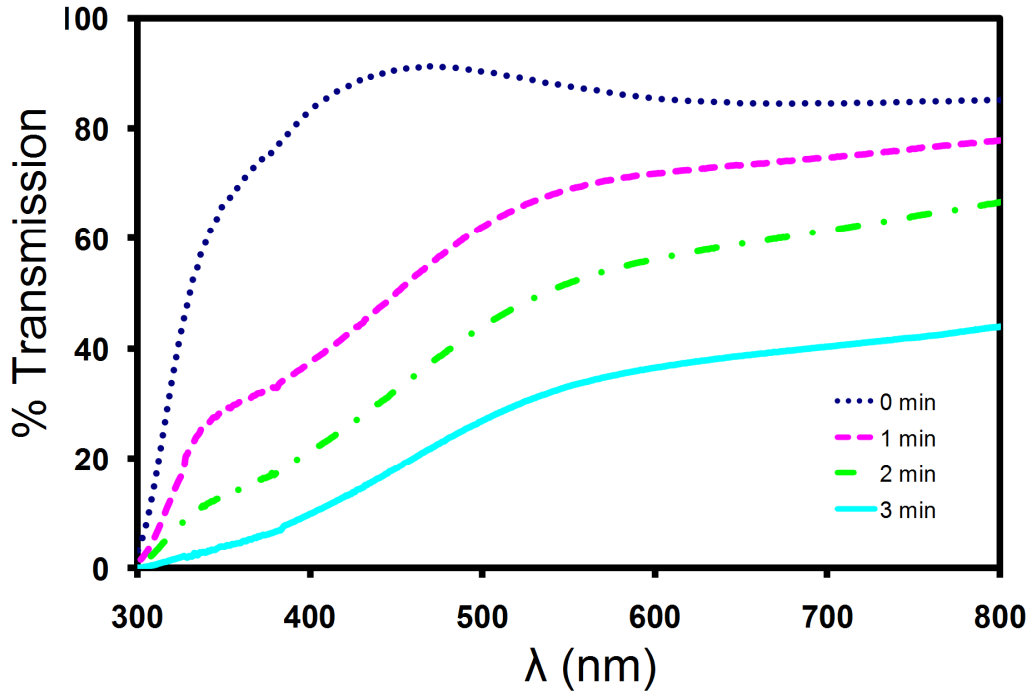

Figure 4.8: Light transmission through ITO films exposed to electrophoretic conditions. The percent transmittance of light through an ITO-based electrophoretic device as a function of total exposure time to electrophoretic conditions.

Although the use of gold lines as counter electrodes may produce non-uniform electric fields within the chamber, microbead assembly was still rapid and uniform across the entire array when 25 μm counter electrode lines at a pitch of 320 μm were used. However, our attempts to assemble similar arrays using lines at a 640 μm pitch were unsuccessful. We developed a 2-D finite element model of the device to examine

the electric field distribution within the chamber for varying counter electrode line pitches and chamber heights. A cross-sectional view of a section of the chamber is illustrated in Figure 4.9A. A screenshot of a portion of a solved model is shown in Figure 4.9B. For each device configuration studied, a horizontal line plot between adjacent counter electrode line centers was generated at a height of 5 μm above the surface of the array. In Figure 4.9C, the chamber height was held at 110 μm while the counter electrode line pitch was varied from 160 μm to 640 μm. At this chamber height, the drop in field strength from a position directly underneath the center of an electrode line to the midpoint between adjacent electrode lines varied from 9.5% at a pitch of 160 μm to 95.7% at a pitch of 640 μm. At a pitch of 320 μm, this drop was 60.0%, and yet we were still able to achieve uniform assembly with this configuration. However, observations made using electrode lines at a 640 μm pitch confirmed that there is a threshold below which assembly cannot be performed. In Figure 4.9D, the pitch was held at 320 μm while the chamber height was varied from 55 μm to 220 μm. At this pitch, the drop in field strength from a position directly underneath the center of an electrode line to the midpoint between adjacent electrode lines varied from 9.9% at a height of 220 μm to 95.4% at a height of 55 μm. This indicates that a uniform electric field could be attained by simply changing the height of the chamber. However, a significant increase in height will prohibit the use of microscope objectives with short working distances and may require a higher voltage for assembly. In our particular model, we do not take into account electrohydrodynamic and convective flow[45, 46], but

future models that include these factors may allow us to optimize further the electrode configurations, device geometry, and electrophoretic conditions.

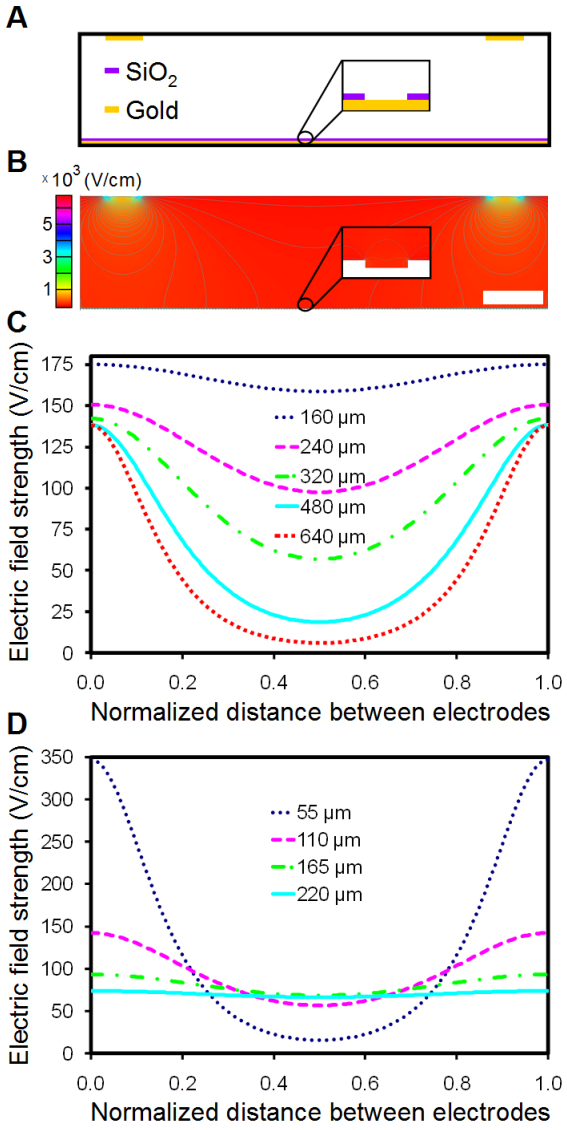

Figure 4.9: Finite element analysis of the electric-field distribution within the microfabricated electrophoretic device.
(A) Cross-sectional illustration of a portion of the device. (B) Surface and contour plot of the y-component of the electric-field strength, E_y, in a scaled COMSOL model of the device. In this particular model, the counter electrode lines are 25 µm wide at a pitch of 320 µm. The chamber is 110 µm high. The inset shows the electric field distribution within a single well. The scale bar is 50 µm. (C) A plot of E_y as a function of the horizontal position between neighboring counter electrode line centers for varying counter electrode line pitches. The channel height was held at 110 µm. (D) A plot of E_y as a function of the horizontal position between neighboring counter electrode line centers for varying chamber heights. The counter electrode line pitch was held at 320 µm. The line plots in (C) and (D) were generated at a fixed height of 5 µm above the surface of the array and the applied potential across the chamber was 3.0 V DC.

We found that 25 μm-wide lines at a pitch of 320 μm allow for excellent microbead assembly as well as unobstructed imaging between them when imaged with a 40x objective and an EMCCD camera with 1004 × 1002 pixels (8 μm × 8 μm pixels). Lines that were too close together lead to the presence of shadows in the images. As shown in Figure 4.10, these shadows diminish the signal from the microbeads up to a distance of ~50 μm from the line. The image was acquired in the FITC channel in a region of the chip where 1 μm antibody-conjugated beads were located directly underneath a 25 μm-wide counter electrode line. Even though the counter electrode lines need to be spaced such that imaging can be performed far enough from the lines to avoid their shadows, this approach offers greater durability and better light transmission than ITO while still providing the means for uniform, efficient assembly of the antibody-conjugated microbeads.

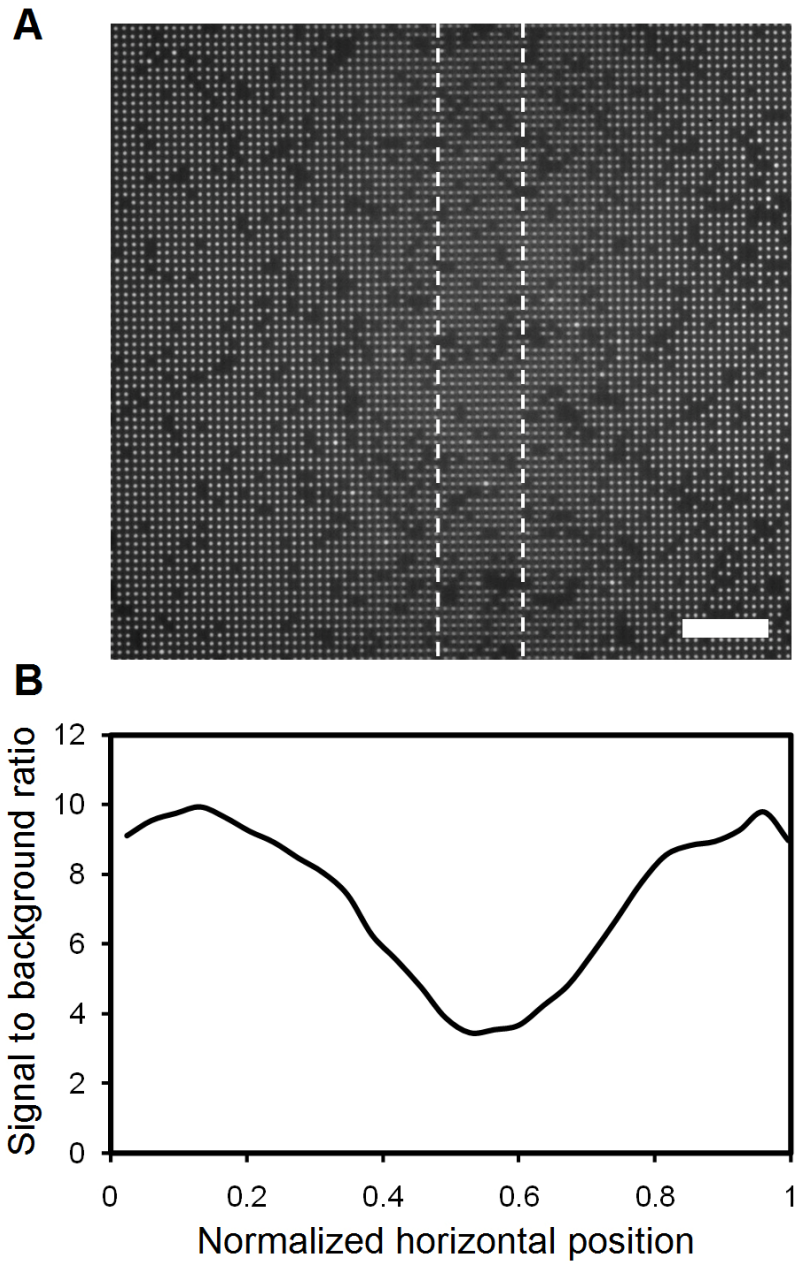

Figure 4.10: Fluorescence signal intensity of assembled antibody-conjugated microbeads under and near a gold counter electrode line.
(A) Fluorescent micrograph of 1 μm antibody-conjugated, fluorescent polystyrene beads assembled near and under a 25 μm gold counter electrode line. The approximate location of the electrode line is given by the dashed lines and is 110 μm above the focal plane in this image. (B) A corresponding fluorescence intensity profile across the entire 200 μm wide image. The scale bar in (A) is 24 μm.

4.5 Conclusions

We have demonstrated that high-density, protein- and antibody-conjugated microbead arrays can be assembled via electrophoretic deposition on microfabricated arrays of wells in silicon dioxide on gold-coated silicon chips. In addition, thin gold lines fabricated on glass coverslips were used as counter electrodes to provide a more robust platform for assembly and enable greater imaging sensitivity than possible with ITO-coated coverslips. Assembly of the microbeads was rapid and resulted in high-density arrays with minimal defects. This platform also enables a simple and yet powerful spatial encoding strategy to replace or compliment fluorescence-based encoding schemes. We have also shown that the assembled antibody arrays could be used to detect test antigens at concentrations as low as 40 pM using sandwich immunoassays. Our microfabricated electrophoretic device and methods will be useful for rapid assembly of encoded antibody arrays for multiplexed detection of proteins. Furthermore, our ability to assemble streptavidin-, NeutrAvidin-, and antibody-conjugated microbeads may be extended to a multitude of other types of protein-conjugated microbeads for other applications such as the analysis of protein-protein interactions.

4.6 Acknowledgements

This work was supported in part by grants from the NIH/NHGRI (R21HG003587, R21HG004130 and 1R01HG005096) and the NSF under a CAREER award to X. H. (BES-0547193). A portion of this work was conducted at the Triangle National Lithography Center at North Carolina State University (NCSU). We thank

David Vellenga and Marcio Cerullo at NCSU for their training, technical support and services, which included DUV photolithography and BARC etching. We thank Jonathan Pierce at the Analytical Instrumentation Facility at NCSU for SEM imaging services during the early stages of this project. A portion of this work was done in the nanofabrication facility at the University of California, Santa Barbara (UCSB), part of the NSF funded NNIN network. We thank Dr. Brian Thibeault for training and technical support at UCSB. Part of this work was also performed in the Nano3 facility at CalIT^2 at the University of California, San Diego (UCSD). We thank Michael Clark for dicing our wafers and Larry Grissom and Ryan Anderson for training and technical support at UCSD. We also thank Nora Theilacker for advice and assistance with antibodies and image analysis routines.

4.7 References

1. Pandey, A. & Mann, M. Proteomics to study genes and genomes. *Nature* **405**, 837-846 (2000).

2. MacBeath, G. Protein microarrays and proteomics. *Nat. Genet.* **32**, 526-532 Suppl (2002).

3. Phizicky, E., Bastiaens, P.I.H., Zhu, H., Snyder, M. & Fields, S. Protein analysis on a proteomic scale. *Nature* **422**, 208-215 (2003).

4. Madoz-Gúrpide, J., Wang, H., Misek, D.E., Brichory, F. & Hanash, S.M. Protein based microarrays: A tool for probing the proteome of cancer cells and tissues. *Proteomics* **1**, 1279-1287 (2001).

5. Knezevic, V., Leethanakul, C., Bichsel, V.E., Worth, J.E., Prabhu, V.V., Gutkind, J.S., Liotta, L.A., Munson, P.J., Petricoin III, E.F. & Krizman, D.B. Proteomic profiling of the cancer microenvironment by antibody arrays. *Proteomics* **1**, 1271-1278 (2001).

6. Bellisario, R., Colinas, R.J. & Pass, K.A. Simultaneous measurement of antibodies to three hiv-1 antigens in newborn dried blood-spot specimens using

a multiplexed microsphere-based immunoassay. *Early Hum. Dev.* **64**, 21-25 (2001).

7. Burbaum, J. & Tobal, G.M. Proteomics in drug discovery. *Curr. Opin. Chem. Biol.* **6**, 427-433 (2002).

8. Renart, J., Reiser, J. & Stark, G.R. Transfer of proteins from gels to diazobenzyloxymethyl-paper and detection with antisera: A method for studying antibody specificity and antigen structure. *Proc. Natl. Acad. Sci. U. S. A.* **76**, 3116-3120 (1979).

9. Engvall, E. & Perlmann, P. Enzyme-linked immunosorbent assay (elisa) quantitative assay of immunoglobulin g. *Immunochemistry* **8**, 871-874 (1971).

10. Silzel, J.W., Cercek, B., Dodson, C., Tsay, T. & Obremski, R.J. Mass-sensing, multianalyte microarray immunoassay with imaging detection. *Clin. Chem.* **44**, 2036-2043 (1998).

11. Arenkov, P., Kukhtin, A., Gemmell, A., Voloshchuk, S., Chupeeva, V. & Mirzabekov, A. Protein microchips: Use for immunoassay and enzymatic reactions. *Anal. Biochem.* **278**, 123 - 131 (2000).

12. MacBeath, G. & Schreiber, S.L. Printing proteins as microarrays for high-throughput function determination. *Science* **289**, 1760 - 1763 (2000).

13. de Wildt, R.M.T., Mundy, C.R., Gorick, B.D. & Tomlinson, I.M. Antibody arrays for high-throughput screening of antibody-antigen interactions. *Nat. Biotechnol.* **18**, 989 - 994 (2000).

14. Holt, L.J., Bussow, K., Walter, G. & Tomlinson, I.M. By-passing selection: Direct screening for antibody-antigen interactions using protein arrays. *Nucleic Acids Res.* **28**, e72- (2000).

15. Zhu, H., Bilgin, M., Bangham, R., Hall, D., Casamayor, A., Bertone, P., Lan, N., Jansen, R., Bidlingmaier, S., Houfek, T. *et al.* Global analysis of protein activities using proteome chips. *Science* **293**, 2101-2105 (2001).

16. Moody, M.D., Van Arsdell, S.W., Murphy, K.P., Orencole, S.F. & Burns, C. Array-based elisas for high-throughput analysis of human cytokines. *Biotechniques*, 186-194 (2001).

17. Haab, B.B., Dunham, M.J. & Brown, P.O. Protein microarrays for highly parallel detection and quantitation of specific proteins and antibodies in complex solutions. *Genome Biology* **2**, 0004.0001-0004.0013 (2001).

18. Huang, R.-P., Huang, R., Fan, Y. & Lin, Y. Simultaneous detection of multiple cytokines from conditioned media and patient's sera by an antibody-based protein array system. *Anal. Biochem.* **294**, 55-62 (2001).

19. Dasso, J., Lee, J., Bach, H. & Mage, R.G. A comparison of elisa and flow microsphere-based assays for quantification of immunoglobulins. *J. Immunol. Methods* **263**, 23-33 (2002).

20. Kellar, K.L. & Iannone, M.A. Multiplexed microsphere-based flow cytometric assays. *Exp. Hematol.* **30**, 1227-1237 (2002).

21. Goodey, A., Lavigne, J.J., Savoy, S.M., Rodriguez, M.D., Curey, T., Tsao, A., Simmons, G., Wright, J., Yoo, S.-J., Sohn, Y. *et al.* Development of multianalyte sensor arrays composed of chemically derivatized polymeric microspheres localized in micromachined cavities. *J. Am. Chem. Soc.* **123**, 2559-2570 (2001).

22. Herrmann, M., Roy, E., Veres, T. & Tabrizian, M. Microfluidic elisa on non-passivated pdms chip using magnetic bead transfer inside dual networks of channels. *Lab Chip* **7**, 1546-1552 (2007).

23. Diercks, A.H., Ozinsky, A., Hansen, C.L., Spotts, J.M., Rodriguez, D.J. & Aderem, A. A microfluidic device for multiplexed protein detection in nano-liter volumes. *Anal. Biochem.* **386**, 30-35 (2009).

24. Qiu, X., Thompson, J.A., Chen, Z., Liu, C., Chen, D., Ramprasad, S., Mauk, M., Ongagna, S., Barber, C., Abrams, W.R. *et al.* Finger-actuated, self-contained immunoassay cassettes. *Biomed. Microdev.* **11**, 1175-1186 (2009).

25. Blicharz, T.M., Siqueira, W.L., Helmerhorst, E.J., Oppenheim, F.G., Wexler, P.J., Little, F.F. & Walt, D.R. Fiber-optic microsphere-based antibody array for the analysis of inflammatory cytokines in saliva. *Anal. Chem.* **81**, 2106-2114 (2009).

26. Sivagnanam, V., Song, B., Vandevyver, C. & Gijs, M.A.M. On-chip immunoassay using electrostatic assembly of streptavidin-coated bead micropatterns. *Anal. Chem.* **81**, 6509-6515 (2009).

27. Easley, C.J., Karlinsey, J.M., Bienvenue, J.M., Legendre, L.A., Roper, M.G., Feldman, S.H., Hughes, M.A., Hewlett, E.L., Merkel, T.J., Ferrance, J.P. *et al.* A fully integrated microfluidic genetic analysis system with sample-in-answer-out capability. *Proc. Natl. Acad. Sci. U. S. A.* **103**, 19272-19277 (2006).

28. Zhong, J.F., Chen, Y., Marcus, J.S., Scherer, A., Quake, S.R., Taylor, C.R. & Weiner, L.P. A microfluidic processor for gene expression profiling of single human embryonic stem cells. *Lab Chip* **8**, 68-74 (2008).

29. Cai, L., Friedman, N. & Xie, X.S. Stochastic protein expression in individual cells at the single molecule level. *Nature* **440**, 358-362 (2006).

30. Newman, J.R.S., Ghaemmaghami, S., Ihmels, J., Breslow, D.K., Noble, M., DeRisi, J.L. & Weissman, J.S. Single-cell proteomic analysis of s. Cerevisiae reveals the architecture of biological noise. *Nature* **441**, 840-846 (2006).

31. Ewalt, K.L., Haigis, R.W., Rooney, R., Ackley, D. & Krihak, M. Detection of biological toxins on an active electronic microchip. *Anal. Biochem.* **289**, 162-172 (2001).

32. Morozov, V.N., Groves, S., Turell, M.J. & Bailey, C. Three minutes-long electrophoretically assisted zeptomolar microfluidic immunoassay with magnetic-beads detection. *J. Am. Chem. Soc.* 129, 12628-12629 (2007).

33. Wu, J., Yan, Y., Yan, F. & Ju, H. Electric field-driven strategy for multiplexed detection of protein biomarkers using a disposable reagentless electrochemical immunosensor array. *Anal. Chem.* 80, 6072-6077 (2008).

34. Ng, J.K., Selamat, E.S. & Liu, W.-T. A spatially addressable bead-based biosensor for simple and rapid DNA detection. *Biosens. Bioelectron.* 23, 803-810 (2008).

35. Michael, K.L., Taylor, L.C., Schultz, S.L. & Walt, D.R. Randomly ordered addressable high-density optical sensor arrays. *Anal. Chem.* 70, 1242-1248 (1998).

36. Han, M., Gao, X., Su, J.Z. & Nie, S. Quantum-dot-tagged microbeads for multiplexed optical coding of biomolecules. *Nat. Biotechnol.* 19, 631-635 (2001).

37. Gunderson, K.L., Kruglyak, S., Graige, M.S., Garcia, F., Kermani, B.G., Zhao, C., Che, D., Dickinson, T., Wickham, E., Bierle, J. et al. Decoding randomly ordered DNA arrays. *Genome Research* 14, 870-877 (2004).

38. Birtwell, S. & Morgan, H. Microparticle encoding technologies for high-throughput multiplexed suspension assays. *Integr. Biol.* 1, 345-362 (2009).

39. Barbee, K.D., Hsiao, A.P., Heller, M.J. & Huang, X. Electric field directed assembly of high-density microbead arrays. *Lab Chip* 9, 3268-3274 (2009).

40. Folcher, G., Cachet, H., Froment, M. & Bruneaux, J. Anodic corrosion of indium tin oxide films induced by the electrochemical oxidation of chlorides. *Thin Solid Films* 301, 242-248 (1997).

41. Abramoff, M.D., Magelhaes, P.J. & Ram, S.J. Image processing with imagej. *Biophotonics Intl.* 11, 36-42 (2004).

42. Anderson, D.J. Determination of the lower limit of detection. *Clin. Chem.* 35, 2152-2153 (1989).

43. Schweitzer, B., Wiltshire, S., Lambert, J., O'Malley, S., Kukanskis, K., Zhu, Z., Kingsmore, S.F., Lizardi, P.M. & Ward, D.C. Immunoassays with rolling circle DNA amplification: A versatile platform for ultrasensitive antigen detection. *Proc. Natl. Acad. Sci. U. S. A.* 97, 10113-10119 (2000).

44. Dziomkina, N.V., Hempenius, M.A. & Vancso, G.J. Symmetry control of polymer colloidal monolayers and crystals by electrophoretic deposition on patterned surfaces. *Adv. Mater.* 17, 237-240 (2005).

45. Trau, M., Saville, D.A. & Aksay, I.A. Assembly of colloidal crystals at electrode interfaces. *Langmuir* 13, 6375-6381 (1997).

46. Cordovez, B., Psaltis, D. & Erickson, D. Trapping and storage of particles in electroactive microwells. *Appl. Phys. Lett.* 90, 024102 (2007).

This chapter, in part, is currently being prepared for publication. Barbee, K.D.; Hsiao, A.P.; Roller, E.E..; Huang, X. Used with permission. The dissertation author was the primary investigator and author of this paper.

5 Fabrication of DNA polymer brush arrays via destructive micropatterning and rolling circle amplification

5.1 Abstract

We report a method for fabricating DNA polymer brush arrays using photolithography and plasma etching followed by solid-phase rolling circle amplification. Oligonucleotide primers were covalently attached to the surface of a glass coverslip. A thin layer of positive-tone photoresist was spin-coated on the coverslip and patterned via photolithography to generate an array of posts in the resist. Oxygen-based plasma was then used to destroy the exposed oligonucleotide primers. The posts were subsequently removed by solvents to reveal the primer array. The glass coverslip with the primer array

was assembled into a microfluidic chip and DNA polymer brushes were synthesized on the oligonucleotide array by rolling circle amplification (RCA). The linear polymers were characterized using fluorescence imaging, enzymatic digestion and gel electrophoresis. We have demonstrated the ability to fabricate high-density arrays of DNA polymer brushes in situ with a high degree of control over the density and the length of the polymers. These polymers may be further functionalized with oligonucleotide primers, antibodies or other biomolecules and may be useful for enhancing the sensitivity of biomolecular assays and the efficiency and yield of solid-phase biochemical reactions by providing a solution-like three-dimensional environment.

5.2 Introduction

High-density arrays of biomolecules can be fabricated by bottom-up approaches using cyclic synthesis and photolithography[1] or robotic ink-jet printing[2]. They can also be fabricated by top-down approaches using robotic deposition with quill-pen[3] and dip-pen lithography[4], microcontact printing[5] or by assembling biomolecule-conjugated microbeads into arrays of wells[6-9]. These technologies have enabled a myriad of high-throughput biological and chemical analyses on an unprecedented scale for genomic[10-12] and proteomic applications[13] despite the fact that the biomolecules on these substrates are presented either in a planar two-dimensional (2D) surface or on the curved surface of a microbead. This is a limitation in that a three-dimensional (3D) environment would likely afford greater biomolecule loading capacities for higher assay sensitivity and a solution-like environment for more efficient biochemical reactions such as DNA amplification[14-18].

Approaches towards the creation of a more optimal, 3D environment for biomolecular assays and reactions include the use of porous polymer films and polymer brushes to contain or attach the biomolecules of interest[14-18]. Compared to the more traditional biomolecule attachment strategies[1-4, 13], the use of these surface-bound polymers have been shown to enhance key parameters such as biomolecule loading capacities and assay sensitivity[15, 18, 19]. These polymer brushes, which serve as flexible linkers for biomolecule attachment and can also help reduce non-specific adsorption[20], are fabricated using either "grafting to" or "grafting from" techniques. The "grafting to" process is a top-down approach in which polymers pre-synthesized in solution[21, 22] are adsorbed or covalently attached to a suitable substrate. This approach is very challenging due to the difficulty in assembling these polymers onto a surface in an efficient manner[23]. Top-down approaches may also suffer from limited packing densities due to the relatively large size of polymers in random coil configurations[24]. In contrast, the "grafting from" method is a bottom-up approach in which polymers are synthesized in-situ using a controlled radical polymerization (CRP) technique[21, 22]. This approach is capable of producing thicker brushes with higher densities but the characterization of these films can be difficult and typically requires complex tools and techniques [23].

As an alternative to the traditional CRP techniques, we have developed an enzymatic approach to the in-situ synthesis of thick, dense polymer brushes. Our process utilizes solid-phase rolling circle amplification (RCA) [25-29] to generate long linear DNA polymers from circularized DNA templates and surface-bound oligonucleotide primers. We have demonstrated that the density and length of these single-stranded DNA polymer brushes can be controlled by simply varying the number of circular template molecules

available for hybridization to the surface-bound primers and the duration of the amplification process, respectively. We have also shown that these DNA polymers can be easily characterized by fluorescence microscopy and basic molecular biology techniques. Various chemical moieties may be added to these polymers by the incorporation of modified nucleotides during synthesis [30] or the post-synthesis hybridization and cross linking of oligonucleotides with desired functional groups [31]. These functionalized DNA polymer brushes may then serve as a means to overcome the limitations of 2D surface-bound biomolecular assays and reactions.

We also report a method for fabricating high-density arrays of these DNA polymer brushes to facilitate high-throughput, multiplexed assays and reactions via spatial separation and confinement. As shown in Figure 5.1, the DNA polymers are synthesized via rolling circle amplification (RCA) on DNA oligonucleotide arrays that have been fabricated via a destructive micropatterning technique. The microfabrication process utilizes photolithography to create a dense array of posts in photoresist on a glass substrate derivatized with DNA oligonucleotides and poly ethylene glycol (PEG) molecules. A subsequent exposure to oxygen plasma is then performed to destroy the biomolecules in the regions that are not protected by the photoresist[32]. The posts are then removed with organic solvents to expose the remaining DNA and PEG molecules. These oligonucleotides later serve as primers for the synthesis of long, single-stranded DNA polymers via RCA on circularized DNA molecules. This reaction is performed within a microfluidic chip that is placed in a device with precision heating and cooling capabilities (Figure 5.2). Upon completion of the reaction and subsequent hybridization of fluorescently labeled DNA probes, the polymers are observed by epifluorescence

microscopy. Enzymatic digestion of the RCA products can also be performed to estimate the length of the polymers, the total amount of DNA synthesized on the array and the polymer density. Our ability to control the length and density of these RCA products will enable us to optimize biomolecule loading and the efficiency of enzymatic reactions performed on these polymers by minimizing steric hindrance[33, 34].

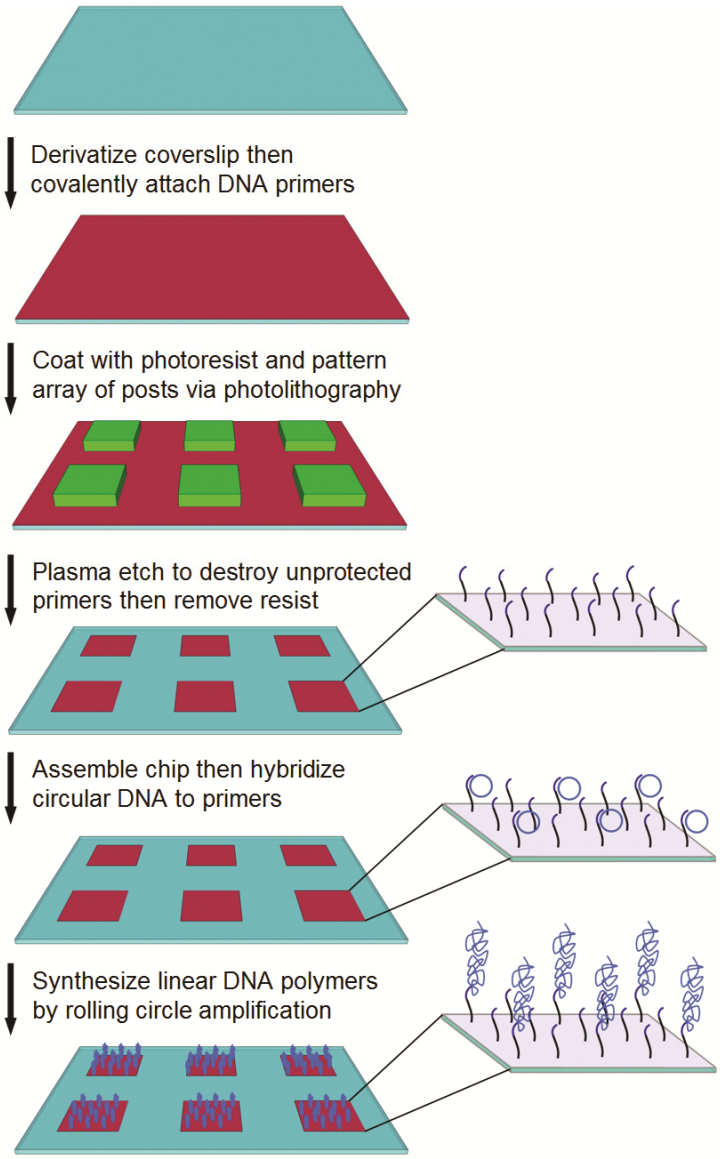

Figure 5.1: Fabrication of linear DNA polymer arrays.
Linear DNA polymer arrays are fabricated on glass coverslips using a destructive micropatterning technique and rolling circle amplification.

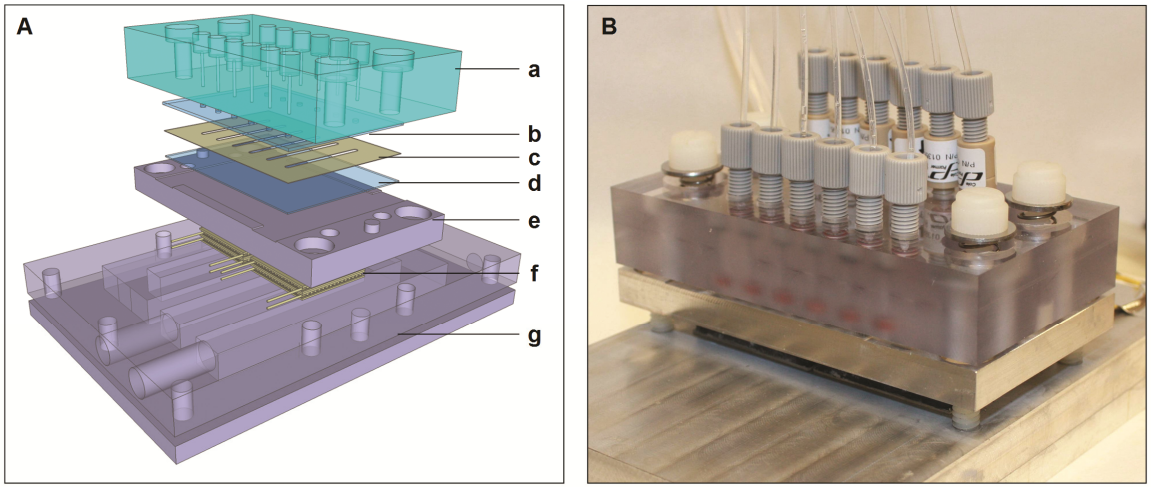

Figure 5.2: Microfluidic device with temperature control.
(A) Exploded view of the device with temperature control and integrated fluidics for automated heating, cooling, reagent loading and washing; a) polycarbonate block with fluidic ports; b) glass slide with drilled holes, c) double-coated silicone adhesive tape; d) glass coverslip containing the DNA primer array; e) aluminum heating and cooling plate; f) thermoelectric modules; g) aluminum heat sink with channels for water cooling. Leak-free connections are made between the glass slide and the polycarbonate block using silicone o-rings (not shown). (B) Photograph of the assembled device.

5.3 Materials and methods

5.3.1 Processing and activation of substrates

Custom glass coverslips with dimensions of 50 mm × 75 mm × 0.170 mm (Erie Scientific Co.) were used as the substrates and derivatized with carboxylate groups on the surface. The coverslips were cleaned by sonication for 1 hr in a 2% solution of Micro-90 (Cole-Parmer Instrument Co.) in batch mode using a custom-built PTFE rack, rinsed five times with deionized water (dH_2O, 18 MΩ-cm, Millipore Milli-Q) and then cleaned in a 1:1:5 solution of NH_4OH:H_2O_2:H_2O at 85 ºC for 1 hr. (Caution: This mixture is extremely dangerous and should be handled with care.) The coverslips were further

cleaned in a 3:1 solution of H_2SO_4:H_2O_2 at 85 ºC for 1 hr and then rinsed extensively with dH_2O. (Caution: This mixture is extremely dangerous and should be handled with care.) The substrates were dipped briefly in ethanol and then soaked in a 2% solution of 3-aminopropyltriethoxysilane in 95:5 of ethanol:dH_2O for 5 min to functionalize the surface with primary amine groups. After rinsing 3 times in acetone, the coverslips were baked at 110 ºC for 10 min. Terminal carboxylic acid groups were then generated by soaking the coverslips for 2 hr in a solution of 250 mM succinic anhydride and 250 mM dry triethylamine in dry dimethyl formamide (DMF). After rinsing three times with acetone, the coverslips were dried by blowing with filtered, compressed air and then stored under vacuum until further use.

On some substrates, a 100 nm layer of silicon dioxide was deposited using a plasma-enhanced chemical vapor deposition (PECVD) system (Plasmalab, Oxford Instruments PLC). Oxide deposition was conducted at 350 °C and 20 W RF using 710 sccm N_2O and 170 sccm SiH_4 at 1 Torr. Upon deposition, the substrates were soaked in a 50% HNO_3 solution for 1 hr, rinsed extensively with dH_2O then dried in a gravity convection at 110 ºC for 10 min. Once cooled, the substrates were derivatized with APTES and then succinic anhydride as described above.

5.3.2 Conjugation of oligonucleotide primes to glass coverslips

The oligonucleotides used in this study were synthesized and purified by Integrated DNA Technologies The amine-labeled primers for covalent attachment to the surface for solid-phase RCA have one of the following two sequences: 5′-NH_2-$(CH_2)_6$-TTT TTT TTT TTT TTT TTT TTT TTT TTT TTT TTT TTT TTT TTT TTT TTT TTT TTA CGT CGT CCG TGC TAG AAG GAA ACA CGC AAT GAT CAC AGC TGA GGA

TAG GAC ATG CGA-3′ or 5′-NH_2-$(CH_2)_6$-TTT TTT TTT TTT TTT TTT TTT TTT TTT TTT TTT TTT TTT TTT TTT TTA TGA TCA CAG CTG AGG ATA GGA CAT GCG AAC GTC GTC CGT GCT AGA AGG AAA CAC GCA ACG TCG TCC GTG CTA GAA GGA AAC ACG CA-3′. The first 50 thymidine residues serve as a spacer between the surface and the priming region. The next 29 bases are present to allow the RCA product to be cut from the surface of the chip using an endonuclease such as BanI or PvuII. The last 29 bases serve as the priming region for the circularized templates described below. The oligonucleotides were covalently attached to the glass or silicon dioxide surface via amide bonds by reacting the primary amine group on the oligonucleotide with the carboxylic acid groups on the substrate. A 1 μM solution of the 5′-amine-labeled oligonucleotides with 180 mM 1-ethyl-3-(3-dimethylaminopropyl) carbodiimide (EDC) in MES-Borate buffer (50 mM MES, 25 mM Borate, pH 4.8) was spotted onto the carboxylated glass coverslip, covered with a second carboxylated coverslip and incubated in a humid chamber for 90 minutes at room temperature. A 22 mm × 22 mm × 0.15 mm coverslip was placed in between the two larger coverslips to maintain adequate separation during the incubation and assist in their separation. Following the derivatization step, the coverslips were rinsed three times with dH_2O and then blown dry with filtered, compressed air.

5.3.3 Conjugation of PEG molecules to glass coverslips

Polyethylene glycol (PEG) molecules were conjugated to the residual carboxyl groups immediately following the DNA conjugation process. A solution containing 10 mM of a methyl-$(OCH_2CH_2)_{24}$-amine compound (Cat. # 26116, Thermo Fisher Scientific) and 100 mM EDC in MES-Borate buffer was spotted onto a DNA-conjugated

coverslip, covered with a second DNA-conjugated coverslip as described above. Following a 30-90 min incubation at room temperature, the coverslips were rinsed with dH_2O then stored in a 5X-SSC-T solution (5X-SSC-T: 5X SSC solution with 0.1% Triton X-100, where a 1X SSC solution contains 15 mM sodium citrate and 150 mM NaCl, pH 7.0) until further use.

5.3.4 Fabrication of primer arrays by photolithography and destructive patterning

Immediately prior to patterning, the coverslips with covalently conjugated oligonucleotide primers were rinsed three times with dH_2O and blown dry with dry nitrogen. The coverslips were then coated with a thin layer of positive photoresist (Shipley Microposit S1813, Rohm & Haas Electronic Materials) by spinning at 6000 rpm for 30 s. The coverslips were baked at 85 ºC on a hotplate for 2 min and then patterned via photolithography on a MA/BA6 contact aligner (SUSS MicroTec). A photomask containing chrome contacts on a clear background was used to create arrays of posts in the resist. The resist was developed for 60-90 s in MF-321 (Rohm & Haas Electronic Materials), rinsed with dH_2O and then blown dry with dry nitrogen. DNA primers not protected by the photoresist were destroyed by exposing the patterned coverslips to oxygen-based plasma for 3 min at 100 W and 300 mTorr in a Technics PE-IIB plasma system. The remaining photoresist was removed by soaking the coverslips in Shipley Microposit Remover 1165 (Rohm & Haas Electronic Materials) at 70 ºC for 15 min. The coverslips were then rinsed 3 times in acetone, 3 times with dH_2O and then stored in a 5X-SSC-T solution until further use. This fabrication process is illustrated in Figure 5.1.

5.3.5 Chip assembly, device fabrication and operation

Holes were drilled in 50 mm × 75 mm × 1 mm glass slides (Product # 2947-75X50, Corning) using a 1-mm diamond-coated drill bit (Cat. # MD16, C.R. Laurence Co) and a high-speed rotary tool (Mod. # 38481, Proxxon) mounted to a CNC milling machine (Mod. # PCNC 1100, Tormach). The drilling process was performed under water or a dilute coolant solution (Formula 77, Kool Mist) The slides were cleaned by the same process used to clean the coverslips and then attached to the patterned coverslips using a ~110 μm-thick, double-sided silicone adhesive tape (Scapa 702, Scapa Group). The coverslips were rinsed three times with dH_2O and blown dry with dry, compressed air immediately prior to the chip assembly process. The cutouts that form the fluidic channels in the chip were designed using AutoCAD (AutoDesk) and Illustrator CS3 (Adobe Systems) then cut out of the tape using a cutting plotter (Mod. # GX-24 CAMM-1, Roland). Each chip contained six 30 mm long and 2 mm wide channels.

5.3.6 Fabrication and operation of the microfluidic device

A device was designed and constructed to enable precise, automated heating and cooling of the chip, and automated delivery of reagents. An exploded view and photograph of this device is shown in Figure 5.2. The heat sink and cold plate were machined out of 6061 aluminum alloy. The coverslip of the assembled chip sits on top of the heating and cooling plate while the fluidic connections are made to the chip via holes in the slide through ports in a thick polycarbonate block. Silicone rubber o-rings (Cat. # 006570, McMaster-Carr Co.) are used at the interface between the glass slide and top block to create leak-free seals. The polycarbonate block is compressed against the chip

with springs. Two pairs of thermoelectric modules (Cat. # VT-199-1.4-1.5, TE Technology) operated in a cascade configuration are used for heating and cooling. The power to the modules is provided by a power supply (Cat. # PS-24-20, TE Technology) via a controller board (Cat. # TC-24-25R, TE Technology). A thermistor (Cat. # MP-2444, TE Technology) is embedded in a shallow groove in the aluminum plate to provide temperature sensing. The temperature of the device is controlled by the proportional-integral-derivative method via a PC using LabVIEW v8.0 (National Instruments). The heat sink is kept at 20 ºC using a refrigerated circulator (RTE-111, Neslab Instruments). A multi-channel syringe pump (Cavro XL 3000, Tecan Group) connected to the device via flangeless fittings (Cat. # P-252/P-259, Upchurch Scientific) is used to deliver reagents and wash solutions. Check valves (Cat. # EW-01355-14, Cole Parmer Instrument Co.) are used to prevent back-flow when removing the polycarbonate block. The pump is controlled via Pump:Link software (Tecan Group).

5.3.7 Preparation of circular DNA molecules

Two different circular DNA molecules, Circle1 and Circle2, were prepared from 78-base long linear oligonucleotides with the following sequences: 5′-phosphate-CTC AGC TGT GAT CAT CAG AAC TCA CCT GTT AGA CGC CAC CAG CTC CAA CTG TGA AGA TCG CTT ATC GCA TGT CCT ATC-3′ (LC1) or 5′-phosphate-CAC GGA CGA CGT ATA TGA TGG TAC CGC AGC CAG CAT CAC CAG ACT GAG TAT CTC CTA TCA CTG CGT GTT TCC TTC TAG CAC GGA CGA CGT-3′ (LC2). A guide oligonucleotide (5′-ATG ATC ACA GCT GAG GAT AGG ACA TGC GA-3′ for Circle1 or 5′-ACG TCG TCC GTG CTA GAA GGA AAC ACG AC-3′ for Circle2), with sequence complementary to both ends of the 78-base linear oligonucleotide was

used to bring the 3′ end and 5′ phosphorylated end to a juxtaposed position for ligation. To purify the circularized DNA molecules, the guide oligos and un-ligated linear oligos were removed by exonuclease digestion. Specifically, the circular DNA molecules were created as follows: 1 μM of the linear oligo was hybridized to 1.1 μM of the guide sequence in a ligase buffer (20 mM of TrisCl, 25 mM KCl, 10 mM $MgCl_2$, 1 mM ATP, 5 mM DTT, 100 μg/mL BSA (Cat. # 10711454001, Roche), pH 7.5) by heating at 75 ºC for 5 minutes and cooling slowly down to 22 ºC. BSA (Cat. # 10711454001, Roche) and T4 DNA Ligase (Cat. # 799099, Roche) were added to the solution to a final concentration of 100 μg/mL and 0.25 U/μL, respectively. The ligation was carried out at 37 ºC for 2 hours and then the ligase was inactivated by heating at 80 ºC for 10 minutes. The pH of the solution was then adjusted to 8.5 by adding an appropriate amount of a 1 M glycine solution (pH 9.5). Exonuclease I and T7 Gene 6 Exonuclease (Cat. #s E70073X and E70025Z, United States Biochemicals) were then added to give a concentration of 1 U/μL each and the digestion was carried out at 37 ºC for 2 hours. The enzymes were deactivated by heating at 80 ºC for 10 min. The circularized DNA was extracted with phenol/chloroform and purified via ethanol precipitation. The DNA was dissolved in 10 mM of TrisCl, pH 7.5, analyzed and quantified by polyacrylamide gel electrophoresis.

5.3.8 Synthesis of linear DNA polymers by rolling circle amplification

Primer-conjugated substrates were re-hydrated by washing the channels with a 2X SSC solution with 1% SDS and heating at 90 ºC for 15 min. The chip was then cooled to room temperature and the channels were washed for 2 min with a 2X-SSC-T solution (2X-SSC-T: 2X SSC solution with 0.1% Triton X-100). A solution containing 20 nM of Circle1 or Circle2 in a 2X SSC solution was then introduced and the chip was heated to

75 ºC for 2 min and cooled to 55 ºC at 2 ºC/min. The temperature was held at 55 ºC for 15 min then cooled to 25 ºC at a rate of 2 ºC/min. The channels were washed for 2 min in a polymerase buffer (20 mM Tris-HCl, 10 mM $(NH_4)_2SO_4$, 10 mM KCl, 2 mM $MgSO_4$, 0.1 % Triton X-100, pH 8.8 at 25 ºC). Bst DNA polymerase large fragment (Cat. # M0275L, New England Biolabs) was introduced at a concentration of 1 U/µL in the polymerase buffer. The chip was then heated to 50 ºC for 15 min to allow the polymerases to bind to the primed circular DNA molecules. The chip was cooled to 4 ºC and a reaction mix containing 1 U/µL Bst DNA polymerase, 100 µg/mL BSA (Cat. # B9001S, New England Biolabs), 1 mM each of dATP, dCTP, dGTP and dTTP (Cat. #s 27-2050-02, 27-2060-02, 27-2070-02 and 27-2080-02, Amersham Biosciences), 4 µM E. coli. single stranded DNA binding protein (SSB) (Cat. # 70032Z, United States Biochemicals) in a Bst buffer (20 mM Tris-HCl, 10 mM $(NH_4)_2SO_4$, 50 mM KCl, 4 mM $MgSO_4$, 0.1 % Triton X-100, pH 8.8 at 25 ºC) was loaded. The chip was heated to 50 ºC for the specified duration. The reactions were terminated by washing the channels with a wash buffer (2X SSC solution with 10 mM EDTA and 0.1% Triton X-100). This process is illustrated in the last two steps in Figure 5.1.

5.3.9 Characterization by fluorescent imaging

Fluorescently labeled oligonucleotides were used to detect the presence of the covalently-bound DNA primers and the RCA products. A Cy5-labeled oligonucleotide, 5′-Cy5- TCG CAT GTC CTA TCC TCA GCT GTG ATC AT-3′, was used to detect the surface-bound primers and a Cy3-labeled oligonucleotide, 5′-Cy3-TCA GAA CTC ACC TGT TAG AC-3′, was used to detect the RCA product from Circle1. The probes were introduced into the channels at a concentration of 1 µM in a 2X SSC solution. The chip

was heated to 75 ºC for 2 min, and then cooled to 25 ºC at a rate of 5 ºC/min. The channels were washed with a 2X-SSC-T solution and imaged using an epifluorescence microscope (Axio Observer.Z1, Carl Zeiss) with a 40x/1.3 NA oil objective and a mercury arc lamp (X-Cite 120, EXFO Photonic Solutions) or a fast wavelength-switching light source with a 300 W xenon arc lamp (Lambda DG-5, Sutter Instrument Co.). Scanning was performed using a BioPrecision 2 XY microscope stage and a MAC 5000 controller system (Ludl Electronics Products) and images were acquired with an EMCCD camera (iXon+885, Andor Technology). Auto-focusing was performed with a Definite Focus system (Carl Zeiss). Custom software was used for all hardware control and image acquisitions. Image analysis was performed with Image J (29).

5.3.10 Characterization by gel electrophoresis

To quantify the amount of DNA polymer synthesized in a given channel, the RCA product generated from Circle2 on a non-patterned surface was digested *in situ* using a restriction enzyme which cuts only once in each repeat unit of the RCA product. First, a complimentary oligonucleotide, 5′-CGA CGT ATA TGA TGG TAC CGC AGC CAG CAT CAC CAG A-3′, was introduced at a concentration of 5.0 μM in a 2X SSC solution and hybridized to the RCA product using the protocol described above. The channels were washed briefly with a reaction buffer (50 mM potassium acetate, 20 mM Tris-acetate, 10 mM magnesium acetate) and an enzyme solution containing 1 U/μL BanI (Cat. # R0118L, New England Biolabs) in 50 mM potassium acetate, 20 mM Tris-acetate, 10 mM magnesium acetate, 100 μg/mL BSA and 1 mM dithiothreitol, pH 7.9 was introduced into the chamber and the chip was incubated at 37 ºC for approximately 12 hr. The digestion solution was collected from the chamber and analyzed using

polyacrylamide gel electrophoresis. Solutions containing known amounts of the LC1 or LC2 oligonucleotides were also loaded onto the same gel for quantification purposes. The gel was stained with SYBR Gold (Cat. # S11494, Invitrogen) and imaged on a Gel Doc imaging system and analyzed using Discovery One software (Bio-Rad Laboratories). An Ultra Low Range Gene Ruler (Cat. # SM1211, Fermentas Life Sciences) was used as a molecular weight marker.

To approximate the average polymer length and rate of DNA synthesis, the individual RCA products were cut and released from the surface of a non-patterned substrate using a restriction enzyme that cuts only at the base of each polymer. Following polymer synthesis, the channels were first washed with the reaction buffer. A mixture consisting of 0.2 U/μL terminal transferase (TdT) (Cat. # M0315L, New England Biolabs), 500 μM dATP, 5 μM ddATP (Cat. # 1008382, Roche) and 0.25 mM $CoCl_2$ in the reaction buffer was then loaded and allowed to incubate at 37 ºC for 30 min to add a poly-A tail onto the 3′ end of each DNA molecule. The enzyme was inactivated by heating the chip at 70 ºC for 10 min. A poly-T oligonucleotide primer, 5′-TTT TTT TTT TTT TTT TTT TTT T-3′ (PT25), at a concentration of 1 μM in a 2X SSC solution was then hybridized to the polyA tails using the procedure described above. A reaction mix containing 0.1 U/uL Phusion High-Fidelity DNA polymerase (Cat. # F530L, New England Biolabs), 1 mM each of dATP, dCTP, dGTP and dTTP, 0.4 μM PT25 and 1X HF buffer (Cat. #F-518L, New England Biolabs) was loaded into the channels and the chip was heated at 67 ºC for 15 min to convert all single-stranded DNA to a double-stranded form. The synthesis reaction was terminated by washing with the wash buffer and then the reaction buffer. A solution containing 2 U/μL of PvuII (Cat. # R0151M,

New England Biolabs) in a digestion buffer (50 mM potassium acetate, 20 mM Tris-acetate, 10 mM magnesium acetate and 1 mM dithiothreitol, pH 7.9) was then loaded into the channels and the chip was incubated at 37 ºC for approximately 12 hr. The solution was then collected from each channel and analyzed using agarose gel electrophoresis. The gel was stained, imaged and analyzed as described above. The length of the RCA products was estimated from the gel using a 1 kb DNA Ladder (Cat. # N0468S, New England Biolabs) and a 1 kb Plus Ladder (Cat. # 10787-026, Invitrogen)

5.4 Results and discussion

5.4.1 Methods and device

We have developed a method for fabricating high-density arrays of oligonucleotides and linear DNA polymers using a destructive micropatterning technique and solid-phase RCA. The micropatterning technique utilizes photolithography to generate an array of posts in photoresist on a DNA-conjugated substrate. Oxygen-based plasma is then used to destroy the oligonucleotides not protected by the photoresist. Once the resist is removed, the remaining oligonucleotides are used to synthesize linear DNA polymers using RCA on circular DNA templates (Figure 5.1). Polymer synthesis is performed within microfluidic channels to minimize reagent use. A device with integrated temperature control and fluidics is employed to enable automated heating, cooling and liquid handling (Figure 5.2). Fluorescently labeled complimentary oligonucleotides can be hybridized to the linear polymers to facilitate qualitative (Figure 5.3) and quantitative (Figure 5.4) analyses by epifluorescence imaging. We also demonstrate the ability to control the polymer density and length by varying the circular template concentrations and RCA

reaction times. Standard molecular biology techniques, which include enzymatic digestion and gel electrophoresis, were utilized for further characterization and quantification of these polymers.

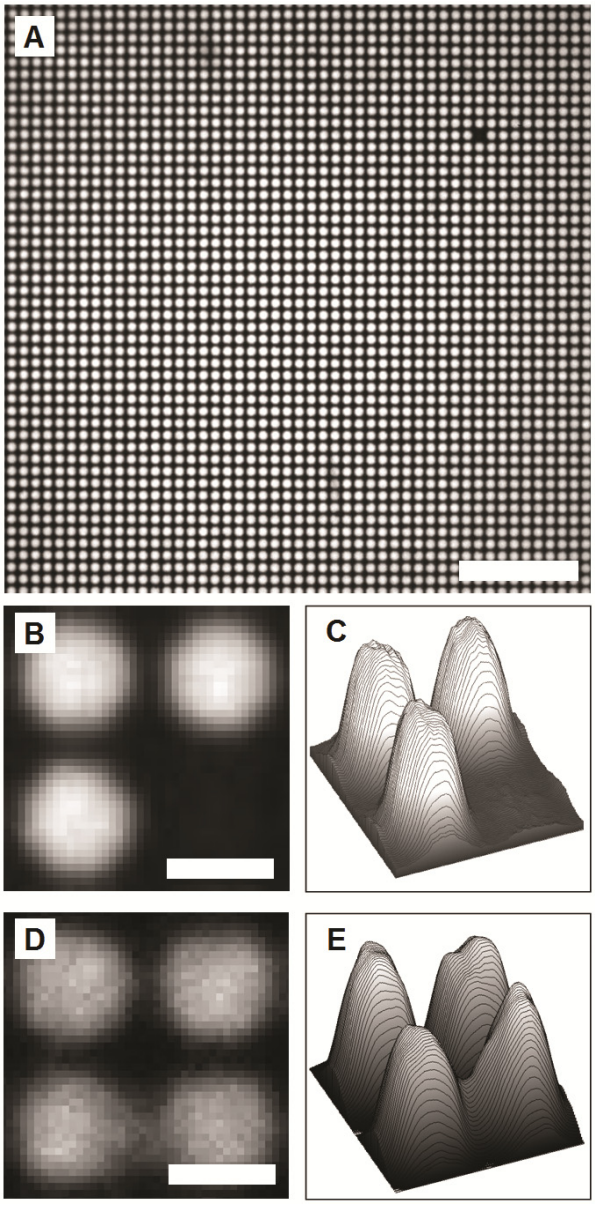

Figure 5.3: High-density arrays of DNA polymer brushes.
(A) Fluorescence image of a portion of an array of linear DNA polymers synthesized using rolling-circle amplification on an array of DNA primers; (B) Close-up view of a portion of the polymer array containing a missing polymer cluster. These dropouts occur when the posts in the photoresist are lost during development. The subsequent plasma treatment results in primer destruction in these unprotected regions; (C) Surface plot of the polymer clusters shown in (C); (D) Close-up view of a portion of the polymer array after a 30 minute RCA reaction. With extended synthesis times, the linear polymers can become long enough to bridge adjacent clusters.; (E) Surface plot of the polymer clusters shown in (D). The scale bar is 40 μm in (A) and 3 μm in (B) and (C).

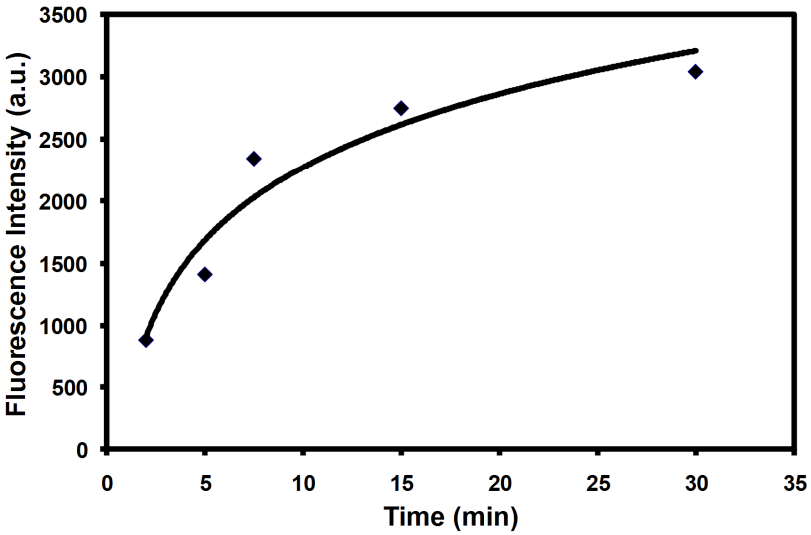

Figure 5.4: Analysis of the linear DNA polymer growth via fluorescence imaging. The polymer growth profile is approximately logarithmic (R^2 = 0.94) as determined by hybridization of a fluorescent probe and subsequent imaging on an automated epifluorescence microscope.

Using the oligonucleotide conjugation strategy described here, we found that it was necessary to cap any free carboxylic acid groups with aminated PEG molecules to enhance photoresist adhesion during the micropatterning process. Without this PEGylation step, a majority of the resist posts would detach from the substrate during development. Because the subsequent plasma etching step was employed to destroy oligonucleotides not protected by photoresist, the lost posts would result in polymer cluster drop-outs. Even with the inclusion of a PEGylation process, this type of defect was still occasionally observed (Figure 5.3). However, this defect rate was typically less than 0.1% and was likely caused by particle contamination on or within the substrate. The only other type of defect we observed was caused by limitations in the resolution and reproducibility of contact lithography. Consistent fabrication of high-density arrays is difficult because slight separation between the photomask and substrate will lead to

significant interference defects. Poor contact can be caused by particle contamination or non-uniform substrate thickness. For a demonstration of principle, we used larger feature sizes in this study to minimize these defects due to the limitations of contact photolithography. However, much smaller feature sizes and higher densities can be achieved by using projection lithography[9].

5.4.2 Control and characterization of the polymer length and density

The polymer density can be controlled by simply adjusting the number of circular templates that are available for hybridization to the surface-bound primers prior to the initiation of the RCA reaction. As shown in Figure 5.5, template concentrations below 2 nM result in a polymer density at which some of the individual polymers can be resolved and counted in a fluorescent micrograph. At 0.2 nM, the polymer density is low enough that nearly every polymer can be resolved and counted. To estimate the polymer density for the higher template concentrations, we have employed a strategy that involves the enzymatic digestion of the polymers on the chip and subsequent analysis by gel electrophoresis. The DNA polymers were either digested into 78-base fragments or cut just once near their base. Oligonucleotides complementary to a specific sequence in each repeat of the RCA products was hybridized to the single-stranded DNA polymers. The sequence contains a recognition site for a restriction enzyme, BanI, which is known to retain its activity even after long incubations. After digesting the polymers with BanI, the solution was reclaimed from the chip and analyzed on a 20% polyacrylamide gel. The result was a major band corresponding to the 78-base repeating unit. Using known amounts of LC1 or LC2 as standards, we were able to quantify the total number of copies

of the 78-base circle that were synthesized on the chip during the RCA reaction (Figure 5.6).

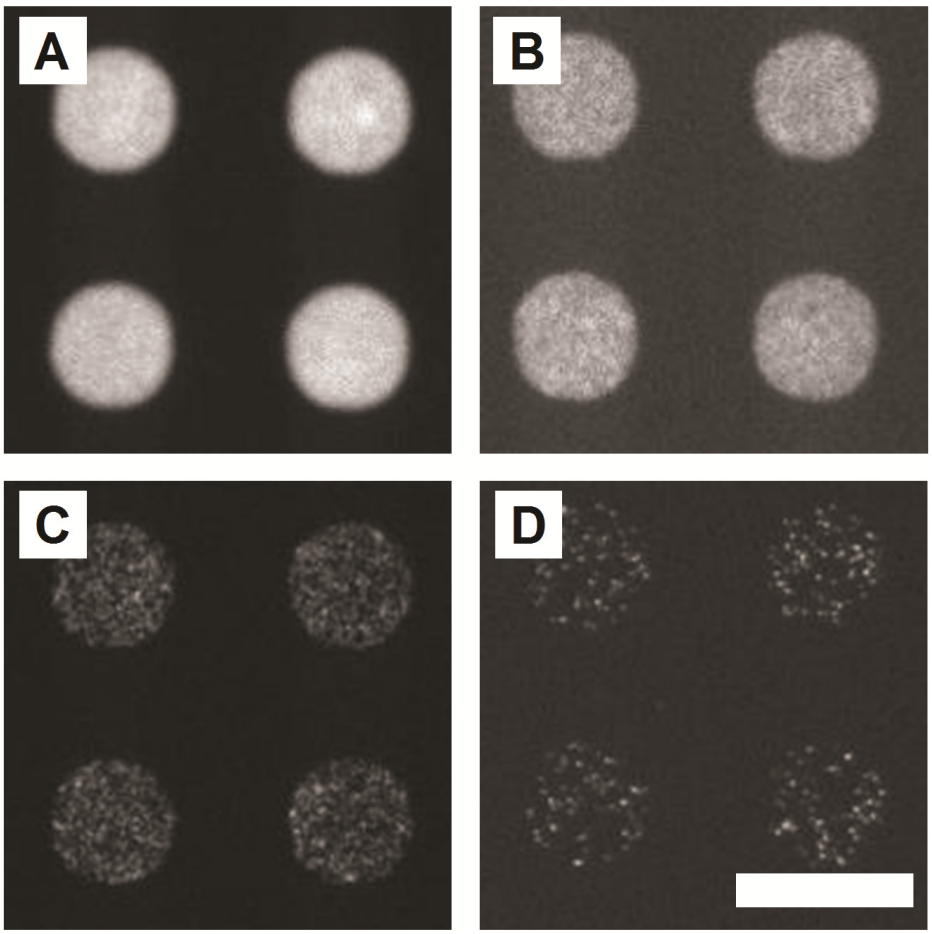

Figure 5.5: Control of the density of the DNA polymer brushes.
Fluorescence images showing the effect of circular DNA template concentration on the density of the linear DNA polymers. The circle concentrations were varied from 200 nM to 0.2 nM: (A) 200 nM, (B) 20 nM, (C) 2 nM, and (D) 0.2 nM. The individual polymers can be resolved at the lower concentrations (C and D). These fluorescent micrographs were acquired with a 40x/1.3 NA oil objective and an EMCCD camera with 8 μm x 8 μm pixels. The scale bar is 15 μm

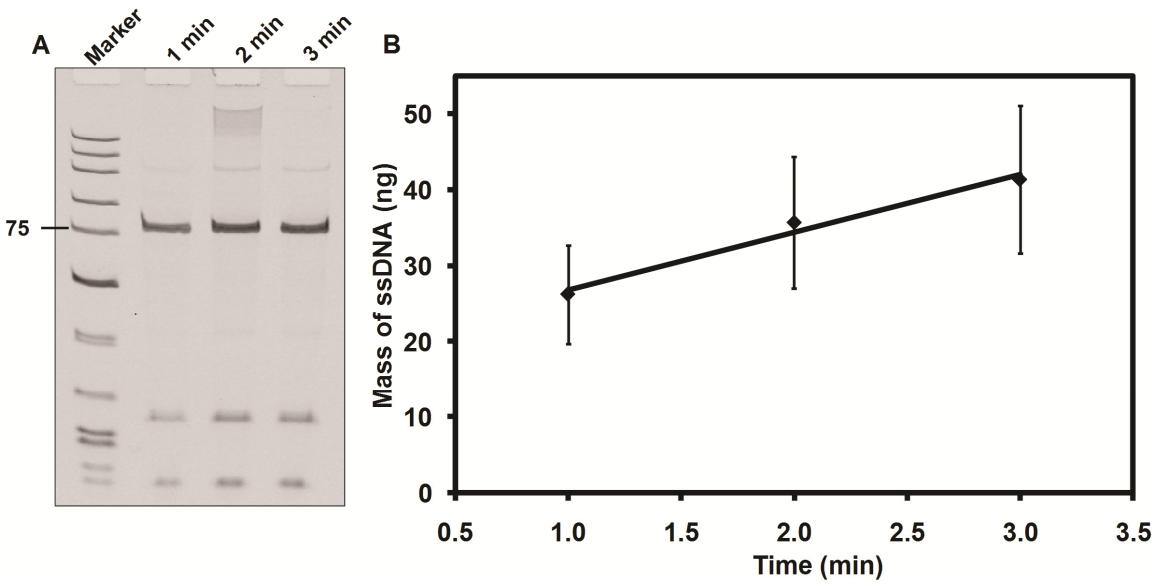

Figure 5.6: Analysis of DNA polymer synthesis by enzymatic digestion and gel electrophoresis.
(A) An image of a 20% polyacrylamide gel showing the result of an enzymatic digestion of the linear DNA polymers synthesized via solid-phase RCA. The primary bands in the right three lanes are 78-base fragments corresponding to the length of the circle used to synthesize the polymers. The higher bands correspond to fragments that are multiples of the 78-base fragment and are a result of incomplete digestion. The lower bands, which are 14 and 23 bases in length, are the digested products of the 37-base oligonucleotides that were hybridized to the polymers to introduce the restriction enzyme cutting sites. (B) A plot of the total amount of DNA synthesized per flow cell as a function of RCA reaction time. The growth rate is approximately linear in this range ($Y = 7.6X + 19.2$, $R^2 = 0.99$)

Enzymatically cutting the polymers near their base allowed for the removal and analysis of full-length polymer strands. First, a poly-A tail with an average length of 100 bases was added by a terminal transferase enzyme to the 3′ end of each strand using 100:1 molar ratio of dATP and ddATP. A short poly-T oligonucleotide was then hybridized to the poly-A tail and a DNA polymerase was used to convert the polymers into a double-stranded form. In addition to the RCA priming sequence, the oligonucleotide covalently attached to the surface of the glass chip contained a sequence with a recognition site for another restriction endonuclease, PvuII. After digestion with

PvuII, the solution was reclaimed from the chip and analyzed on a 0.5% agarose gel with known DNA standards to determine the average length of the polymers (Figure 5.7).

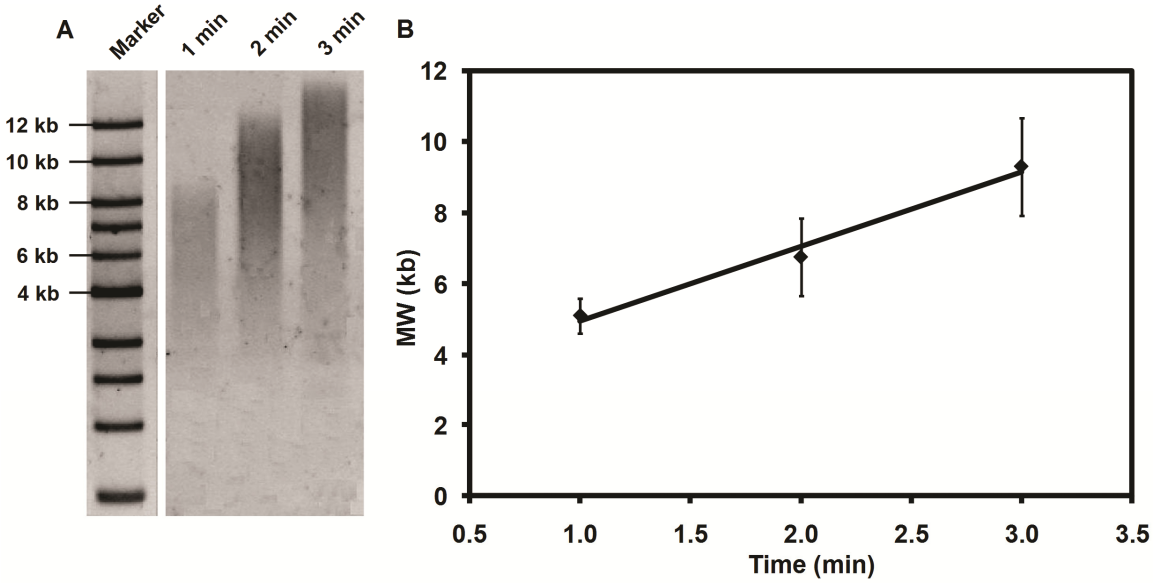

Figure 5.7: Analysis of the linear DNA polymer length by enzymatic digestion and gel electrophoresis.
(A) An image of a 0.5% agarose gel showing the average linear DNA polymer lengths for three different time points. The polymers were synthesized via solid-phase RCA, converted into a double-stranded form and then released from the substrate by cutting the molecules near the base with a restriction enzyme. (B) A plot of the average polymer length in kilobase pairs as a function of RCA reaction time. The polymer growth rate is approximately linear in this range ($Y = 2.1X + 2.9$, $R^2 = 0.98$)

The surface density of the DNA polymer brushes was estimated using the enzymatic digestion and gel electrophoresis data. First, the total number of 78-base tandem repeats synthesized within a given channel was obtained from the BanI digest data shown in Figure 5.6. Next, the average polymer length was estimated from the PvuII digestion data shown in Figure 5.7. Then the number of polymers synthesized within a given channel was obtained by dividing the total number of the tandem repeats by the average polymer length for a given reaction time. Finally, the average polymer density was calculated by dividing the total number of polymers synthesized within a given

channel by the channel surface area. For an RCA reaction that began with the hybridization of a circular template at a concentration of 20 nM, the average polymer density on a non-patterned surface was 153 molecules/μm^2. As shown in Figure 5.5, this density can be modified by adjusting the concentration of the circular template that is hybridized onto the surface-bound oligonucleotide primers. However, an extremely high polymer density may inhibit analysis by enzymatic digestion due to steric constraints[33, 34]. Fortunately, this problem may be overcome through the use of various chemical cleavage methodologies[36].

The limitations of these characterization methods include errors introduced by large polymer length distributions and the detection and sizing limits of gel electrophoresis. The polymer length distribution is minimized by pre-loading the primer-circle constructs with the DNA polymerase to synchronize the individual RCA reactions. Gel sizing limitations were dealt with by using relatively short RCA reaction times to keep the polymer lengths within reason. These short reaction times also helped to prevent the RCA molecules from growing long enough to bridge the gap between adjacent pads on the array (Figure 5.3D). The lower detection limit of gel electrophoresis was avoided by using non-patterned surfaces and circular template concentrations of at least 20 nM. These steps helped ensure an adequate amount of DNA was synthesized within a given channel. However, a more sensitive gel electrophoresis system may enable the characterization of polymer brushes with even lower densities

5.4.3 Applications

In one potential application, these DNA polymer brushes may serve as long, flexible supports for the attachment of various biomolecules. For instance, attaching

multiple PCR primers along the length of these polymers may enable greater primer accessibility for more efficient DNA amplification than what can be achieved using traditional solid-phase PCR (SP-PCR). The inefficiencies of SP-PCR[16], which requires a large number of reaction cycles to achieve a relatively small number of template copies[36, 37], is attributed to poor hybridization efficiencies and steric constraints. However, the use of polymer-bound oligonucleotide primers may provide a more favorable environment for PCR, which is likely to result in the synthesis of more template copies in fewer cycles. In essence, the DNA polymers create a 3D, solution-like environment that may enable more efficient reactions than possible on 2D substrates[16]. In addition, the greater loading capacities afforded by the third dimension of the polymers may allow for the synthesis of many more template copies on a spot on an array[14] or on the surface of a microbead[38], which may be advantageous to both microbead- and surface-based DNA sequencing platforms[39-41]. This third dimension may also enable further reductions in the spot size on DNA microarrays without compromising the dynamic range needed for gene expression analysis[42].

Another potential advantage of the technology presented here is the isolation of the polymer clusters afforded by the array format. With each cluster of DNA polymers spatially separated from one another, the products of individual clonal DNA amplification reactions, or amplicons, would also remain separated from each other[14, 36]. The ability to confine these reactions may prove beneficial to current DNA sequencing platforms by eliminating amplicon overlap and controlling amplicon size. These issues represent significant challenges in that DNA template concentrations must be carefully controlled to ensure an optimal amplicon density is obtained[36, 41]. High amplicon

densities typically result in excessive overlap whereas low densities result in poor throughput. Restricting the outward growth of the amplicon may even result in higher template densities if the amplification process continues to generate additional template copies that would effectively fill in the gaps within a given amplicon[14, 37]. Furthermore, the use of an array format allows for higher imaging efficiencies to be obtained by reducing the number of unused pixels in each image and allowing each amplicon to be imaged with a minimal number of pixels[7].

5.5 Conclusions

In summary, we have developed a method for fabricating high-density arrays of oligonucleotide primers using a destructive micropatterning technique. We have demonstrated that circular DNA molecules can be hybridized to these primers and amplified by RCA to generate an array of DNA polymer brushes. We have also shown that these DNA polymers brushes can be well characterized by fluorescence imaging, enzymatic digestion and gel electrophoresis. These long, linear polymers may be useful for enhancing the sensitivity and dynamic range of biomolecular assays by enabling higher loading capacities and more efficient biomolecular binding. The 3D, solution-like environment created by these DNA polymer brushes may also enable more efficient enzymatic reactions such as solid-phase DNA amplification.

5.6 Acknowledgements

This work was supported in part by grants from the NIH/NHGRI (R21HG003587, R21HG004130 and 1R01HG005096) and the NSF under a career award to X. H. (BES-0547193). A portion of this work was performed in the Nano3 facility at CalIT^2 at

UCSD. We thank Larry Grissom and Ryan Anderson for training and technical support at Nano3. We thank Aric Joneja for advice regarding enzymes, primers and DNA amplification strategies. We also thank Eric Roller for programming the automated imaging system.

5.7 References

1. Fodor, S.P., Rava, R.P., Huang, X.C., Pease, A.C., Holmes, C.P. & Adams, C.L. Multiplexed biochemical assays with biological chips. *Nature* **364**, 555-556 (1993).

2. Lausted, C.G., Warren, C.B., Hood, L.E. & Lasky, S.R. Printing your own inkjet microarrays. *Methods Enzymol.* **410**, 168-189 (2006).

3. Schena, M., Shalon, D., Davis, R.W. & Brown, P.O. Quantitative monitoring of gene expression patterns with a complementary DNA microarray. *Science* **270**, 467-470 (1995).

4. Piner, R.D., Zhu, J., Xu, F., Hong, S. & Mirkin, C.A. "Dip-pen" Nanolithography. *Science* **283**, 661-663 (1999).

5. Lange, S.A., Benes, V., Kern, D.P., Horber, J.K.H. & Bernard, A. Microcontact printing of DNA molecules. *Anal. Chem.* **76**, 1641-1647 (2004).

6. Ferguson, J.A., Steemers, F.J. & Walt, D.R. High-density fiber-optic DNA random microsphere array. *Anal. Chem.* **72**, 5618-5624 (2000).

7. Barbee, K.D. & Huang, X. Magnetic assembly of high-density DNA arrays for genomic analyses. *Anal. Chem.* **80**, 2149-2154 (2008).

8. Blicharz, T.M., Siqueira, W.L., Helmerhorst, E.J., Oppenheim, F.G., Wexler, P.J., Little, F.F. & Walt, D.R. Fiber-optic microsphere-based antibody array for the analysis of inflammatory cytokines in saliva. *Anal. Chem.* **81**, 2106-2114 (2009).

9. Barbee, K.D., Hsiao, A.P., Heller, M.J. & Huang, X. Electric field directed assembly of high-density microbead arrays. *Lab Chip* **9**, 3268-3274 (2009).

10. Chee, M., Yang, R., Hubbell, E., Berno, A., Huang, X.C., Stern, D., Winkler, J., Lockhart, D.J., Morris, M.S. & Fodor, S.P. Accessing genetic information with high-density DNA arrays. *Science* **274**, 610-614 (1996).

11. Schena, M., Shalon, D., Heller, R., Chai, A., Brown, P.O. & Davis, R.W. Parallel human genome analysis: Microarray-based expression monitoring of 1000 genes. *Proc. Natl. Acad. Sci. U. S. A.* **93**, 10614-10619 (1996).

12. Gunderson, K.L., Steemers, F.J., Lee, G., Mendoza, L.G. & Chee, M.S. A genome-wide scalable snp genotyping assay using microarray technology. *Nat. Genet.* **37**, 549-554 (2005).

13. Zhu, H., Bilgin, M., Bangham, R., Hall, D., Casamayor, A., Bertone, P., Lan, N., Jansen, R., Bidlingmaier, S., Houfek, T. *et al.* Global analysis of protein activities using proteome chips. *Science* **293**, 2101-2105 (2001).

14. Mitra, R. & Church, G. In situ localized amplification and contact replication of many individual DNA molecules. *Nucleic Acids Res.* **27**, e34- (1999).

15. Miller, J.C., Zhou, H., Kwekel, J., Cavallo, R., Burke, J., Butler, E.B., Teh, B.S. & Haab, B.B. Antibody microarray profiling of human prostate cancer sera: Antibody screening and identification of potential biomarkers. *Proteomics* **3**, 56-63 (2003).

16. Pemov, A., Modi, H., Chandler, D.P. & Bavykin, S. DNA analysis with multiplex microarray-enhanced PCR. *Nucleic Acids Res.* **33**, e11- (2005).

17. Ishihara, K. & Takai, M. Bioinspired interface for nanobiodevices based on phospholipid polymer chemistry. *J. R. Soc. Interface* **6**, S279-S291 (2009).

18. Jain, P., Baker, G.L. & Bruening, M.L. Applications of polymer brushes in protein analysis and purification. *Annu. Rev. Anal. Chem.* **2**, 387-408 (2009).

19. Kusnezow, W. & Hoheisel, J.D. Solid supports for microarray immunoassays. *J. Mol. Recognit.* **16**, 165-176 (2003).

20. Hucknall, A., Kim, D.-H., Rangarajan, S., Hill, R.T., Reichert, W.M. & Chilkoti, A. Simple fabrication of antibody microarrays on nonfouling polymer brushes with femtomolar sensitivity for protein analytes in serum and blood. *Adv. Mater.* **21**, 1968-1971 (2009).

21. Zhao, B. & Brittain, W.J. Polymer brushes: Surface-immobilized macromolecules. *Prog. Polym. Sci.* **25**, 677-710 (2000).

22. Matyjaszewski, K. & Xia, J. Atom transfer radical polymerization. *Chem. Rev.* **101**, 2921-2990 (2001).

23. Tomlinson, M.R., Cousin, F. & Geoghegan, M. Creation of dense polymer brush layers by the controlled deposition of an amphiphilic responsive comb polymer. *Polymer* **50**, 4829-4836 (2009).

24. Flory, P.J. & Jr., T.G.F. Molecular configuration and thermodynamic parameters from intrinsic viscosities. *J. Polym. Sci.* **5**, 745-747 (1950).

25. Fire, A. & Xu, S.Q. Rolling replication of short DNA circles. *Proc. Natl. Acad. Sci. U. S. A.* **92**, 4641-4645 (1995).

26. Liu, D., Daubendiek, S.L., Zillman, M.A., Ryan, K. & Kool, E.T. Rolling circle DNA synthesis: Small circular oligonucleotides as efficient templates for DNA polymerases. *J. Am. Chem. Soc.* **118**, 1587-1594 (1996).

27. Lizardi, P.M., Huang, X., Zhu, Z., Bray-Ward, P., Thomas, D.C. & Ward, D.C. Mutation detection and single-molecule counting using isothermal rolling-circle amplification. *Nat. Genet.* **19**, 225-232 (1998).

28. Hatch, A., Sano, T., Misasi, J. & Smith, C.L. Rolling circle amplification of DNA immobilized on solid surfaces and its application to multiplex mutation detection. *Genet. Anal. - Biomol. Eng.* **15**, 35-40 (1999).

29. McCarthy, E.L., Bickerstaff, L.E., Cunha, M.P.d. & Millard, P.J. Nucleic acid sensing by regenerable surface-associated isothermal rolling circle amplification. *Biosens. Bioelectron.* **22**, 1236-1244 (2007).

30. Kuwahara, M., Hososhima, S.-i., Takahata, Y., Kitagata, R., Shoji, A., Hanawa, K., Ozaki, A.N., Ozaki, H. & Sawai, H. Simultaneous incorporation of three different modified nucleotides during PCR. *Nucleic Acids Res. Symp.* **3**, 37-38 (2003).

31. Pieles, U. & Englisch, U. Psoralen covalently linked to oligodeoxyribonucleotides: Synthesis, sequence specific recognition of DNA and photo-cross-linking to pyrimidine residues of DNA. *Nucleic Acids Res.* **17**, 285-299 (1989).

32. Flounders, A.W., Brandon, D.L. & Bates, A.H. Patterning of immobilized antibody layers via photolithography and oxygen plasma exposure. *Biosens. Bioelectron.* **12**, 447-456 (1997).

33. Castronovo, M., Radovic, S., Grunwald, C., Casalis, L., Morgante, M. & Scoles, G. Control of steric hindrance on restriction enzyme reactions with surface-bound DNA nanostructures. *Nano Lett.* **8**, 4140-4145 (2008).

34. Bar, M. & Bar-Ziv, R.H. Spatially resolved DNA brushes on a chip: Gene activation by enzymatic cascade. *Nano Lett.* **9**, 4462-4466 (2009).

35. Abramoff, M.D., Magelhaes, P.J., Ram, S.J. Image processing with imagej. *Biophotonics Intl.* **11**, 36-42 (2004).

36. Fedurco, M., Anthony Romieu, Scott Williams, and, I.L. & Turcatti, G. BTA, a novel reagent for DNA attachment on glass and efficient generation of solid-phase amplified DNA colonies. *Nucleic Acids Res.* **34**, e22 (2006).

37. Adessi, C., Matton, G., Ayala, G., Turcatti, G., Mermod, J.-J., Mayer, P. & Kawashima, E. Solid phase DNA amplification: Characterisation of primer attachment and amplification mechanisms. *Nucleic Acids Res.* **28**, e87- (2000).

38. Dressman, D., Yan, H., Traverso, G., Kinzler, K.W. & Vogelstein, B. Transforming single DNA molecules into fluorescent magnetic particles for detection and enumeration of genetic variations. *Proc. Natl. Acad. Sci. U. S. A.* **100**, 8817-8822 (2003).

39. Margulies, M., Egholm, M., Altman, W.E., Attiya, S., Bader, J.S., Bemben, L.A., Berka, J., Braverman, M.S., Chen, Y.J., Chen, Z. *et al.* Genome sequencing in microfabricated high-density picolitre reactors. *Nature* **437**, 376-380 (2005).

40. Shendure, J., Porreca, G.J., Reppas, N.B., Lin, X., McCutcheon, J.P., Rosenbaum, A.M., Wang, M.D., Zhang, K., Mitra, R.D. & Church, G.M. Accurate multiplex polony sequencing of an evolved bacterial genome. *Science* **309**, 1728-1732 (2005).

41. Bentley, D.R., Balasubramanian, S., Swerdlow, H.P., Smith, G.P., Milton, J., Brown, C.G., Hall, K.P., Evers, D.J., Barnes, C.L., Bignell, H.R. *et al.* Accurate whole human genome sequencing using reversible terminator chemistry. *Nature* **456**, 53-59 (2008).

42. Dufva, M. Fabrication of high quality microarrays. *Biomol. Eng.* **22**, 173-184 (2005).

This chapter, in part, has been submitted for publication. Barbee, K.D.; Chandrangsu, M.; Huang, X. Used with permission. The dissertation author was the primary investigator and author of this paper.

6 Conclusions

6.1 Summary of work

6.1.1 Magnetic assembly of high-density microbead arrays

In this work, we have developed a scalable method for fabricating large-scale, high-density arrays of DNA-conjugated superparamagnetic microbeads on glass substrates. The fabrication process is simple and the assembly process is extremely fast and efficient. Our low-defect arrays are free of background caused by non-specifically bound beads and are compatible with automated processes, microfluidics devices and conventional microscopy. The highly ordered arrays, when properly sized and aligned to a given CCD sensor, can also greatly improve imaging efficiency and reduce the complexities of image processing. These properties give our approach significant advantages over existing bead array technologies. By combining these arrays with the emerging sequencing technologies, the time and cost required to sequence a human

genome could be reduced by at least one order of magnitude. The described method can also be used for fabricating and assembling arrays of other molecules such as antigens, lipids and proteins.

6.1.2 Electric field directed assembly of high-density microbead arrays

In this work, we have demonstrated the ability to use electric fields to rapidly assemble high-density arrays of protein-conjugated microbeads. Wafer-scale arrays of wells are fabricated in an epoxy-based photoresist on gold electrodes and hundreds of millions of microbeads can be assembled within these wells in seconds by applying a series of DC electrical pulses. Defect rates are extremely low and the assembly process is very efficient as demonstrated by filling rates as high as 99.9%. This method may be applied to the assembly of arrays of microbeads conjugated to various biomolecules for use in high-throughput assays. In addition, the use of such a platform may provide a means of accelerating diffusion-limited assays by actively concentrating molecules of interest via an electric field.

6.1.3 Multiplexed protein detection on antibody-conjugated microbead arrays

In this work, we have demonstrated that high-density, antibody-conjugated microbead arrays can be assembled via electrophoretic deposition on microfabricated arrays and that these arrays could be used to detect multiple test antigens at concentrations as low as 40 pM using a sandwich immunoassay. For greater reliability and flexibility, this device uses an array of wells fabricated in silicon dioxide on gold-coated silicon chips. In addition, thin gold lines fabricated on glass coverslips were used

as counter electrodes to provide a more robust platform for assembly and enable greater imaging sensitivity than possible with ITO-coated coverslips. We demonstrated the ability to perform a simple and yet powerful spatial encoding strategy to replace or compliment fluorescence-based encoding schemes. Our ability to assemble streptavidin-, NeutrAvidin-, and antibody-conjugated microbeads may be extended to a multitude of other types of protein-conjugated microbeads for other applications such as the analysis of protein-protein interactions.

6.1.4 Fabrication of DNA polymer brush arrays

In this work, we have demonstrated a method for fabricating high-density arrays of oligonucleotide primers using photolithography and plasma etching. Furthermore, we have demonstrated that linear DNA polymers can be generated on these primer arrays using rolling circle amplification. These long, single-stranded DNA molecules could potentially be further functionalized, for example, by hybridization and cross-linking of oligonucleotides at each repeating unit of the polymer. The 3D nature of the polymer brush arrays will provide a solution-like environment for efficient enzymatic reactions with higher yields, which may be useful for applications such as solid-phase DNA amplification.

6.2 Future directions

We plan to scale the features on our platforms down to the nanoscale to determine the lower limits of our assembly techniques and to enable the fabrication and assembly of single molecules. This may involve alternative lithographic techniques such as nanoimprint and deep-UV lithography. We also plan to demonstrate that a multitude of

assays can be enhanced via the use of electric fields on our electrophoretic microchips. These improvements may include enhanced DNA hybridization kinetics and accelerated antigen capture for fast and sensitive genotyping and protein detection, respectively. Furthermore, we plan to demonstrate that our polymer arrays can be used to enhance solid-phase DNA amplification and can serve as a suitable platform for high-throughput DNA sequencing.